UNIVERSITÁ DEGLI STUDI DI MILANO

FACOLTÁ DI MEDICINA E CHIRURGIA

DOTTORATO DI RICERCA IN FISIOLOGIA

SETTORE SCIENTIFICO DISCIPLINARE BIO-09

CICLO XXV°

Tesi di Dottorato di Ricerca

Ion channels pathophysiology and biophysics:
1. The role of the expression of CLIC1 ion channels in cancer stem cells from human glioblastoma;
2. Ca^{2+} and voltage dependent structural changes in the human BK channel during operation revealed by voltage clamp fluorometry.

Dottorando: Dott. Nicoletta Savalli

Matricola: R08853

Tutor: Prof. Michele Mazzanti
Dept. of Biosciences, University of Milan

Co-tutor: Prof. Riccardo Olcese
Dept. of Anesthesiology, University of California Los Angeles

Coordinatore: Prof. Paolo Cavallari

Anno Accademico 2011-2012

INDEX

CHAPTER 2: Ca^{2+} and voltage dependent structural changes in the human BK channel during operation revealed by voltage clamp fluorometry

ABSTRACT

Ion channels are transmembrane proteins that create a pathway for charged ions (sodium, potassium, calcium, and chloride) to pass through the otherwise impermeant lipid membranes. They are present both at the plasma membrane level and in the membrane of intracellular organelles. Ion channels engage in fundamental functions, such as muscle contraction, cell excitability, hormone secretion, mechanosensitivity, just to mention a few. Thus, the understanding of their physiology and pathophysiology remains an important task for science. This thesis embraces two projects involving two different ion channels: the Chloride Intracellular Channel 1 (CLIC1) and the large conductance Ca^{2+}-voltage activated K^+ channel (BK).

The goal of the first project aimed to understand the role of CLIC1 channels in glioblastoma cancer stem cells. Among brain tumors, glioblastomas are very frequent and have the worst outcome. They are composed of two cell types: a small population of cells able to self-renew and generate progeny (cancer stem cells, CSCs) and a larger population possessing a limited division capacity and committed to a precise fate (bulk cells). Glioblastomas are very aggressive tumors because of CSC brain infiltration efficiency and their resistance to chemotherapies. Therefore, CSCs are the most tumorigenic component of glioblastomas and we have focused our efforts on this small population of cells. Several forms of glioblastomas show a high level of expression of CLIC1 compared to normal brains. CLIC1 is a protein mainly localized to the cytoplasm and nucleoplasm that is able to translocate to the plasma membrane and to the nuclear membrane where it acts as a Cl^- channel. The soluble form of CLIC1 belongs to the glutathione S-transferase superfamily. Upon oxidation, the protein forms a dimer that translocates to the membrane and operates as an ion channel. Four human glioblastomas (all expressing CLIC1) have been studied. Human glioblastoma biopsies were cultured in a medium selecting for CSCs. By knocking down CLIC1 protein using siRNA viral infection (siCLIC1), we found that CLIC1-deficient cells migrated about 50% less efficiently than control cells treated with siRNA for luciferase (siLUC). Is this phenotype the result of CLIC1 absence in plasma membranes? To answer this question, we performed electrophysiological experiments from perforated patches for both siLUC and siCLIC1 cells. Cl^- currents mediated by CLIC1 were isolated using a specific inhibitor (IAA94 100 µM). The results showed that siCLIC1 cells did not display IAA94-sensitive currents, while siLUC cells presented the CLIC1-mediated chloride current. Interestingly, in the four glioblastomas analyzed, there is a direct correlation between tumor aggressiveness and the relative abundance of IAA94 sensitive current: the more aggressive the tumor, the greater the relative abundance of CLIC1 current. These results point

to the view that CLIC1 is involved in glioblastoma CSCs migration. However, the mechanism has yet to be elucidated.

The second project investigated the Ca^{2+}-voltage dependent structural rearrangements of the human BK channel during its activation. BK channels are Ca^{2+}-voltage-activated K^+ channels. They are potent regulators of cellular excitability involved in processes such as neuronal firing, synaptic transmission, cochlear hair cell tuning and smooth muscle tone. The BK channel's unique activation pathway is a consequence of its structurally distinct regulatory domains, including four transmembrane voltage sensors (VSD) and four pairs of intracellular Ca^{2+} sensors, RCK1 and RCK2 (Regulation of K^+ Conductance). RCK1 includes residues D362/D367 involved in high-affinity Ca^{2+} sensing, while RCK2 encompasses a stretch of five Asps (D894-898 or Ca bowl) that coordinate Ca^{2+}. In the functional tetrameric channel, the two RCK domains from each subunit assemble into a superstructure called the "gating ring". To understand the allosteric interplay between these sensing apparata (VSD and RCK1/RCK2 in the gating ring), we have simultaneously tracked the conformational status of the VSD and the pore while activating the Ca^{2+} sensors in the gating ring by combining voltage clamp fluorometry with UV-photolysis of caged Ca^{2+}. In WT channels, we found that the VSD conformational changes were triggered not only by voltage but also by $[Ca^{2+}]$ increase, demonstrating that Ca^{2+}-induced rearrangements of the BK intracellular gating ring allosterically propagate to the transmembrane VSD. The impairment of the Ca bowl in the RCK2 domain (D894-898N mutations) abolished the VSD facilitation induced by the rapid increase of $[Ca^{2+}]$. However, the neutralization of the Ca^{2+} sensor in RCK1 (D362A/D367A mutations) did not prevent VSD facilitation by Ca^{2+} (as in WT channels, but to a lesser extent). Thus, RCK1 and RCK2 domains play different functional roles in the Ca^{2+}-dependent activation of the human BK channel. A statistical-mechanical model has been implemented to quantify the thermodynamics of the functional coupling between intracellular and transmembrane regulatory domains in BK channels. This model includes one pore, four VSDs, four RCK1 Ca^{2+} sensors and four RCK2 Ca^{2+} sensors. All these domains are regulated by equilibrium constants and linked by allosteric factors.

CHAPTER 1: The role of the expression of CLIC1 ion channels in cancer stem cells from human glioblastoma

1.A INTRODUCTION

Cancer Stem Cells

‘‘The cancer stem cell hypothesis’’ states that both solid and liquid tumors are composed of i) a relatively small subset of slowly-cycling cells that undergo self-renewal for an unlimited period of time (cancer stem cells or CSCs) and ii) a larger population of cells committed to a precise fate and with finite division capacity (or bulk cells) (Reya et al., 2001). CSCs are defined, in analogy to normal stem cells, as cells that possess the capacity to self-renew and give rise to the variety of differentiated cells found in the malignancy (Vermeulen et al., 2008; Baccelli and Trumpp, 2012). To date, the practical translation of this definition is the ability to generate a phenocopy of the original tumor in immuno-compromised mice (Figure 1).

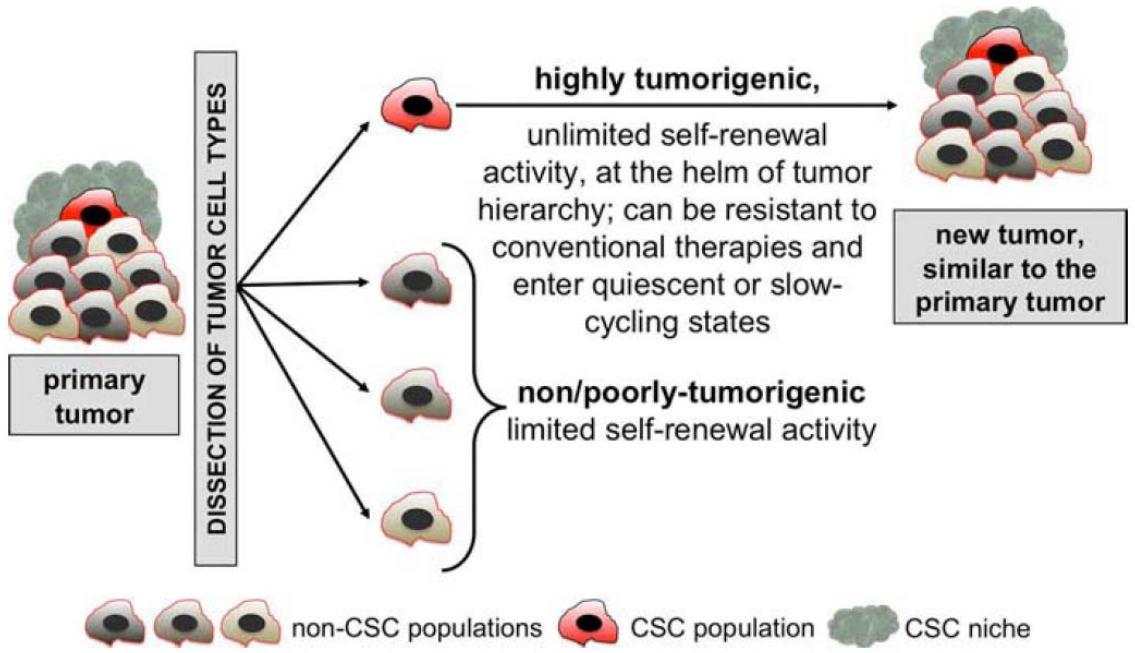

Figure 1. Scheme of the “cancer stem cell” (CSC) hypothesis. Tumors are heterogeneous and hierarchically organized. Upon dissociation and transplantation into an immuno-compromised animal, human CSCs can reinitiate and grow a similar heterogeneous tumor *in vivo* (Baccelli and Trumpp, 2012).

CSCs have been first identified in 1997 in human acute myeloid leukemia (Bonnet and Dick, 1997). Bonnet and Dick found that some hematopoietic stem cells could undergo a tumorigenic event that in turn generated the acute myeloid leukemia. These stem cells not only are multi-potent and able to self-renew but also possess cancer properties, such as karyotypic anomalies and unlimited proliferation ability (Huse and Holland, 2010). In the following years, it has been shown that different tumors contain CSCs, including brain tumors (Singh et al., 2004; Galli et al.,

2004). Alike to neuronal stem cells, brain CSCs express stemness markers (as CD133), are localized in perivascular niches and grow as neurospheres *in vitro* (Huse and Holland, 2010; Calabrese et al., 2007; Jones and Holland, 2010; Charles and Holland, 2010; Stiles and Rowitch, 2008).

The origin of CSCs remains controversial. These cells may derive from normal tissue stem cells. However, another possibility includes the introduction of oncogenes in committed progenitors that can give rise to malignant clones. For example, it has been shown that when ras and c-myc are introduced into oligodendrocyte progenitors, tumors with a glioblastoma multiforme phenotype arise upon in vivo transplantation (Barnett et al., 1998). This indicates that for tumors to occur there is no absolute prerequisite for genetic mutation of normal stem cells (Vermeulen et al., 2008).

CSCs are difficult targets for cancer therapeutics because (1) they cycle slowly, (2) they express high levels of drug-export proteins (chemotherapy resistance), (3) the anti-apoptotic pathways of DNA repair are efficiently activated (radiotherapy resistance) and (4) they may not express the oncoproteins targeted by the new generation of drugs (chemotherapy resistance) (Stiles and Rowitch, 2008; Bao et al., 2006).

Moreover, according to the CSC hypothesis, metastasis-initiating cells should be a subset of CSCs, since they are the cells capable of initiating and driving tumor growth and express migration markers (Baccelli and Trumpp, 2012).

Glioblastoma Multiforme

Gliomas are highly aggressive tumors of the central nervous system (CNS), originating from the neoplastic degeneration of glia cells, including astrocytes and oligodendrocytes (Sanai et al., 2005; Huse and Holland, 2010; Chen et al., 2012). In the United States, about 80% of the CNS malignant tumors are gliomas, which are essentially incurable such that the overall 5-year survival rate remains less than 5% (CBTRUS, 2009).

In general, cancer cells of origin are normal cells in which tumorigenic mutations first occur and accumulate to form a malignancy (Chen et al., 2012). In gliomas, astrocytes were thought to be the origin cells, as the only known replication-competent population (Figure 2). The malignant transformation process in this scenario requires a ‘‘dedifferentiation’’ process by which cells regain immature glial and progenitor properties. The recent discovery of neuronal stem cells (Reynolds and Weiss, 1992; Zhao et al., 2008) provided an alternative candidate for the glioma cell of origin (Figure 2). In neuronal stem cells, the oncogenic process can be viewed as losing control over their self-renewal and differentiation properties.

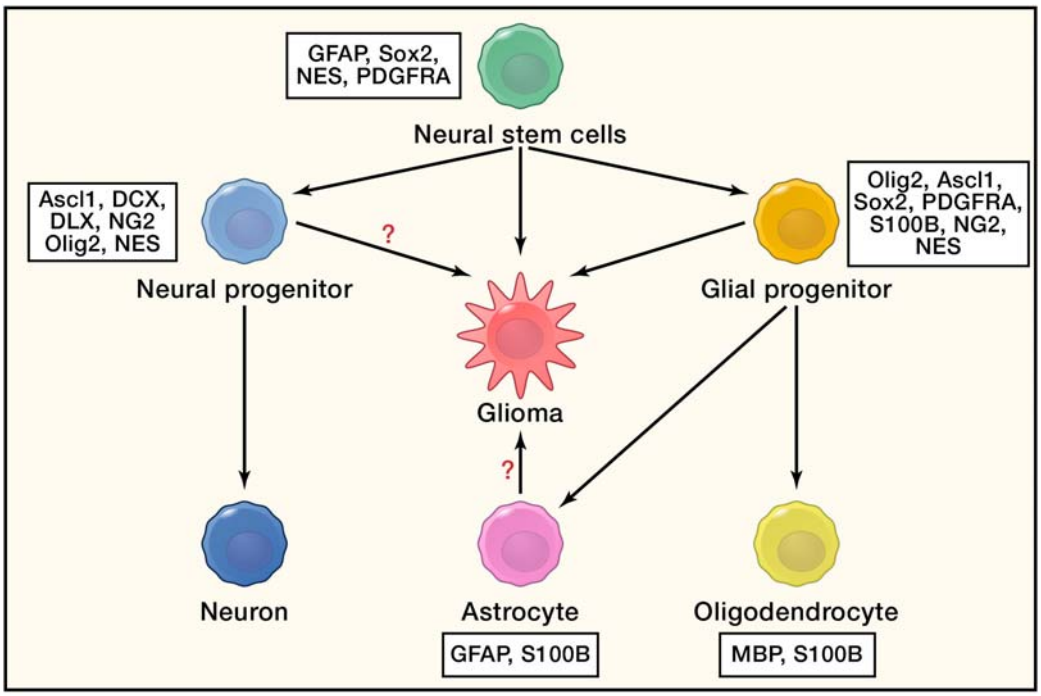

Figure 2. The origin of gliomas. Adult neural stem cells that undergo extensive mutations are sufficient to drive malignant glioma formation *in vivo*. Also, progenitors or mature astrocytes are found as cells of origin (Chen et al., 2012).

The World Health Organization has classified gliomas in four groups (grade I-IV) based on their histology, pleomorphism, localization and expression pattern: the higher the grade the worst the prognosis (Maher et al., 2001; Huse and Holland, 2010; Denysenko et al., 2010). Thus, the most aggressive glioma is the grade IV, or glioblastoma multiforme (GBM), which is characterized by unlimited proliferation ability, neovascularization, infiltration and necrosis. Unfortunately, the occurrence of the GBM is more frequent than all the other glioma types, as reported in Figure 3 (Jones and Holland, 2010).The life expectancy for patients diagnosed with GBM is between 12 and 15 month (Chamberlain, 2010; Maher et al., 2001). The reason for this poor prognosis mainly resides in the fact that GBMs are resistant to radiotherapy and chemotherapy. Moreover, due to its high invasiveness in the brain tissue, surgery is normally not successful and the tumor relapses within a few months (Lefranc et al., 2005).

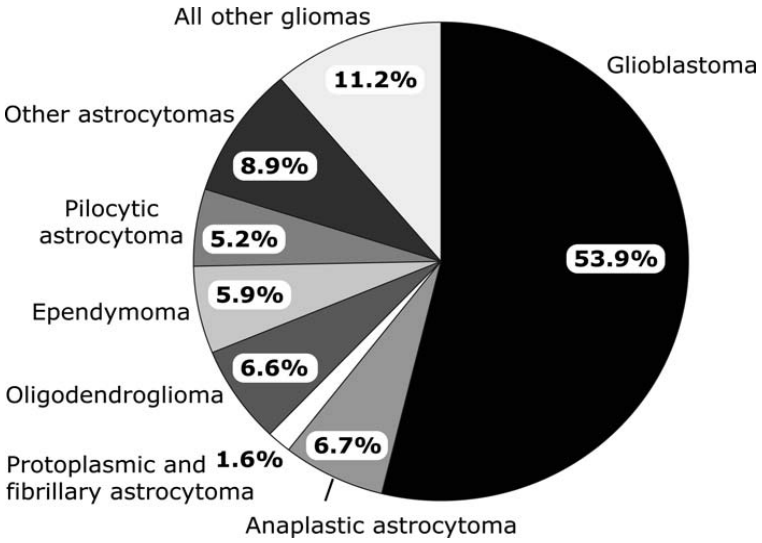

Figure 3. The plot shows the frequency of new primary gliomas in USA between 2004 and 2006. The glioblastoma represents more than 50% of all the gliomas (CBTRUS 2010).

GBMs are characterized by an extensive angiogenesis. The new blood vessels favor tumor growth and infiltration by providing oxygen and nutrients to tumor cells (Denysenko et al., 2010; Sanai et al., 2005; Jones and Holland, 2010). Furthermore, blood vessels and white matter offer a support along which tumor cells invade the brain tissue (Furnari et al., 2007; Sanai et al., 2005; Vescovi et al., 2006). Differently from the other solid tumors, gliomas do not take advantage of the linfantic and blood streams to spread and form metastasis outside of the CNS (Maher et al., 2001).

To explain how GBMs initiate and develop, to date two alternative models are present (Figure 4). The stochastic model proposes that tumor cells are heterogeneous, and virtually all of them can function as a tumour-founding cell. On the other hand, the hierarchical model implies that only a small subpopulation of tumour stem cells can proliferate extensively and sustain the growth and progression of a neoplastic clone (Vescovi et al., 2006). The latter hypothesis fits with the cancer-stem-cell theory.

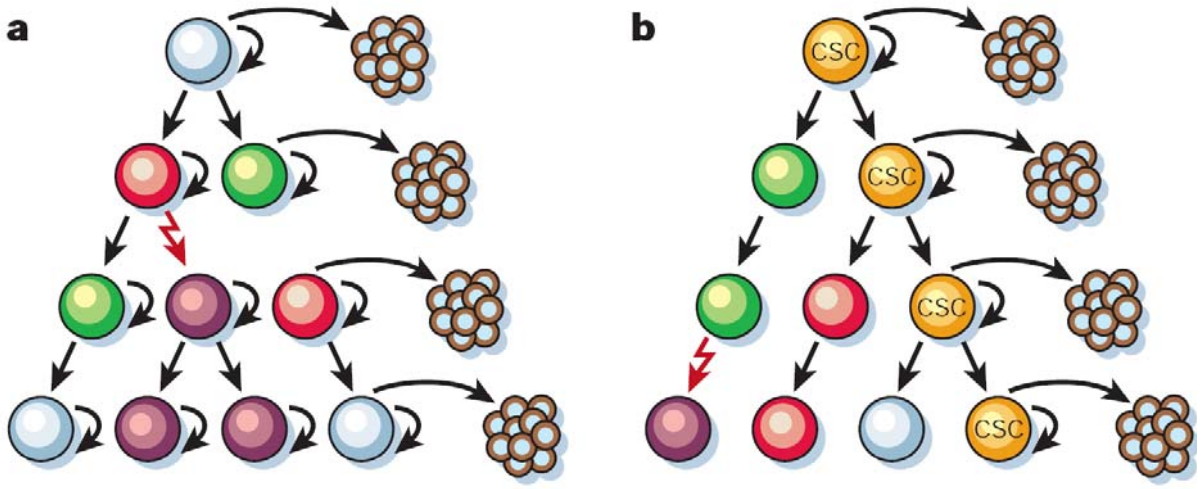

Figure 4. Tumor initiation models. (A) The stochastic model predicts that all the cells in a tumor have a similar tumorigenic potential, which is activated asynchronously and at a low frequency. (B) The hierarchical model predicts that only a rare subset of cells within the tumor (CSC) has significant proliferation capacity and the ability to generate new tumors (Reya et al., 2001).

Ion channels and tumor migration

Ion channels are transmembrane proteins responsible for the passive exchange of ions across the plasmamembrane and the other membranes in the cell. There are many types of ion channels, which at the functional level are traditionally classified by either the stimulus that gates them or the ion species that they pass. Ion channels are involved in all the fundamental cellular processes, such as cell cycle, differentiation, homeostasis and apoptosis (Kunzelmann, 2005; Wonderlin and Strobl, 1996; Prevarskaya et al., 2010). They also play an important role in tumors. The involvement of different types of ion channels has been shown in defining each of the six cancer hallmarks: 1) self-sufficiency in growth signals, 2) insensitivity to antigrowth signals, 3) avoidance of programmed cell death (apoptosis), 4) unlimited replicative potential, 5) angiogenesis and 6) tissue invasion and metastasis (Figure 5) (Prevarskaya et al., 2010; Fraser and Pardo, 2008).

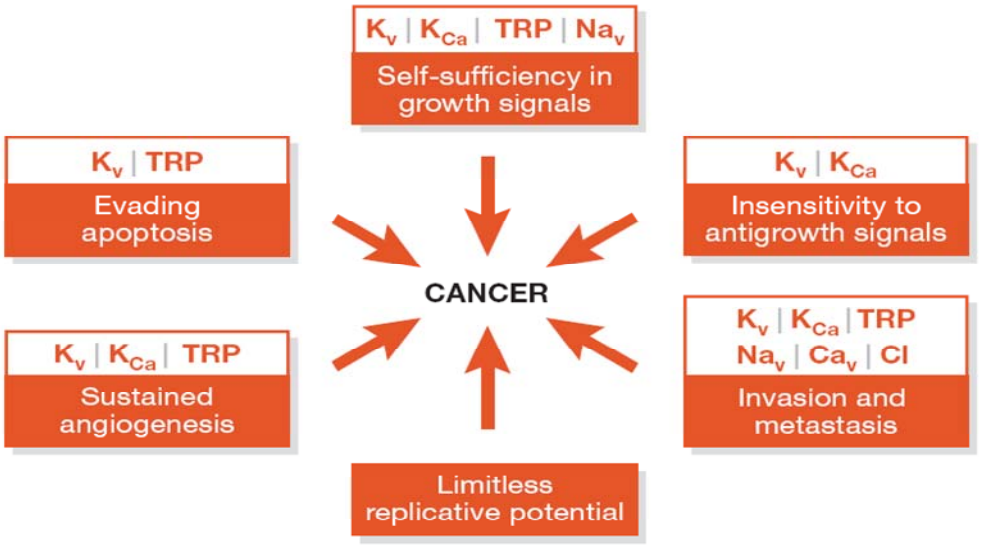

Figure 5. Different types of ion channels are involved in each of the six cancer hallmarks (Fraser and Pardo, 2008).

Specifically, tissue invasion and metastasis involve cell migration, which consists of common mechanisms both in physiological and pathological processes (Schwab, 2001; Friedl and Gilmour, 2009; Schwab et al., 2012). Migrating cells are polarized and move along a front-to-back axis. Migration engages a repeated cycle of protrusion of lamellipodia/invadipodia, cylindrical extroflections that provide the forward movement of the cell, and retraction of the rear part of the cell. The polarization of migrating cells also comprises the subcellular distribution of membrane proteins such as chemokine receptors and transport proteins as well as the composition of the plasma membrane itself (Schwab, 2001; Lefranc et al., 2005; Schwab et al., 2012). In particular, ion channels facilitate migration by conducting ions towards the extracellular milieu, leading to the osmotic movement of water. Thus, ion channels are able to efficiently regulate global cell volume or create local osmotic gradients facilitating the swelling or shrinking of cellular processes (Figure 6) (Cuddapah and Sontheimer, 2011).

As anticipated, cell migration is critical to cancer metastasis and malignant progression. In gliomas, cells move from the tumor central mass to adjacent parenchyma by migrating through the narrow extracellular space. This is facilitated by the overexpression of ion channels involved in cytoplasmic volume regulation, mainly K^+ channels and Cl^- channels that concomitantly release K^+ and Cl^- ions, leading to the osmotic release of water. This in turn leads to cytoplasmic volume decrease, allowing cells to squeeze through narrow extracellular spaces. It has been recently shown that invading glioma cells decrease their volume by 30 –35% (Cuddapah and Sontheimer, 2011; Watkins and Sontheimer, 2011). This percentage resembles the maximally achievable cellular volume decrease, suggesting that invading cells secrete all free, unbound cytoplasmic water to maximize their chance of crossing narrow barriers.

Moreover, exchangers like the Na^+/H^+ exchanger facilitate malignant cell invasion by acidifying the extracellular space to digest the extracellular matrix (Cuddapah and Sontheimer, 2011).

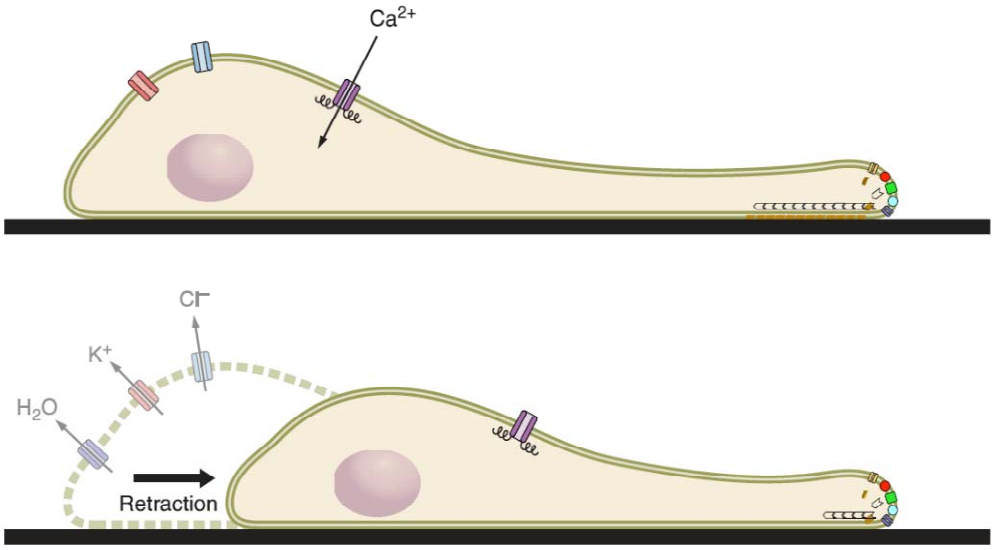

Figure 6. Cell volume rearrangements during cell migration. Cell migration consists of a continuous cycle of protrusion of the cell front (top) and retraction of the trailing end (bottom). This can be modeled as a localized volume increase at the cell front and volume decrease at the rear end, involving mainly K^+ and Cl^- conductances and aquaporins. The disassembly of focal adhesion components at the rear part of migrating cells involves the Ca^{2+} -sensitive family of calpain proteases (Schwab et al., 2012).

Glioblastoma cells maintain high intracellular Cl^- (80–100 mM), similar to immature neurons (Habela et al., 2009; Sontheimer, 2008). Thus, even at a relatively depolarized resting potential (~ -40 mV), opening of Cl^- channels causes Cl^- efflux. The high intracellular $[Cl^-]$ is accomplished by the activity of the $Na^+/K^+/Cl^-$ co-transporter, which is highly expressed in invadipodia of glioblastoma cells (Haas and Sontheimer, 2010).

The most relevant channels expressed in glioblastoma are:

- a splice variant of the Ca^{2+}- and voltage- activated K^+ (BK) channel named gBK; it contains a 34 amino acid insert near the Ca^{2+} sensor of the channel that increases Ca^{2+} sensitivity (Liu et al., 2002);

- acid-sensing Na^+ channels (ASIC) (Berdiev et al., 2003);

- ClC-2 and ClC-3 Cl^- channels; ClC-3 channels localize to the same specialized lipid domains on the invadipodia that also contain gBK channels (Sontheimer, 2008);

- the water channel aquaporin-4, also contained in the same lipid raft domains as gBK and ClC-3 (McCoy and Sontheimer, 2007).

The chloride intracellular channel 1 (CLIC1)

In the late ‘80, the first Chloride Intracellular Channel (CLIC) protein, p64 (now known as CLIC5b), was isolated from bovine tracheal apical epithelium and kidney cortex microsomal membrane fractions (Landry et al., 1993; Redhead et al., 1992).

The CLIC family possesses six known members (CLIC1-6) with differential tissue distribution and function both in the plasmamembrane and intracellular organelles. They share structural homology with members of the omega glutathione S-transferase (GST) superfamily (Singh, 2010; Littler et al., 2010; Averaimo et al., 2010; Edwards and Kahl, 2010). A unique feature of CLIC proteins is their ability to exist in two different forms: a soluble globular form and an integral membrane protein, suggested forming functional ion channels. However, the presence of a single putative transmembrane domain has led to doubt over their ability to function as ion channels (Duran et al., 2010; Jentsch et al., 2002).

CLIC1 was cloned in 1997 from a human monocytic cell line and localized in the cell nucleus and cytoplasmic organelles (Valenzuela et al., 1997). This protein adopts at least two stable tertiary structures, with redox status controlling the transition between them thus making CLIC1 a member of the rare category of ‘‘metamorphic proteins” (Murzin, 2008; Littler et al., 2010). In fact, it has been shown that the effect of oxidation on CLIC1 allows the protein to undergo a reversible transition between a reduced, soluble monomeric state and an oxidized, soluble dimeric state (Figure 7) (Littler et al., 2004). The non-covalent dimer interface comprises a flat, hydrophobic surface that could favor the protein insertion into a lipid bilayer. Thus, the half dimer structure may represent the membrane docking form of CLIC1 (Littler et al., 2004).

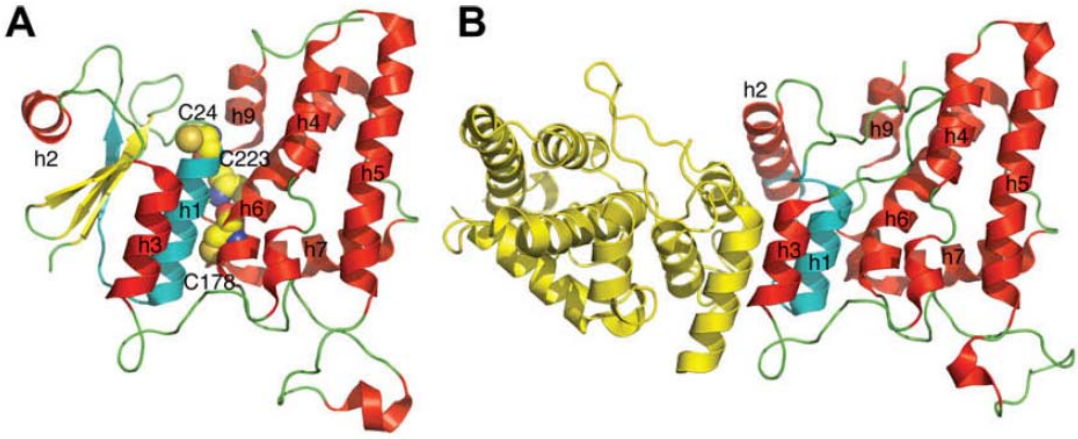

Figure 7. CLIC1 crystal structure. (A) The monomeric structure of CLIC1 in the soluble, reduced form (α-helices in red, β-strands in yellow, loops in green). The putative TM region is in cyan (residues 25–46). (B) The crystal structure of the oxidized CLIC1 dimer: the left subunit is colored yellow, while the right subunit is colored and oriented as the CLIC1 monomer in panel A. The four-stranded mixed β-sheets that are characteristic of the thioredoxin fold transformed into α-helices and loops (Littler et al., 2010).

However, a different study suggests that the dimerization process during oxidation is not necessary for the insertion of the protein into membranes (Goodchild et al., 2009). In this model, CLIC1 monomer interacts by itself with the membrane surface and successively the oxidation promotes the structural changes that allow the protein to cross the membrane.

The ion channel activity of CLIC1 has been characterized in both cells and artificial bilayers. The first evidence of a CLIC1-mediated current was shown in CLIC1 transfected CHO-K1 cells through cell and nuclear patch clamp (Tonini et al., 2000). By transfecting these cells with CLIC1 bearing either a N- or C-terminal FLAG epitope tag and using an antibody anti-FLAG, it was demonstrated that CLIC1 spans the plasma membrane an odd number of times with the C-terminus in the cytoplasm (Tonini et al., 2000). Further electrophysiological studies in CHO-K1 cells indicate that CLIC1 chloride current varies according to the stage of the cell cycle, being expressed only on the plasma membrane of cells in G2/M phase (Valenzuela et al., 2000). In addition, the purified CLIC1 protein has been functionally reconstituted in artificial bilayer by different laboratories (Warton et al., 2002; Singh et al., 2007; Tulk et al., 2002) to show that CLIC1 forms functional ion channels in the absence of ancillary protein. The main single channel conductance in 140 mM KCl symmetric solution is approximately 30 pS (Tulk et al., 2002; Warton et al., 2002). The only effective channel blocker so far identified is the Indanyloxyacetic acid 94 (IAA94), with an EC_{50} of 8.6 μM (Tulk et al., 2000). To further support the ion channel nature of CLIC1, it has been reported that a single point mutation (C24A) in CLIC1 putative transmembrane region results in alterations of the electrophysiological characteristics of the channel (Singh and Ashley, 2006).

CLIC1 is widely expressed in epithelial and non-epithelial cell types where it shows tissue- and cell-specific patterns of subcellular localization (Ulmasov et al., 2007). However, CLIC1 physiological function is not fully understood. Several studies address the question of CLIC1 function. The human gene is located within the major histocompatibility complex class III region, one of the most conserved and important regions in the genome. It has been recently generated a *Clic1* KO mouse that does not show any embryonic lethality but only a mild bleeding disorder and decreased platelet activation (Qiu et al., 2010). Different lines of evidence support the hypothesis of a fundamental role of CLIC1 protein in activated microglia. For example, CLIC1 expression increases by 60% in the hippocampus of mild/moderate Alzheimer patients (Parachikova et al., 2007). Moreover, in a mouse model of Alzheimer disease, CLIC1 is mainly localized in the plasma membrane of activated microglia (Figure 8) (Milton et al., 2008). The blockade of CLIC1 functional expression with specific inhibitors or its downregulation by small interference RNA impairs the production of reactive oxygen species, limiting the detrimental effects of microglia over activation (Milton et al., 2008; Novarino et al., 2004). In these conditions, neurodegeneration may be limited without affecting the phagocytic ability of microglia (Paradisi et al., 2008).

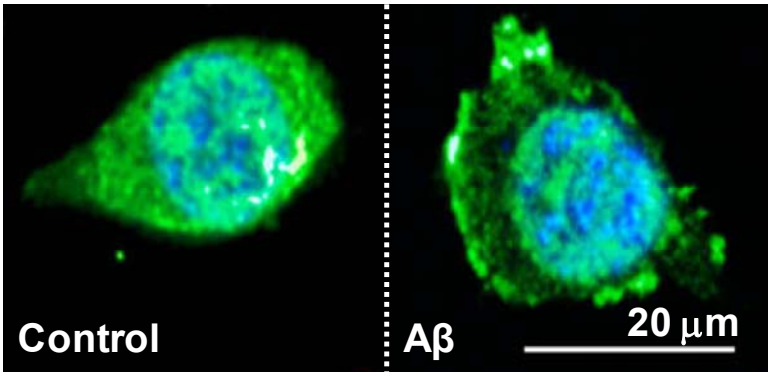

Figure 8. CLIC1 subcellular localization. Immunolocalization of CLIC1 (green, antibody directed against the N-terminus of the protein) in BV2 cells (nuclei are stained in blue, DAPI). Following b-Amyloid (Ab) stimulation, which induces oxidative stress, CLIC1 translocates into the plasma membrane (Milton et al., 2008).

CLIC1 in tumors

CLIC1 appears to have a main role in all the diseases that involve oxidative stress, including tumors (Averaimo et al., 2010). As reported above, CLIC1 is detected on the plasma membrane of cells in the G2/M phase of the cell cycle (Valenzuela et al., 2000). During this phase, the current density is approximately twice the one recorded in the G1/S phase. Moreover, CLIC1 blockade prolongs the average duration of the cell cycle. Since oxidative fluctuations drive the cells through the cell cycle phases (Menon and Goswami, 2007), it is not surprising that CLIC1 may be very active as an ion channel in cancer cells, which are cells in a highly proliferative state.

It has been shown that CLIC1 plays a role in a variety of human solid tumors such as human gastric carcinoma (Chen et al., 2007), colorectal cancer (Petrova et al., 2008), gallbladder carcinoma (Wang et al., 2009), hepatocarcinoma (Li et al., 2012) and glioma (Kang and Kang, 2008; Wang et al., 2012). In this latter case, data from Oncomine (oncomine.com) show that CLIC1 is overexpressed in brains from glioblastoma patients compared to patients with no tumor (Figure 9). Furthermore, it has been recently reported that CLIC1 expression at both mRNA and protein levels is increased in high-grade (Grade III~IV) glioma tissues compared with that in low-grade (Grade I~II) (Wang et al., 2012).

This thesis project focuses on the role of CLIC1 in human glioblastomas, and specifically in the subpopulation of cells that are most likely responsible for tumor infiltration and so far resistant to therapies: the cancer stem cells.

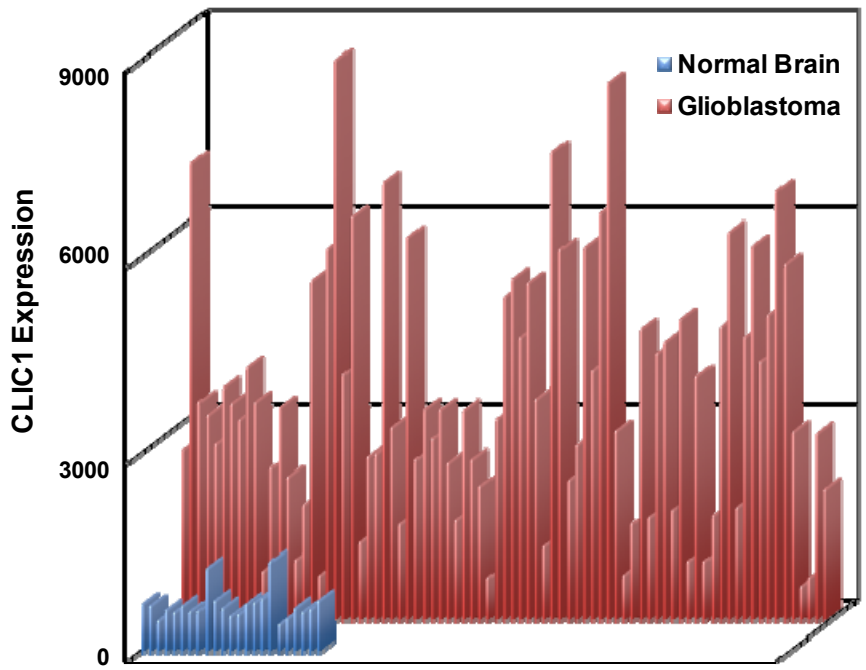

Figure 9. CLIC1 is overexpressed in glioblastomas. The figure shows the RNA expression profile on arrays for CLIC1 in a subset of 81 glioblastomas and 23 non-tumoral tissues.

1.B METHODS

Tumor sample preparation

Tumor specimens classified as GBM were collected from consenting patients at the Istituto Neurologico Carlo Besta, Department of Neurosurgery, Milan (Italy). Tissues were enzymatically processed with papain (2mg/ml) (Worthington Biochemical, Lakewood, NJ) at 37°C and mechanically dissociated until a single cell suspension was achievement (Figure 10).

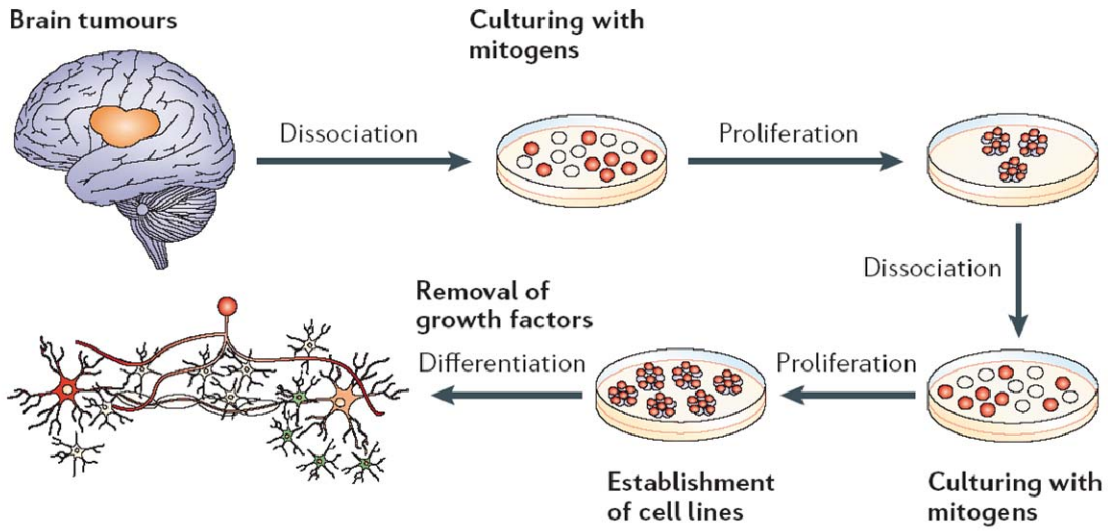

Figure 10. Human brain tumor biopsys were dissociated and cultured in a specific medium that allows only CSCs to grow (no serum, plus EGF and FGF) (Vescovi et al., 2006).

Cell culture

Cancer stem/progenitor cells were grown in suspension as spheroid aggregates (neurospheres), each deriving from a single cancer stem cell (Figure 11). The neurosphere assay is a defined serum-free culture system that allows the isolation and propagation of CNS-derived stem cells. Adult precursors from human GBM were dissociated and plated in NeuroCult medium (StemCell Technologies, Vancouver, BC, Canada) supplemented with 20 ng/ml epidermal growth factor (EGF), 10 ng/ml basic fibroblast growth factor (bFGF) (PeproTech, Rocky Hill, NJ), and 0.0002% heparin (Sigma-Aldrich, St. Louis, MO)(Ortensi et al., 2012). Because of the lack of serum and the low plating density (~100 cells/cm^2), differentiated cells die, while cells that divide in response to

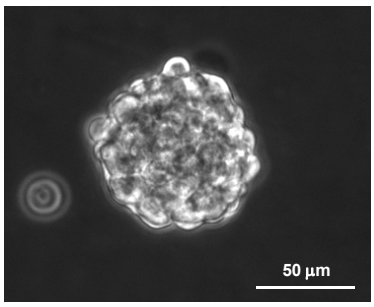

Figure 11. Neurospheres from glioblastoma CSCs are grown in suspension in a serum-free medium.

the stem-cell mitogens survive. The growth-factor-responsive cells proliferate to form floating clusters of cells that are referred to as neurospheres. These can be further mechanically dissociated into a single-cell suspension and then re-plated in fresh medium to produce secondary neurospheres every 5-10 days. The process can be repeated, resulting in a geometric expansion in the number of cells that are generated at each passage (Figure 10) (Vescovi et al., 2006).

Lentiviral infection

RNA interference (RNAi) was first recognized as a natural antiviral defense mechanism in plants wherein long double-stranded RNAs are cleaved into short 21–23 nucleotide double-stranded RNA molecules called small interfering RNAs (siRNAs) that mediate sequence-specific gene silencing. Experimentally, RNAi can be induced by the direct introduction of synthetic siRNA into the cells or by intracellular generation of siRNA from vector driven expression of the precursor small hairpin (sh) RNAs (Figure 12) (Manjunath et al., 2009). In the latter method, a double-stranded oligonucleotide containing the siRNA sequence linked by a ~9 nucleotide loop is cloned in plasmid or viral vectors to endogenously express shRNA which is subsequently

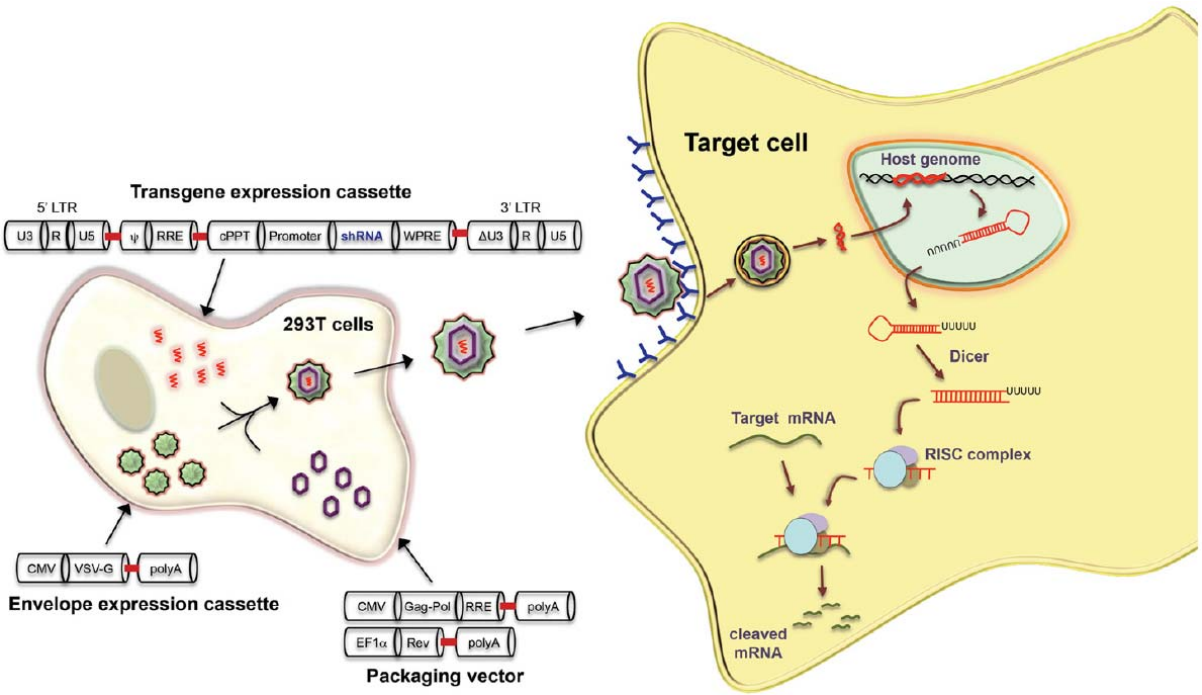

Figure 12. Scheme of non-replicating lentiviral vector for stable shRNA expression. Host cells (293T cells) are transfected with a mixture of plasmids: i) an shRNA expression cassette, ii) a packaging cassette and iii) a heterologous viral envelope expression cassette. The generated lentivirus is then used to transduce the desired cell type for shRNA expression. Because only the vector containing the shRNA expression cassette integrates into the host cell genome in the transduced cells, shRNA is continually expressed but infectious virus is not produced (Manjunath et al., 2009).

processed in the cytoplasm to siRNA. Lentiviruses may be particularly suited for long-term shRNA expression and gene silencing since the viral DNA gets incorporated in the host genome.

Short hairpins specific to human CLIC1 (5'-GATGATGAGGAGATCGAGCTC-3') and to firefly luciferase (5'-CGTACGCGGAATACTTCGA-3') mRNAs were cloned into the PLentiLox 3.7 lentiviral vector using the XhoI/HpaI sites. The PLentiLox 3.7 lentiviral vector also includes the puromycine gene to select infected cells and the Green Fluorescent Protein (GFP) gene to evaluate transduction efficiency. Lentiviral and packaging plasmids (vpMDLg/pRRE, pRSV-REV and pMD2G) were amplified in the E.Coli-strain Top10 and purified using a QUIAGEN MAXI KIT. HEK 293T cells were used to amplify the viral particles and they were grown in IMDM (Iscove's Modified Dulbecco's Medium, plus Glutamax, Invitrogen) with 10% FBS and 25 U/ml Penicillin/Streptomycin. HEK 293T cells were co-trasfected with all the plasmids using the calcium phosphate method according to established procedures (TronoLab). The viral particles were collected and concentrated using PEG-it. The transducing unit (TU) concentration was then determined by GFP expression. The viral suspension was used to infect dissociated CSCs from human GBM (104 TU/µl). 72 hours after infection, cells were positively selected with 1.5 mg/ml puromycine.

Western Blot

Western blot analysis uses denaturating gel electrophoresis to separate proteins by their size; the proteins are then transferred to a membrane (typically nitrocellulose or PVDF), where they are immunostained with specific antibodies. This technique was used to evaluate the interference efficiency 72 hours after selection with puromycine. Neurosphere samples were collected by centrifugation and pellets were lysated on ice in 50-100 µl of lysis buffer (50 mM Tris–Cl buffer, 10 mM $CaCl_2$, 5mM EGTA, 250 mM NaCl , 10% Glycerol, 1% triton-x 100, pH 8) containing a cocktail of proteinase inhibitors (50 mM NAF, 10 mM NAPP, 10mM NaOrtoV, 0.1mg/ml PMSF, Leupeptin , Apoprotinin). Concentration of protein lysates was assessed by Bradford assay (Biorad). Each lysate (10 µg) was loaded onto a SDS-polyacrylamide gel electrophoresis (PAGE) under reducing conditions, and resolved proteins were transferred onto Nitrocellulose membranes (Protran ®) of 0.2 µm pore size. Membranes were incubated overnight at 4°C with anti-CLIC1 mouse monoclonal antibody and anti-Vinculin diluted in Tris-Buffered Saline and Tween 20 (TBS-T [50mM Tris, 150mM NaCl, 0.05% Tween 20]) supplemented with 5% Milk Powder. Antibody binding was assessed by horseradish peroxidase (HRP)-conjugated secondary antibody (Sigma Aldrich, 1:10000 dilution). Immunoreactive bands were detected with enhanced chemiluminescence reagents (GE Healthcare Bio-Sciences).

Boyden chamber assay

The Boyden chamber is a useful tool to study cell migration. It consists of two chambers separated by a filter that was originally constructed by Boyden (BOYDEN, 1962) Cells are

placed into the upper chamber, while the chemotactic substance is added into the lower one. The size of the motile cells to be investigated determines the pore size of the filter (Figure 13).

To assess the migration efficiency of glioblastoma CSCs, 50,000-100,000 cells were seeded in the upper chamber in 100 µl of growth factor-free medium, while the lower chamber was filled with 600 µl of EGF-FGF supplemented medium as chemoattractants (Figure 13). After 48-72h transwells were removed and stained with crystal violet solution for 10 minutes and then thoroughly washed with water. Crystals were solubilized in 10% acetic acid solution and quantified by absorbance (λ=600 nm).

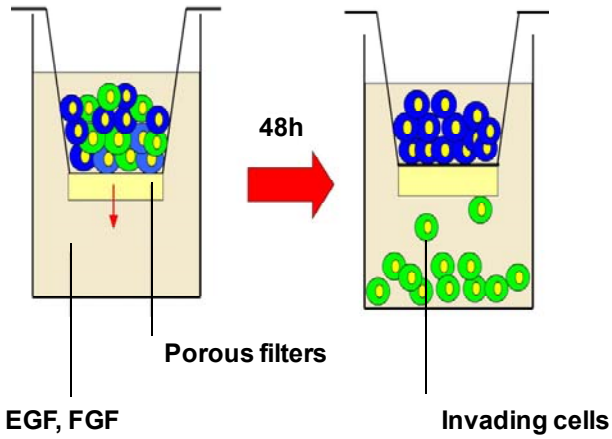

Figure 13. Schematic drawing of a Boyden Chamber. Cells are seed in the upper chamber, while in the bottom chamber there are the chemoattractants agents (EGF, FGF). After 48h, cell migration ability through the porous filter (8 µm diameter) into the lower chamber is assessed.

Patch clamp

The patch clamp technique allows to measure the ionic currents passing through ion channels (Neher and Sakmann, 1992; Neher and Sakmann, 1976; Sakmann and Neher, 1984). In this technique a small heat-polished glass pipette is pressed against the cell membrane where the ion channels are embedded and forms an electrical seal with a resistance of ~1-10 GΩ (Figure 14) (Hamill et al., 1981). The high resistance of the seal ensures that most of the currents originating in a small patch of membrane flow into the pipette, and from there into current-measurement circuitry. An electrode (a silver wire coated with AgCl), located inside the glass pipette and connected to the circuitry, converts the ionic current into electrical current. This configuration is defined as cell-

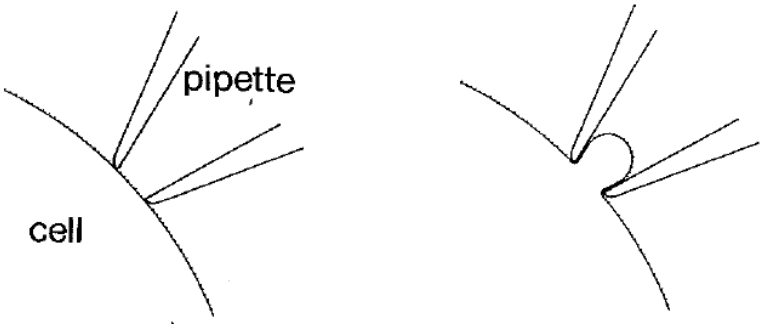

Figure 14. Schematic diagrams showing a pipette pressed against the cell membrane (left), and after formation of a gigaseal when a small patch of membrane is drawn into the pipette tip (right) (Hamill et al., 1981).

attached. Other possible configurations are (Hamill et al., 1981; Neher and Sakmann, 1992; Horn and Patlak, 1980):

- inside-out configuration, where the pipette is rapidly withdrawed from the cell-attached configuration without destroying the giga-seal, leaving a cell-free membrane and allowing current recordings in known intracellular solutions;

- whole-cell configuration, where after giga-seal formation the membrane patch is disrupted providing a direct low resistance access to the cell interior allowing for recordings from the ion channels in the whole cell membrane (Figure 15);

- outside-out configuration, where the pipette is gently withdrawed from the whole-cell configuration without destroying the giga-seal, leaving a cell-free membrane patch exposing in the bath solution the outer leaflet of the lipid bilayer;

- perforated patch, where the pipette contains specific antibiotics (such as gramicidin, anphotericin B or nystatin) that, once inserted in the plasmamembrane, provide electrical access to the cell interior preserving the cytoplasm content (Figure 15).

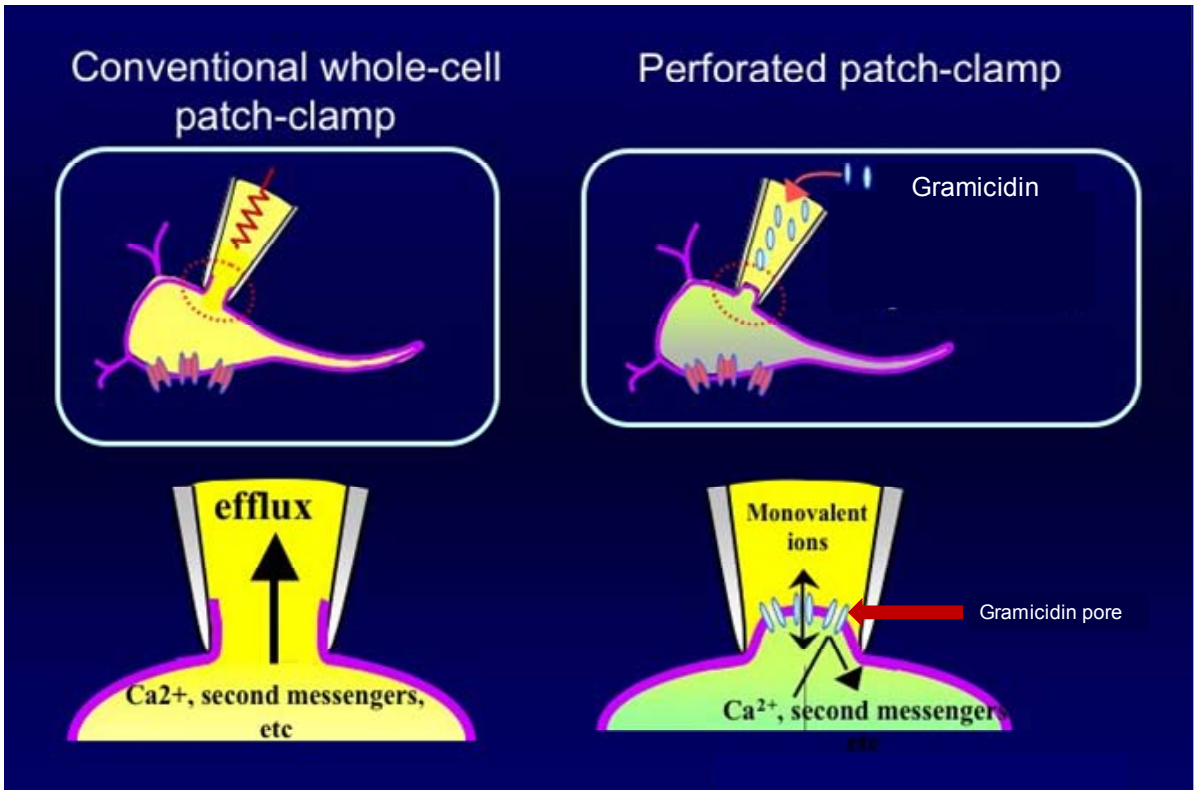

Figure 15. Comparing the conventional whole cell patch-clamp configuration (left) and the perforated patch technique (right), it is evident that the advantage of the latter is to preserve the intracellular milieu. In perforated patch, the electrical access to the cell is achieved taking advantage of the pore forming ability of certain antibiotics (such as gramicidin).

Detailed protocol for the patch clamp experiments reported in this thesis: Cancer stem cells from human glioblastomas primary cultures (h70.01.42, hGBMR1, h60.90.12 and h60.50.51) were voltage-clamped using an Axopatch 200 B amplifier (Molecular Devices) in the perforated patch configuration. Ionic currents were digitized at 5 kHz and filtered at 1 kHz. The bath solution (mM) contained: 130 NMDG-Cl, 2 $MgCl_2$, 2 $CaCl_2$, 10 HEPES, 10 Glucose, 5 TEA-Cl (pH=7.4). The pipette solution was (mM): 145 KCl, 1 $MgCl_2$, 10 HEPES (pH=7.25); prior experiments, 2.5 µg/ml Gramicidin (Sigma) was added to the solution. Gramicidin is an antibiotics capable to insert into plasma membranes and form pores permeable only to monovalent cations, allowing to gain electrical access to the cell as well as preserve the $[Cl^-]_i$ and the cytoplasm content. The voltage protocol consisted of 800 ms pulses from -80 mV to +80 mV (20 mV voltage steps); the holding potential was set according to the resting potential of the cell (between -40 and -80 mV). CLIC1-mediated Cl^- currents were isolated from the other ionic currents in the cells by perfusing a specific inhibitor (Indanyloxyacetic acid 94, IAA94 100 µM) dissolved in the bath solution using a Rapid Solution Changer (RSC-200, BioLogic). Other Cl^- currents were isolated using the aspecific inhibitor DIDS 200 µM (Disodium 4,4′-diisothiocyanatostilbene-2,2′-disulfonate).

Analysis: Offline analysis was performed using Clampfit 9.0 (Molecular Devices), OriginPro 8.5 and Excel routines. IAA94-sensitive (I_{IAA94}) and DIDS-sensitive (I_{DIDS}) currents were estimated by analytical subtraction of ionic currents after addition of either inhibitor from the total current (I_{TOT}) of the cell at each membrane potential tested. Current/Voltage relationships (or I/V curves) were constructed by plotting the averaged ionic current data points in the last 100 ms of the pulse against the corresponding membrane potential. IAA94-sensitive and DIDS-sensitive currents were normalized to the total ionic current of the cell (I_{IAA94}/I_{TOT} and I_{IAA94}/I_{TOT}, respectively); I_{IAA94}/I_{TOT}% and I_{IAA94}/I_{TOT}% from the same cell types were averaged and plotted against the membrane potential. Error bars are the standard error of the mean in all plots.

1.C RESULTS

This study aimed to investigate the role of CLIC1 protein in cancer stem cells (CSCs) from human glioblastoma to ultimately understand new mechanistic information about tumor invasiveness. In particular, our attention was focused on CLIC1 fraction in the plasmamembrane in that it would eventually result in a more accessible therapeutic target.

Knock-down of CLIC1 expression in human glioblastoma CSCs

The early stages of this project have been developed in Dr Pelicci laboratory, our collaborator at the European Institute of Oncology. They established primary cultures of CSCs from four different human glioblastomas (h70.01.42, hGBMR1, h60.90.12 and h60.50.51). In the appropriate medium, CSCs grow as neurospheres in suspension and they can be propagated in culture by mechanical dissociation, following the method implemented by Vescovi and colleagues (Vescovi et al., 2006).

CLIC1 expression was explored in these four glioblastomas. Western blot analysis was performed on neuropsheres lysates, showing that all the tumors expressed CLIC1 (Figure 16).

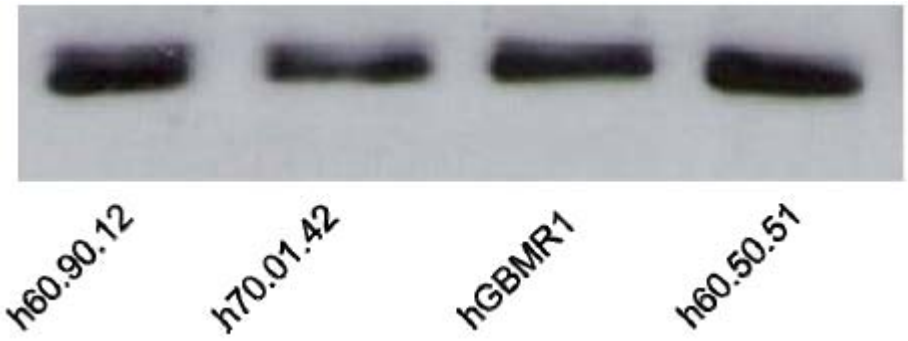

Figure 16. CLIC1 expression in four human glioblastomas. Neurospheres from the four different tumors were lysed and assessed for CLIC1 expression by western blot analysis. CLIC1 band is detectable in al the tumors analyzed.

In order to study CLIC1 role in CSCs from glioblastoma, the strategy applied was to knock-down its expression level taking advantage of the RNA interference (RNAi) technique. A lentiviral vectors carrying the shRNA (short hairpin RNA) against human CLIC1 (siCLIC1) or against the firefly luciferase (siLuc) were engineered and transduced into CSCs from h70.01.42 and hGBMR1 tumors. To verify the extent of CLIC1 silencing in the different glioblastomas, a western blot was performed on both the infected cells and the control cells (no infection). By probing the membrane with antibodies anti-CLIC1 and anti-Vinculin, we found that CLIC1 protein expression was reduced in both tumors (Figure 17A). Densitometry analysis revealed

that the efficiency of CLIC1 silencing was 60% in h70.01.42 cells and 50% in hGBMR1 cells (Figure 17B).

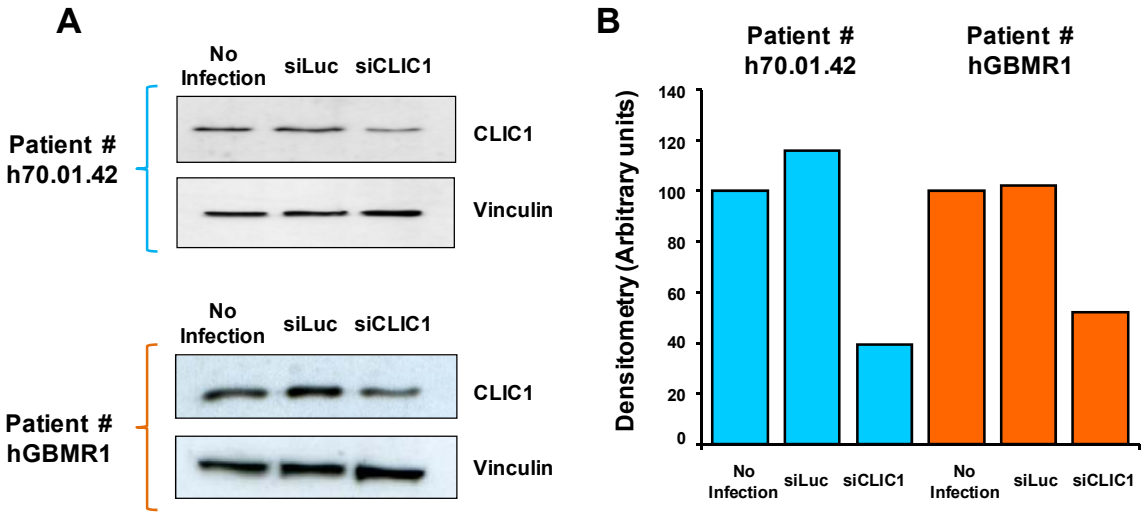

Figure 17. Efficiency of CLIC1 silencing in CSC from human glioblastomas. (A) Western blot analysis was performed on whole lysates from siLUC, siCLIC1 and not-infected cells and probed with anti-CLIC1 and anti-Vinculin antibodies. (B) Histograms show the normalization of CLIC1 signal to Vinculin signal: the reduction of CLIC1 protein in siCLIC1 cells is about 50% in both patients compared to siLUC and not-infected cells.

CLIC1 silencing decreases migration ability of glioblastoma CSCs

Since glioblastomas are highly invasive tumors, we asked whether the silencing of CLIC1 –a Cl^- channel- could impact on the ability of CSCs to migrate.

The migration assay was performed using the Boyden chambers, two chambers separated by a porous filter (8 µm pore diameter). 100,000 siCLIC1 or siLUC CSCs were seeded in the top chamber in a growth-factor-free medium. Chemoattractants factors (FGF, EGF) were added in the bottom chamber to stimulate CSCs to migrate through the filter pores. After 48h the cells that reached the bottom chamber were fixed and stained with Crystal violet. The quantification was achieved by measuring the absorbance (A) at λ = 600 nm with a spectrophotometer (Figure 18). In the h70.01.42 tumor, we found that in the siLUC cells A was 0.49 + 0.08 (n = 3), while in the siCLIC1 cells A was reduced to 0.29 + 0.08 (n = 3). Similar results were obtained for the hGBMR1 tumor: in the siLUC cells A was 0.99 + 0.34 (n = 4) and in the siCLIC1 cells A decreased to 0.50 + 0.29 (n = 4). The student's t-test showed that the reduced migration ability of the cells partially lacking CLIC1 was significant ($p < 0.05$).

Taken together, these data show that the migration efficiency of CSCs from two different human glioblastomas was reduced when CLIC1 was silenced.

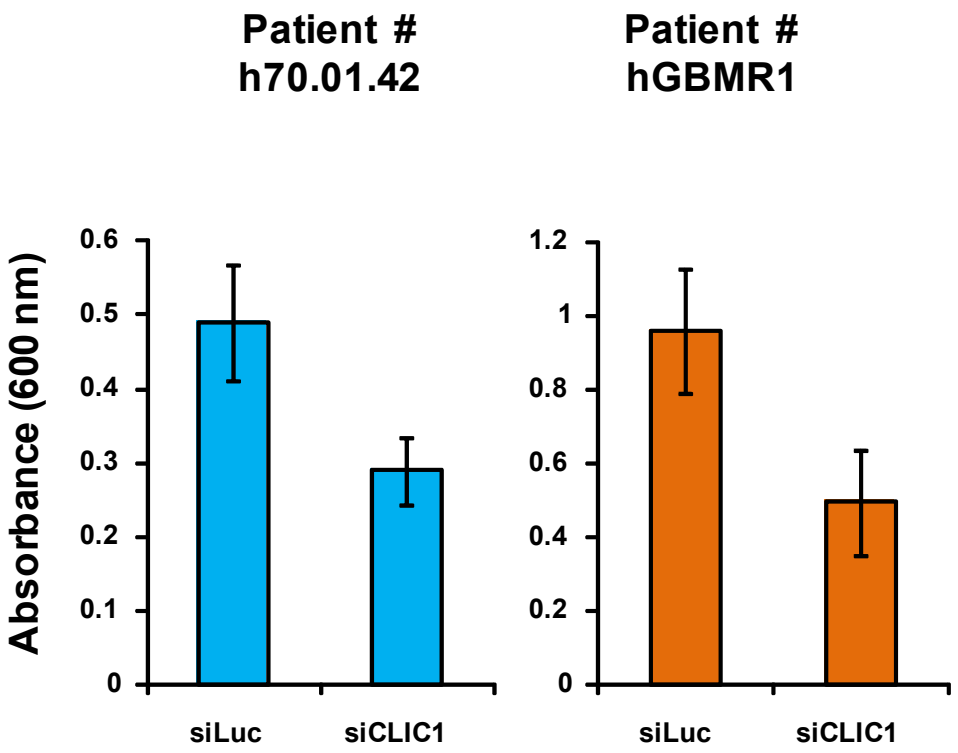

Figure 18. CLIC1 silencing decreases migration ability of glioblastoma CSCs. The histograms represent the average absorbance (λ= 600 nm) for h70.01.42 (n=3) or hGBMR1 (n=4) siCLIC1 and siLUC cells following Boyden chamber assay.

siRNA against CLIC1 abolishes CLIC1-mediated currents in glioblastoma CSCs

As we stated above, CLIC1 possesses at least two stable conformations: one in the cytoplasm and one in the lipid bilayer. We asked whether CLIC1 as an ion channel was responsible for the decreased migration efficiency of CSCs or its soluble counterpart.

To address this question, we took advantage of the patch clamp, a very powerful technique to measure ionic conductances in cells. Specifically, we used the perforated patch clamp technique, which differs from the classical whole-cell configuration in that after gigaseal formation there is no suction to rupture the patch membrane. Instead, the electrode solution contains antibiotics that, by inserting into the membrane, provide electrical access to the cell interior. In the experiments presented here, we used gramicidin, which forms pores permeable only to monovalent cations. This has the advantage of reducing the dialysis of the cell: in particular the intracellular [Cl^-] and the soluble CLIC1 are preserved inside the cell.

In a typical experiment, after gigaseal formation, it took 10-20 minute for the gramicidin to insert into the plasmamembrane; this was ascertained by monitoring the capacitive current increase and the resting potential stabilization. The resting potential could vary between -30 mV and -80 mV and the holding potential of each experiment was set according to the resting potential of that specific cell. Once the gramicidin is inserted in the membrane, bath solution, 100 μM IAA94 (CLIC1 inhibitors) and 100 μM IAA94 + 200 μM DIDS (Cl^- channels inhibitor that does not affect CLIC1 current) were sequentially perfused on the cell and ionic currents were recorded at different imposed membrane potentials. By analytical subtraction IAA94- and DIDS-sensitive currents were isolated from the total current of the cell (I_{tot}). Since the absolute values of these currents were different from cell to cell, they were normalized to I_{tot} obtaining the percentage of IAA94-sensitve current (% I_{IAA94}) and DIDS-sensitive current (% I_{DIDS}) (also see methods for more details).

In Figure 19, perforated patch experiments are shown for cells from the patient h70.01.42: not infected cells and siLuc or siCLIC1 cells. The IAA94-sensitve current was detectable in both not infected and siLuc cells, while it was absent in the siCLIC1 cells (Figure 19A). The Current/Voltage relationships clearly show the lack of IAA94-sensitive current in siCLIC1 cells (Figure 19B). For example, at 20 mV % I_{IAA94} was 24.55% + 6.6% (n = 6), 16.72% + 3.21% (n = 8) and -0.76% + 2.04% (n = 7) in not infected, siLuc and siCLIC1 cells respectively. These results strongly suggest that CLIC1 silencing affects the proteins in the plasmamembrane. On the other hand, DIDS-sensitive currents were recorded from all the groups of cells: at +20 mV % I_{DIDS} was 38.67% + 9.93% (n = 6) in not infected cells, 35.33% + 5.44% (n = 8) in siLUC cells and 37.43% + 6.20% (n = 4) in siCLIC1 cells (Figure 21).

The experimental observations from cells of the hGBMR1 tumor provided qualitatively similar results to data from h70.01.42 cells (Figure 20). In siCLIC1 cells, IAA94-sensitve current was abolished by silencing CLIC1 protein, unlike DIDS-sensitive current that were recorded from all cell groups. For example, at 20 mV % I_{IAA94} was 21.75% + 3.91% (n = 5), 28.05% + 3.97% (n = 7) and 2.38% + 0.91% (n = 5) in not infected, siLuc and siCLIC1 cells respectively; while I_{DIDS} was 23.88% + 4.63% (n = 5) in not infected cells, 21.09% + 5.65% (n = 4) in siLUC cells and 28.45% + 13.05% (n = 3) in siCLIC1 cells (Figure 21).

Averaging all the experiments performed at each membrane potential, we found that, in both tumors, siCLIC cells displayed a complete abolishment of the CLIC1-mediated current, while the DIDS-sensitive current were unaltered, underlying the specificity of siRNA effect (Figure 21).

Overall, the results from h70.01.42 and hGBMR1 cells support the view that CLIC1 silencing affects both CLIC1 expression and ion channel activity, revealed as the lack of IAA94-sensitive current in CLIC1 silenced cells.

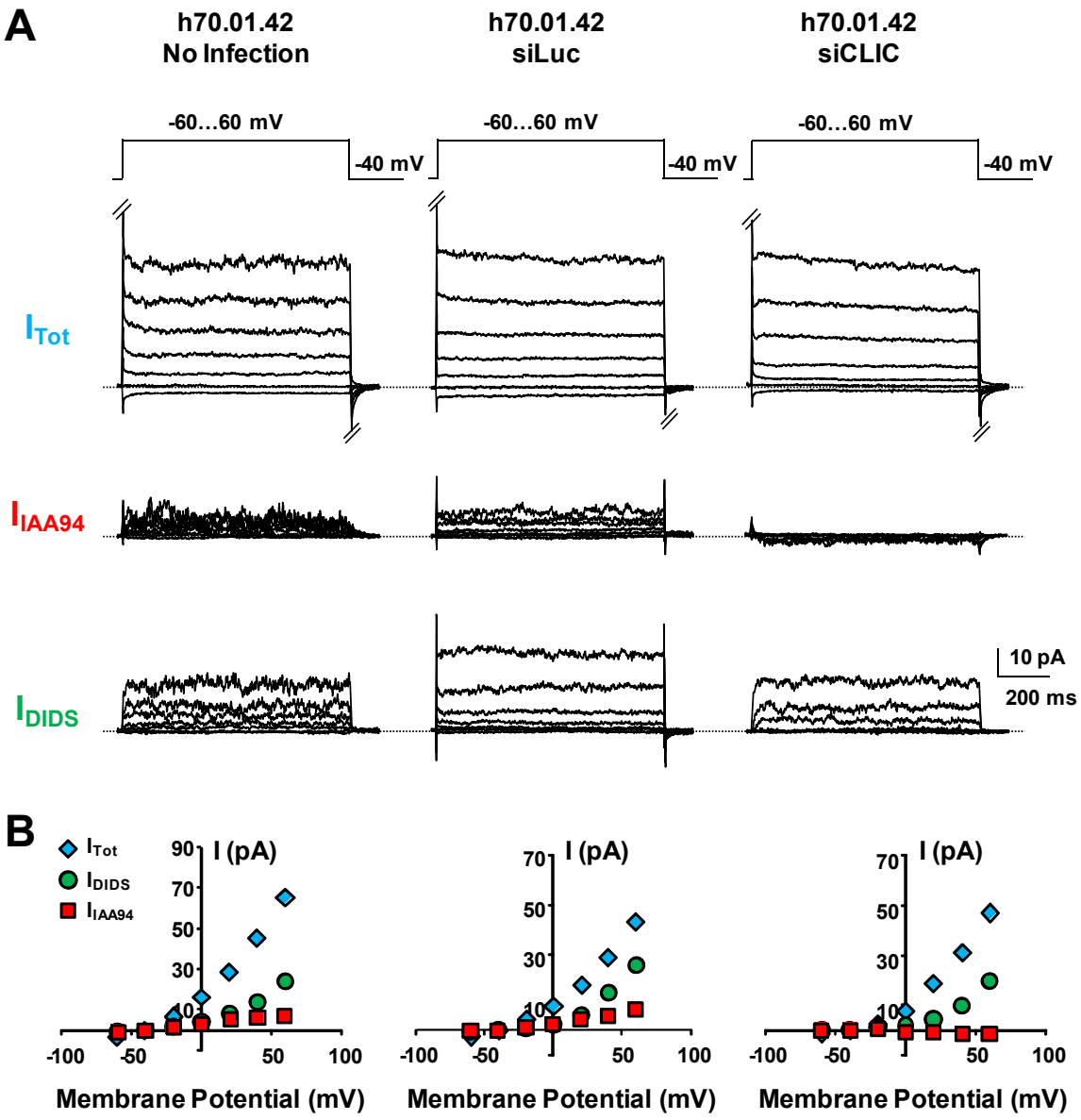

Figure 19. siRNA abolishes CLIC1 currents in h70.01.42 CSCs. (A) Rapresentative ionic current traces from perforated patches of CSCs from h70.01.42 tumors (not infected, siLuc and siCLIC1 cells). The voltage protocol is shown above the traces. By analytical subtraction of the ionic current after 100 μM IAA94 addition from the total current of the cell, we obtained the IAA94-sensitive current (I_{IAA94}); the DIDS-sensitive current (I_{DIDS}) is calculated by subtracting the current after 200 μM DIDS addition from the current after IAA94 effect. (B) shows I/V relationships for the corresponding experiments in A. Note that siCLIC cells display a complete abolishment of the CLIC1-mediated current, while the DIDS-sensitive current is unaltered.

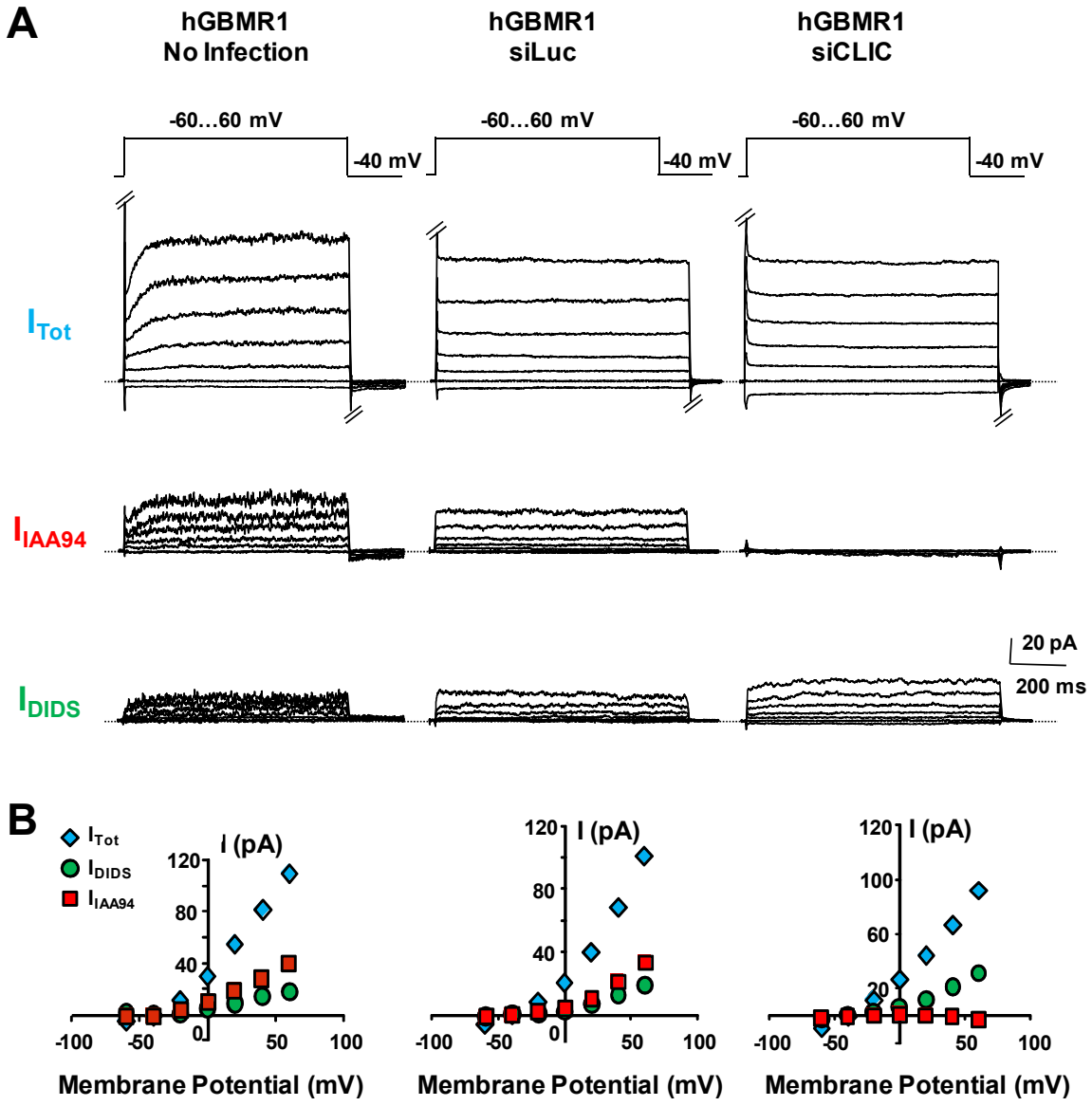

Figure 20. siRNA abolishes CLIC1 currents in hGBMR1 CSCs. (A) Rapresentative ionic current traces from perforated patches of CSCs from h70.01.42 tumors (not infected, siLuc and siCLIC1 cells). The voltage protocol is shown above the traces. By analytical subtraction of the ionic current after 100 μM IAA94 addition from the total current of the cell, we obtained the IAA94-sensitive current (I_{IAA94}); the DIDS-sensitive current (I_{DIDS}) is calculated by subtracting the current after 200 μM DIDS addition from the current after IAA94 effect. (B) shows I/V relationships for the corresponding experiments in A. As for 70.01.42 CSCs, siCLIC cells display a complete abolishment of the CLIC1-mediated current, while the DIDS-sensitive current is unaltered.

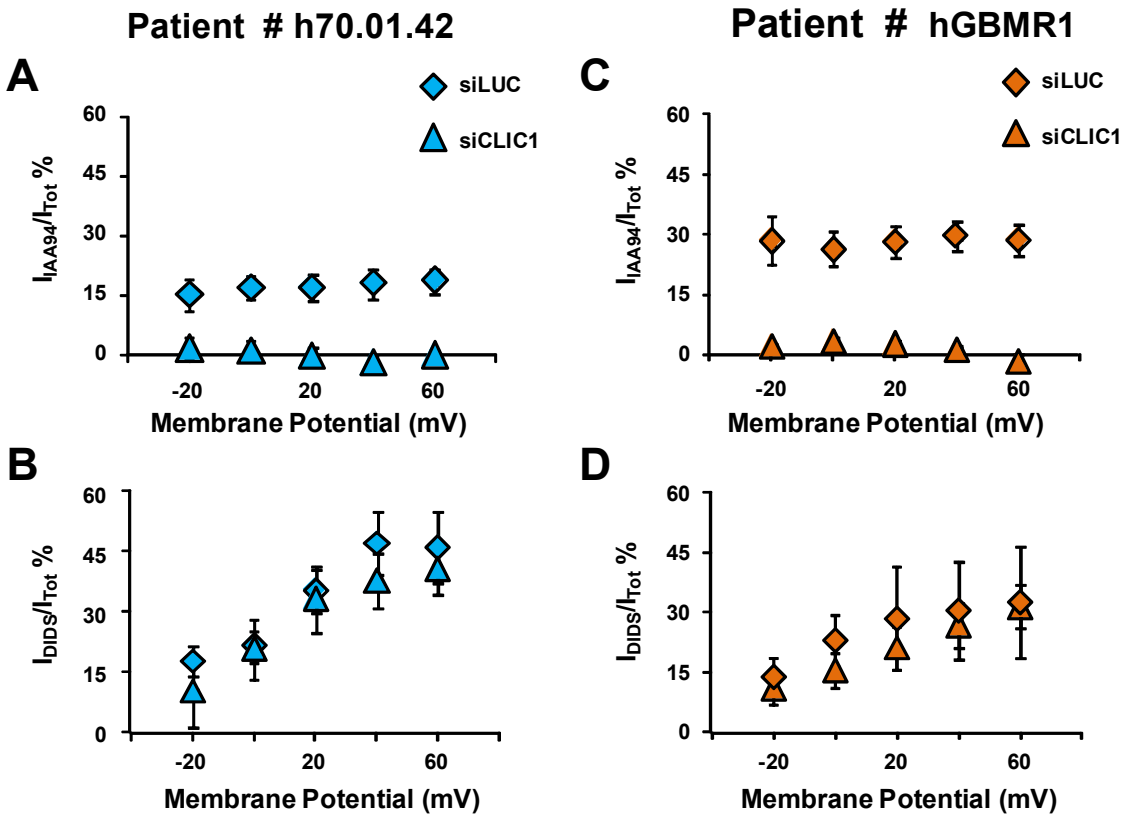

Figure 21. CLIC1 Silencing Reduces the Protein Plasma Membrane Fraction in Glioblastoma CSCs. These plots report the averages of the ratio of IAA94-sensitive currents (A, C) and DIDS-sensitive currents (B, D) over the total current of the same cell, for experiments performed in h70.01.42 (A, B) and hGBMR1 (C, D) glioblastomas CSCs.

Positive correlation between the relative abundance of CLIC1-mediated current and glioblastoma aggressiveness

In order to estimate how CLIC1-mediated current was represented compared to the other Cl^- currents in h70.01.42 and hGBMR1 cells, we calculated the I_{IAA94}/I_{DIDS} ratio, defined as the relative abundance of CLIC1-mediated current.

As shown in Figure 22, not infected and siLuc cells displayed a very similar I_{IAA94}/I_{DIDS} pattern at all membrane potentials explored, indicating that the lentiviral infection by itself did not affect ion channels function. On the other hand, in siCLIC1 cells the I_{IAA94}/I_{DIDS} ratio was close to zero in both tumors. For example at 0 mV, in not infected cells from h70.01.42 tumor we found that the I_{IAA94}/I_{DIDS} ratio was 0.65 + 0.16 (n = 9), in siLuc cells 0.52 + 0.15 (n = 10) and in siCLIC1 cells -0.05 + 0.04 (n = 7) (Figure 22A). For hGBMR1 tumor, at 0 mV the I_{IAA94}/I_{DIDS} ratio was: not infected cells 1.10 + 0.41 (n = 5), siLUC cells 1.20 + 0.18 (n = 7) and siCLIC1 cells 0.07 + 0.03 (n = 5) (Figure 22B). Interestingly, in not infected hGBMR1 cells the relative abundance of CLIC1-mediated current was about two fold bigger than in not infected h70.01.42 cells at

membrane potentials comprised between -20 mV and +40 mV. Considering that the hGBMR1 tumor is more aggressive than the h70.01.42 tumor, we asked whether the positive correlation between I_{IAA94}/I_{DIDS} ratio and tumor aggressiveness was a random coincidence or a real trend (where the aggressiveness is the time needed for CSCs inoculated in nude mice to generate a lethal tumor).

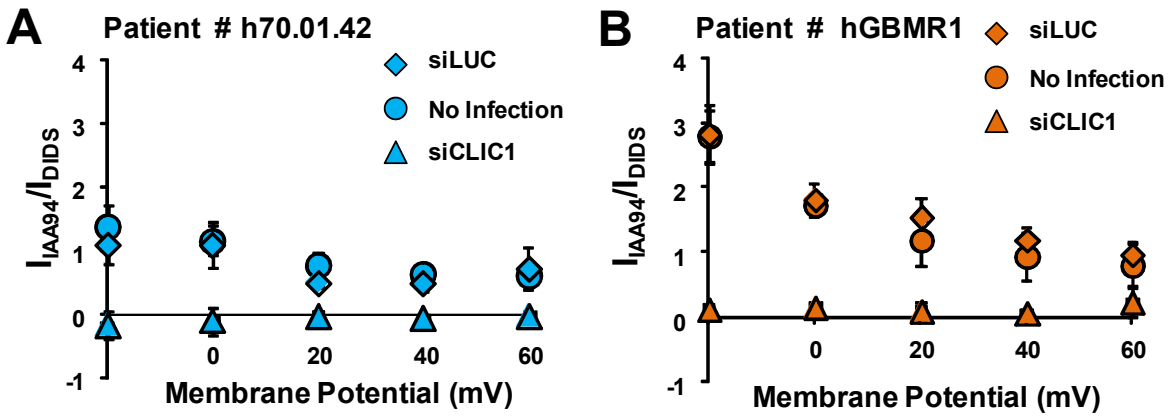

Figure 22. The relative abundance of CLIC1-mediated current compared to the other Cl^- conductances in CSCs. (A, B) The ratio of IAA94-senstive current over DIDS-sensitive current is defined as the relative abundance of CLIC1-mediated current and is reported against membrane potential, for h70.01.42 (A) and hGBMR1 (B) glioblastomas CSCs.

To address this question, we included in our study other two human glioblastomas: h60.50.51 and h60.90.12 (Figure 23). Perforated patch experiments on not infected CSCs revealed that also in these two tumors CLIC1-mediated current was constitutively present. For example at 20 mV, the IAA94-sensitive current was 12.89% + 2.66% (n = 6) in the h60.90.12 cells and 22.09% + 2.68% (n = 12) in the h60.50.51 cells. Thus, it appears that, in this last tumor, the average percentage of CLIC1-mediate current is more relevant than in the h60.90.12 CSCs.

In Figure 24, it is shown a cumulative plot summarizing all the data collected from not infected CSCs in four different human glioblastomas. We found that the relative abundance of CLIC1-mediated current positively correlated with tumor aggresiveness, meaning that the longer the latency of tumor formation in nude mice the least aggressive the glioblastoma. For example, at 0 mV membrane potential the ratio I_{IAA94}/I_{DIDS} was 0.5 + 0.12 (n = 6) in h60.90.12 cells, 1.18 + 0.23 (n = 9) in h70.01.42 cells, 1.74+ 0.1 (n = 6) in hGBMR1 cells and 2.32 + 0.42 (n = 12) in h60.50.51 cells. In the tumors analyzed in this study, the average survival of nude mice inoculated with CSCs was: 152 ± 2 days for tumor h60.90.12, 128 ± 2 days for tumor h70.01.42, 55 ± 4 days for tumor hGBMR1 and 88 + 4 days for tumor h60.50.51. Thus, in CSCs from the glioblastoma hGBMR1 CLIC1-mediated current is more represented than the other Cl^- currents in the cells compared to the other tumors.

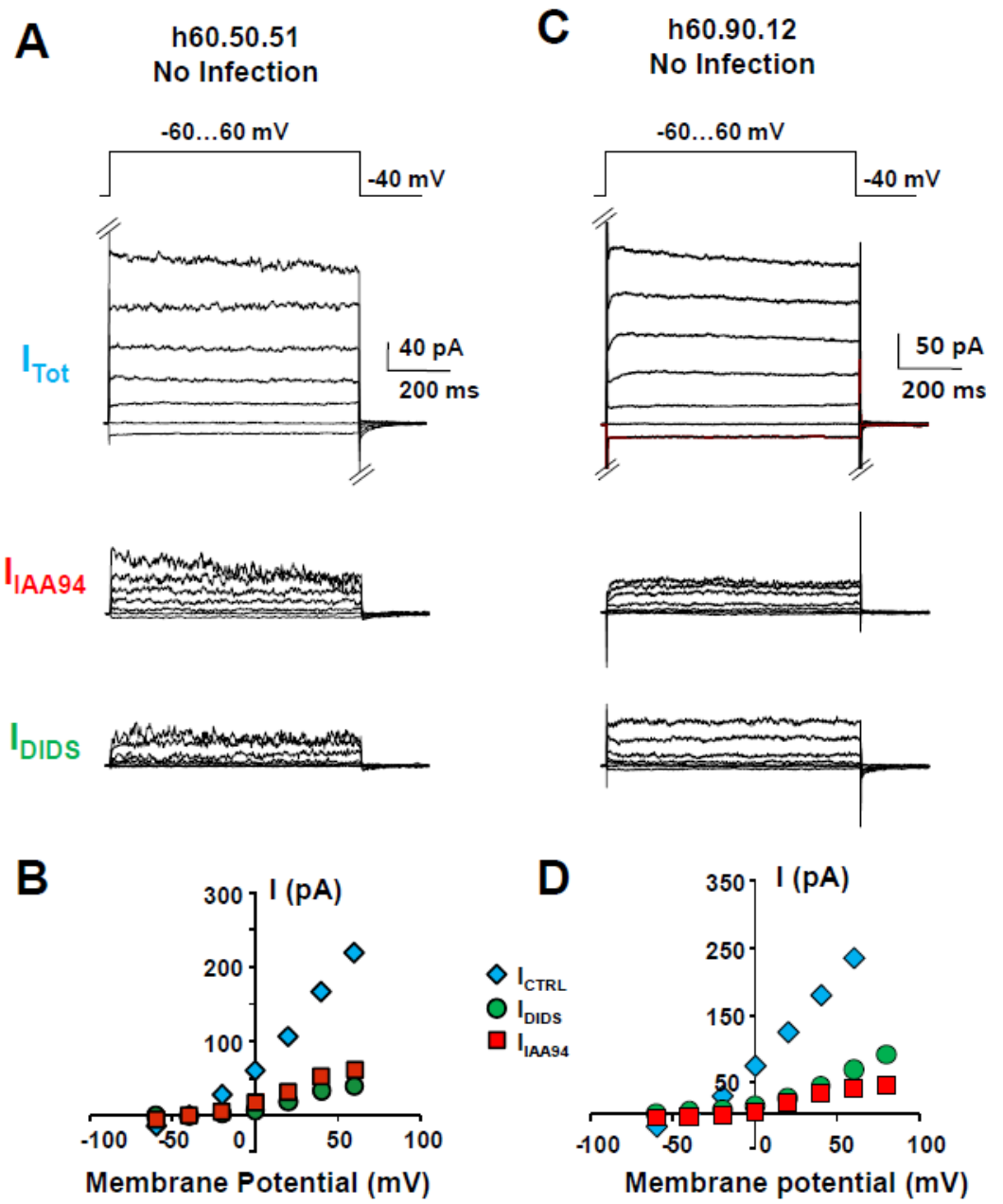

Figure 23. CLIC1 currents in h60.50.51 and h60.90.12 CSCs. (A, C) Rapresentative ionic current traces from perforated patches of CSCs from h60.50.51 (A) or h60.90.12 (C) tumors (not infected). The voltage protocol is shown above the traces. By analytical subtraction of the ionic current after 100 μM IAA94 addition from the total current of the cell, we obtained the IAA94-sensitive current (I_{IAA94}); the DIDS-sensitive current (I_{DIDS}) is calculated by subtracting the current after 200 μM DIDS addition from the current after IAA94 effect. (B, D) show I/V relationships for the corresponding experiments in A and C, respectively.

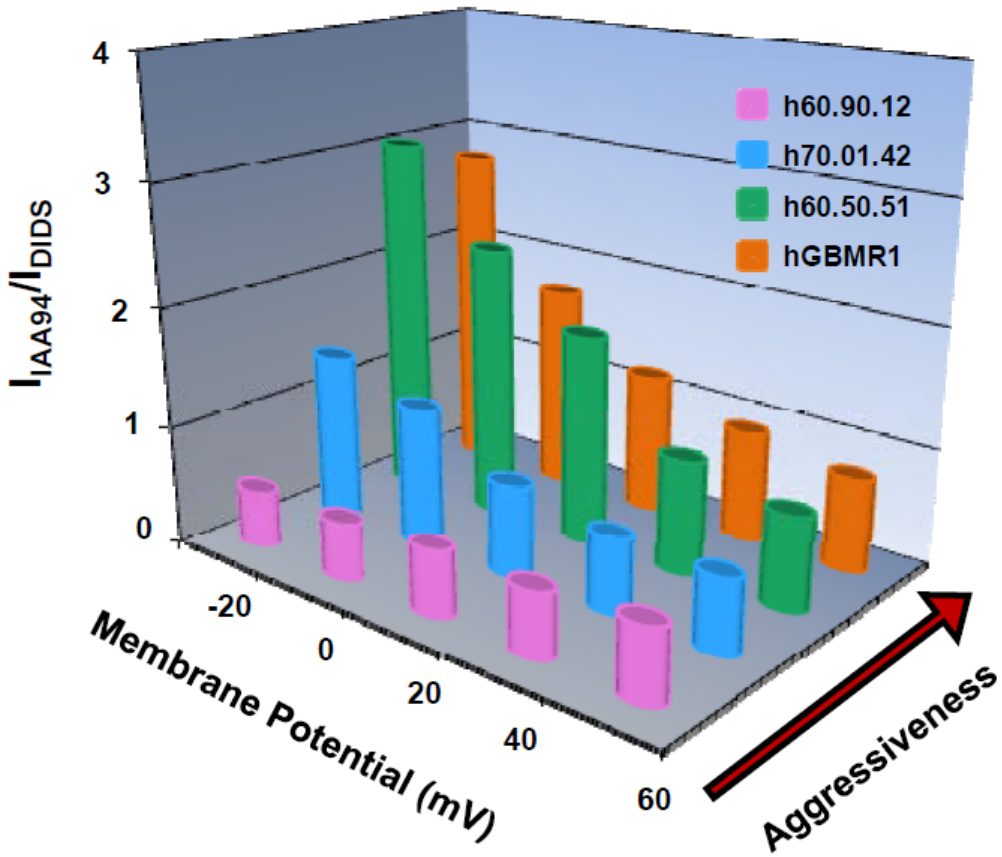

Figure 24. Positive correlation between CLIC1 relative abundance and glioblastoma aggressiveness. This 3D plot correlates the relative abundance of CLIC1-mediated current (I_{IAA94}/I_{DIDS}), the membrane potential and the tumor aggressiveness (defined as the latency of tumor formation occurring after inoculation of CSCs in nude mice) for four different human glioblastomas.

1.D DISCUSSION

Glioblastoma remains one of the deadliest forms of cancer, in that infiltrating cancer cells in the surrounding brain prevents complete tumor removal upon surgery or radiation. Furthermore, the existence of cancer stem cells (CSCs) may explain the resistance of these tumors to conventional chemotherapies (Nduom et al., 2012). Indeed, CSCs are predicted to be difficult targets for therapeutics because (1) they cycle slowly, (2) express high levels of drug export proteins, and (3) they may not depend upon the oncoproteins targeted by the new generation of drugs. These observations would suggest that a new class of agents should be designed to specifically target CSCs (Figure 25) (Stiles and Rowitch, 2008). Thus, fundamental questions about the mechanisms of CSC tissue invasion need to be addressed. In fact, preventing tumor invasion would lead to more successful surgeries or radiation therapies. This thesis project explores the possibility that CLIC1 protein represents an important player in glioblastoma infiltration.

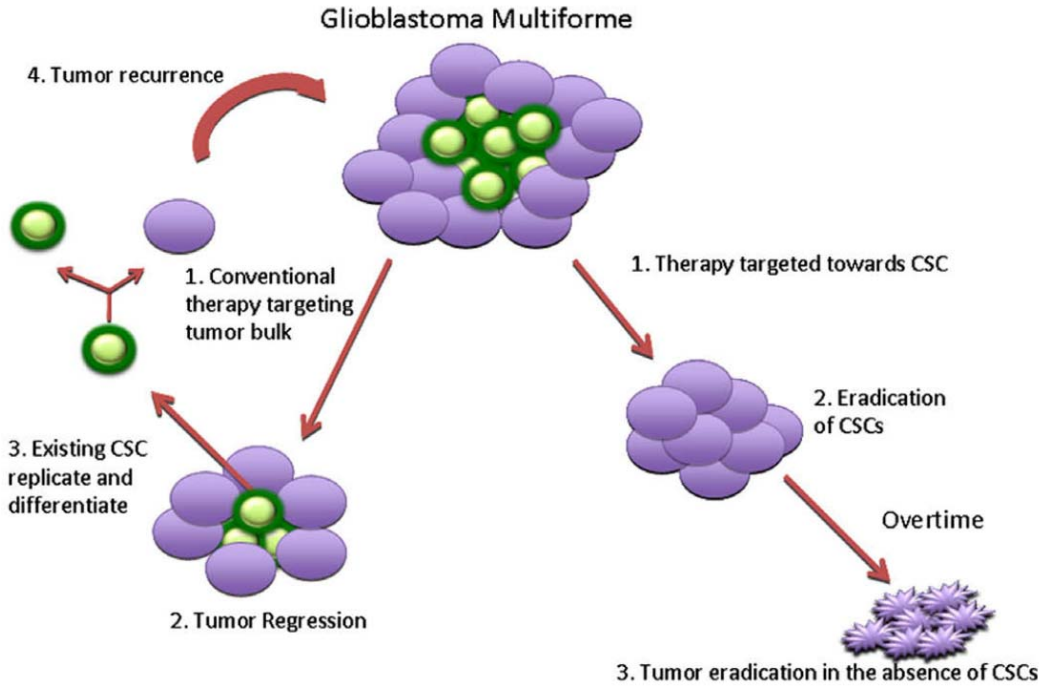

Figure 25. Conventional therapies targeting glioblastoma tumor bulk cells (violet circles) lead to tumor regression, however, the presence of CSCs (green circles) in the residual tumor allows for tumor recurrence. To eradicate the tumor, new therapies should be targeted against CSCs (Dey et al., 2010).

CLIC1 appears to have a main role in diseases that involve oxidative stress, including tumors (Averaimo et al., 2010). Damage to living tissues is often initiated and propagated by oxidative stress. Since cancer is deeply related to inflammation and tissue repair (Mantovani, 2009),

CSCs are recruited and activated like in a healing wound: they migrate out of their niches and begin to make new tissue. Oxidative stress is not only the drive that recruits CSCs, but also what regulates their migration. For this task, the cytoplasmic local redox potential coordinates membrane protrusion at the cell front (Rac-dependent) and contraction at the trailing edge (Rho-dependent) during cell migration (Figure 26) (Pani et al., 2010). CLIC1 appears to properly fit in this context, as it is a protein modulated by the oxidative status of the cell: upon oxidation, the cytoplasmic form of CLIC1 undergoes an extensive conformational change that leads to its translocation into the plasmamembrane (Averaimo et al., 2010; Singh, 2010). Here, acting as a Cl^- channel, it may play a role in volume regulation and consequently migration. Moreover, CLIC1 is highly expressed in high grade gliomas (Wang et al., 2012).

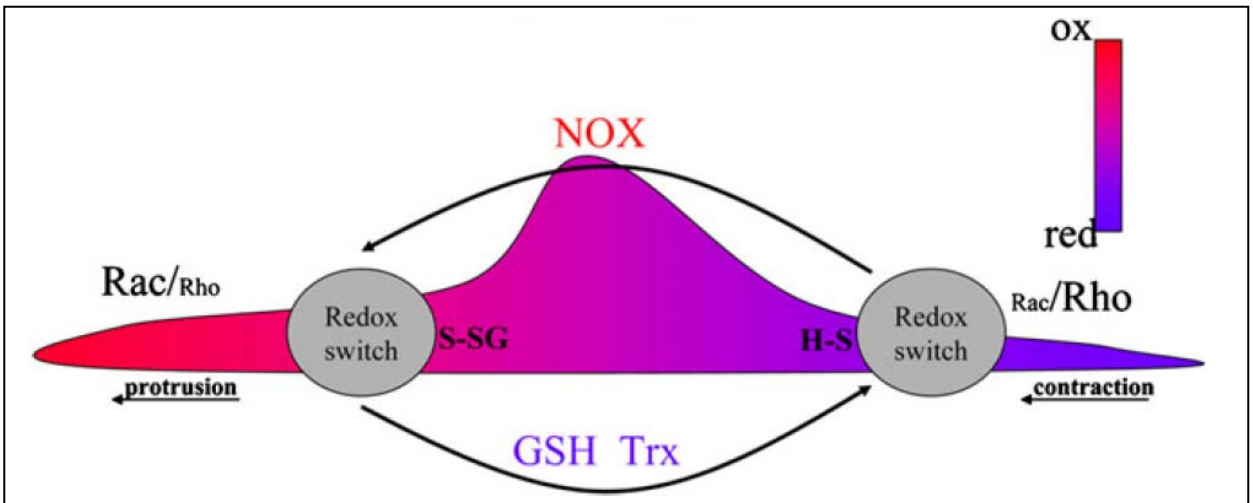

Figure 26. Protrusion/retraction dynamics regulated by a redox mechanism. Membrane protrusion at the leading edge of a migrating cell is promoted by a prevalence of oxidative events (red), with the opposite occurring at the retracting edge (purple) (Pani et al., 2010).

On this line of thoughts, we established primary cultures of CSCs from four different human glioblastomas biopsies. To investigate CLIC1 role, the cells are infected with lentiviruses engineered to bicistronically express siRNA against our protein and the Green Fluorescent Protein (GFP). GFP is used to assess transduction efficiency and to be able to recognize infected cells during electrophysiological experiments (where only green cells are studied). Western blot analysis reveals that CLIC1 protein is partially but efficiently silenced in siCLIC1 cells from all the glioblastomas (50-80% protein reduction, depending on the tumor), but not in siLuc cells, suggesting that the viral infection *per se* is not affecting CLIC1 knock down (Figure 17). The migration assay of CSCs shows that the efficiency of migration largely decreases (~50 %) when CLIC1 is silenced (Figure 18). Being the intrinsic nature of CLIC1 the one of a dimorphic protein, it is legitimate to ask whether the migration impairment is mediated by the cytoplasmic protein fraction or by the transmembrane one.

Interestingly, electrophysiological recordings from siCLIC1 cells show that the IAA94-sensitive current (likely corresponding to the CLIC1-mediated current) is completely abolished, while in siLuc or not infected cells it ranges between 10-30% of the total current depending on the tumor analyzed. This is not an obvious result since CLIC1 silencing is partial in all the glioblastomas. Thus, the residual proteins could have been residing in the membrane and act as ion channel. Although the electrophysiology approach allows us to study only one cell at the time, it is important to note that the standard error of the mean for the percentage of CLIC1-mediated current in siCLIC1 cells is extremely small in all of the tumors analyzed (mostly inside the symbols, Figure 21 A&C), strengthening the results and pointing to little variability from cell to cell. On the other hand, DIDS-sensitive current shows more variability in amplitude, but not a significant difference between siCLIC1 and siLuc cells from the same tumor (Figure 21 B&D). This is not surprising being DIDS an aspecific Cl^- channel inhibitor.

Taken together, these data strongly support the view that the CSCs migration impairment measured with the Boyden chamber assay is due to the lack of a functional CLIC1 protein as an ion channel. This action could be mediated through several mechanisms:

- by allowing Cl^- ions out of the cell, CLIC1 may participate in the volume rearrangements needed for a cell to change shape and infiltrate in narrow interstitial spaces;

- since it has been shown that CLIC1 interacts with the F-actin (Singh et al., 2007), it may participate in the reorganization of the cytoskeleton that leads to invadopodia formations;

- CLIC1 may act by supporting the function of the NADPH-oxidase (shown to be active during tumor cell migration (Pani et al., 2010) and balancing the superoxide negative charges produced by this enzyme (Averaimo et al., 2010; Milton et al., 2008).

If CLIC1 plays such a key role, it is important to quantify the relative abundance of CLIC1-mediated currents compared to the other Cl^- conductances in human glioblastomas CSCs that are not infected with lentiviruses. We find that the bigger is the relative abundance of CLIC1-mediated current, the more aggressive is the glioblastoma (Figure 24). However, western blot data show that the total protein (from all cellular compartments) does not correlate with tumor aggressiveness. Thus, the plasmamembrane fraction of CLIC1, and not the cytoplasmic one, appears to confer a worst outcome to the tumor. These findings suggest CLIC1 as a possible pharmacological target to contrast the invasiveness of glioblastoma. Being the transmembrane, and more accessible, fraction of this protein involved, it will be relatively easier to design a drug against CLIC1. Also, the other functions carried out by the cytoplasmic portion of this protein will be likely unaffected. Further experiments are needed to discriminate among the possible mechanisms that involve CLIC1 in glioblastoma infiltration to possibly find other pharmacological targets.

CHAPTER 2: Ca^{2+} and voltage dependent structural changes in the human BK channel during operation revealed by voltage clamp fluorometry

2.A INTRODUCTION

Allostery

Allostery is an intrinsic property of all proteins, which allows distant sites to be energetically coupled, resulting in a common and efficient regulation of many biological processes. Allostery can originate from binding events, covalent modifications, mutations or changes in the environment (Goodey and Benkovic, 2008; del et al., 2009; Morange, 2012). The word 'allosteric' was introduced by Jacques Monod to explain how an inhibitor binding to another site induced a conformational change of the protein that modified the active site (MONOD and JACOB, 1961). The long-range interactions between amino acids in different parts of a protein are remarkable, and the effects of binding, covalent modification or mutation can be felt through great distances. Proteins exist in a dynamic equilibrium of preexisting conformations and their ligands shift the distribution of conformers by increasing entropy via amino acid side-chain dynamics (Tsai et al., 2008).

According to this wide definition, also ion channels are modulated by allosteric processes. Indeed, their gating mechanism(s) relies on the allosteric coupling between the pore and other modulatory domains, specialized to sense different stimuli, such as changes in membrane potential, temperature, mechanical stress and concentration of signaling molecules. In particular, the large-conductance Ca^{2+}- and voltage-gated K^+ (BK) channel is an excellent example of allosteric protein.

The BK Channel

BK channels allosterically open in response to membrane depolarization and binding of different ligands, such as Ca^{2+}, Mg^{2+}, Heme, H_2O_2, lipids (Latorre et al., 2010; Cui et al., 2009; Lee and Cui, 2010; Hou et al., 2009). Physiological and pathophysiological roles played by BK channels are diverse. For example, in some neurons, activation of BK channels contributes to fast after-hyperpolarization (Muller et al., 2007), regulating action potential firing frequency (Gu et al., 2007) and neurotransmitter release (Figure 27) (Hu et al., 2001; Lancaster et al., 2001). In smooth muscle cells, opening of BK channels promotes muscle relaxation (Nelson and Quayle, 1995). Furthermore, in endocrine and exocrine cells, BK channels control hormone release (Petersen and Maruyama, 1984). Other physiological phenomena involving BK channels include skeletal muscle fatigue (Tricarico et al., 2005), regulation of circadian rhythm (Meredith et al., 2006), ethanol tolerance (Cowmeadow et al., 2006), and nociception (Hendrich et al., 2012). As expected from these diverse roles, a variety of pathological consequences may arise from BK channel impairment, including erectile dysfunction (Werner et al., 2005), incontinence, hypertension (Grimm and Sansom, 2010), asthma (Seibold et al., 2008), epilepsy and dyskinesia (Du et al., 2005).

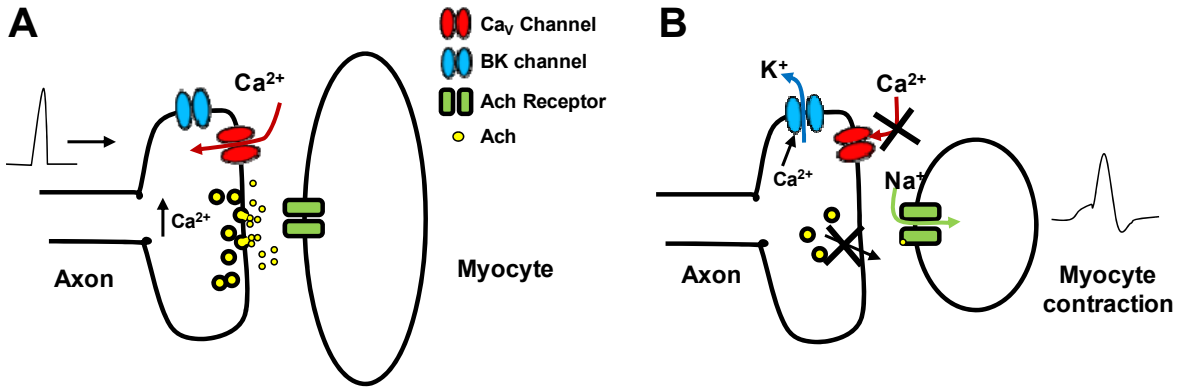

Figure 27. A model for the functional role of BK channels in the neurotransmitter release. (A) Schematic representation of a neuromuscular junction: when the axon depolarizes upon action potential arrival, voltage gated Ca^{2+} (Ca_V) channels open and intracellular [Ca^{2+}] increases, allowing acetylcholine (Ach)-containing vesicles to fuse with the membrane. Ach binds to Ach ionotropic receptors that let Na^+ into the myocyte, inducing a depolarization that triggers an action potential and myocyte contraction. (B) Ca^{2+} in the pre-sinaptic terminus also activates BK channels, accelerating repolarization: Ca_V channels close and Ach release stops. A similar mechanism, involving a tight coupling between BK and Ca_V channels, also exists in smooth muscle cells and in hormone-secreting cells.

BK channel different functions are made possible by their structural and functional diversity conferred by multiple mechanisms. For example, while only one gene encodes for the pore-forming subunit (KCNMA1, Slo1), its transcript is extensively spliced (Fodor and Aldrich, 2004; Adelman et al., 1992). Also, co-assembly with auxiliary subunits β1, β2, β3, β4, and leucine-rich repeat-containing proteins (LRRCs; γ subunits) increases functional diversity by modulating Ca^{2+} and voltage sensitivity as well as their kinetic properties (Wallner et al., 1995; Yan and Aldrich, 2012; Jiang et al., 1999). Participation in formation of macromolecular complexes with other proteins and posttranslational modifications further expand the BK channel functions (Lu et al., 2006; Berkefeld et al., 2010).

One functional BK channel is composed of four identical subunits (Shen et al., 1994), each containing ~1,100 residues (Figure 28). In addition to transmembrane helices S1-S6, which are found in voltage-dependent K^+ (K_V) channels, a seventh transmembrane segment (S0) exists in BK, such that its N terminus faces the extracellular side (Figure 28) (Meera et al., 1997; Wallner et al., 1996). An atomic structure of the transmembrane domain of the BK channel is not yet available. However, homology models have been constructed using the atomic structure of the Kv1.2/2.1 chimeric channel (Long et al., 2007) as the template (Figure 29). The location of S0 has been inferred from functional studies utilizing disulfide crosslinking of engineered cysteine residues (Liu et al., 2010) and collisional fluorescence quenching (Pantazis and Olcese, 2012), placing S0 close to S3 and S4. Transmembrane segments S0--S4 represent the voltage sensor

domain (VSD) of each subunit (four VSD per channel), in that they are rich in charged amino acids. Helices S5 and S6 from all four subunits form the pore domain.

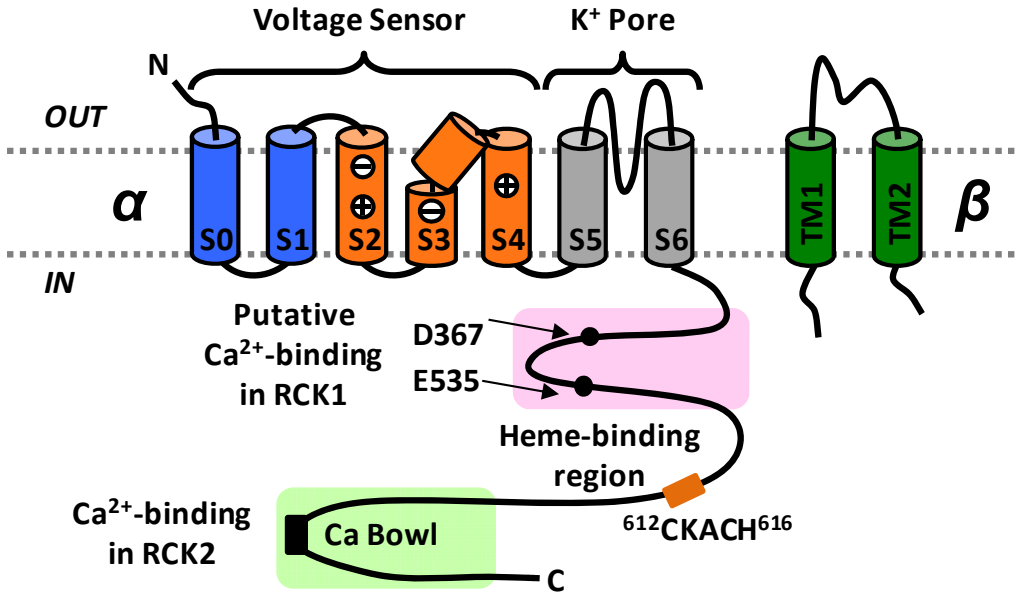

Figure 28. Membrane topology of BK α and β subunits. Transmembrane helices S1-S6 are homologous to those of other K_V channels, but S0 is unique in BK channels. Helices S2-S4 bear charged, voltage-sensing residues, indicated according to their valence. The BK intracellular C-terminus encompasses the RCK1 and RCK2 regulatory domains (each with one high-affinity Ca^{2+} sensor) and the heme-binding motif. Auxiliary β subunits consist of two transmembrane domains (TM1 and TM2) and a large extracellular loop.

The transmembrane region of BK channel includes about a third of the total amino-acid residues, and the remainder forms the cytoplasmic C-terminal domain, which is structurally organized into two tandem RCK (regulator of conductance for K^+) domains (RCK1 and RCK2). Despite their modest primary sequence similarity, RCK1 and RCK2 exhibit a three-dimensional structural similarity (Figure 29) (Yuan et al., 2010; Yuan et al., 2011; Wu et al., 2010). Each RCK domain possesses a micromolar-affinity Ca^{2+} sensing region: the RCK1 Ca^{2+} sensor (Xia et al., 2002; Yusifov et al., 2010) and the RCK2 Ca^{2+} sensor (Yusifov et al., 2008), referred to as the "Ca bowl" (Schreiber and Salkoff, 1997). A short stretch of about 20 residues connects the transmembrane helix S6 and RCK1 (S6-RCK1 linker), while ~100 residues link RCK1 and RCK2.

In the tetrameric BK channel, four pairs of RCK1-RCK2 domains assemble to form a large cytoplasmic structure called the "gating ring" (Figure 29) (Wu et al., 2010; Yuan et al., 2010; Yuan et al., 2011). The transmembrane and gating ring domains are proximal enough for close reciprocal functional interactions (Yang et al., 2008). The exact distance and radial alignment

between the transmembrane and cytoplasmic domains remains unknown. The outer diameter of the gating ring is ~15 nm and the diameter of the central star-shaped hole in the gating ring is ~4 nm.

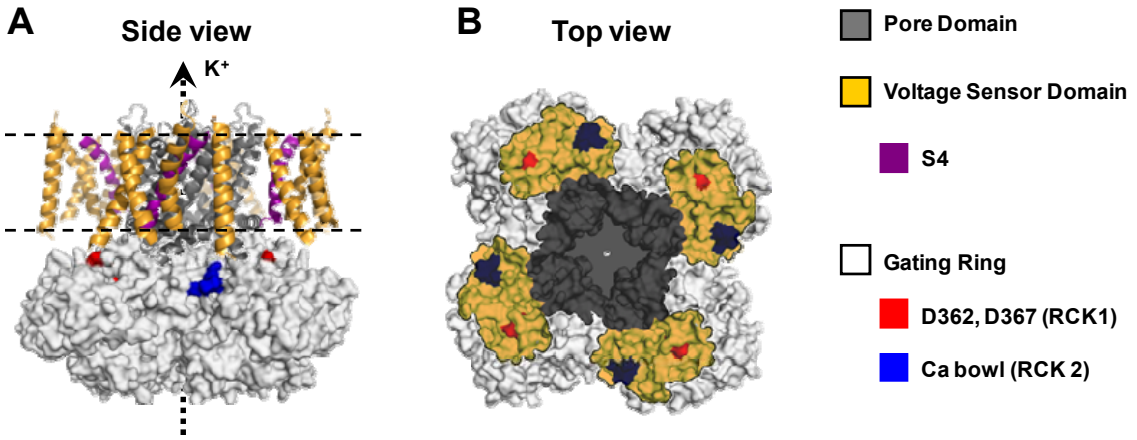

Figure 29. BK channel putative structure. (A) Side view of a putative structural model of the BK channel, composed of the BK gating ring structure (PDB# 3NAF, white), manually associated with the transmembrane portion of the K_V1.2-2.1 paddle chimera (PDB #2R9R), and S0 ideal helices positioned according to Liu and coworkers (Liu et al., 2010; Long et al., 2007; Wu et al., 2010). The pore domain is shown in gray, while VSD helices are shown in orange, except S4 (purple). (B) Top view of the gating ring structure overlaid by the "footprint" of the K_V1.2-2.1 transmembrane domains. The high affinity Ca^{2+} binding site in RCK2 (Ca bowl) is highlighted in red, while two of the putative Ca^{2+}-coordinating residues in RCK1 are in red.

The recent crystal structures of BK gating ring have shown that both the RCK1 and RCK2 Ca^{2+} sensing sites are located close to the transmembrane region of the channel (Figure 29) (Wu et al., 2010; Yuan et al., 2010; Yuan et al., 2011). Furthermore, BK channels have been recently found to be modulated by the prosthetic group heme through the heme-binding motif CKACH in the RCK1-RCK2 linker (Figure 28) (Horrigan et al., 2005; Tang et al., 2003).

The voltage sensor domain

In cells, a lipid bilayer membrane separates the cytoplasm from the external medium. The concentration of different ionic species equilibrates across the bilayer according to their electrochemical gradient (Bezanilla, 2008; Swartz, 2008). This generates a charge separation across the membrane, which translates into a membrane potential that is ranging between ~-40mV and ~–100 mV (negative inside the cell) depending on the cell type and the cell cycle phase. An electric charge or an electric dipole can be re-orientated within a transmembrane protein when the electric field across the membrane changes, eventually producing a protein

structural change that may regulate its function (Bezanilla, 2008). The movement of the charge or the dipole induces a transient current (gating current) that can be measured (Armstrong and Bezanilla, 1973). In proteins, the electric field is sensed through different mechanisms (Figure 30). Charged amino acids such as Asp, Glu, Arg, Lys and His are likely candidates since they can orientate in the field (Figure 30a). Alternatively, amino acid side chains with an intrinsic dipole moment such as Tyr (Figure 30b) may sense the voltage. Although not yet identified as a voltage sensor, the α-helix with its intrinsic dipole moment represents a potential voltage-sensing structure (Figure 30c). Proteins also contain cavities where free ions can associate; changes in an electric field might move the free ion, likely resulting in a conformational change of the protein (Figure 30d) (Bezanilla, 2008).

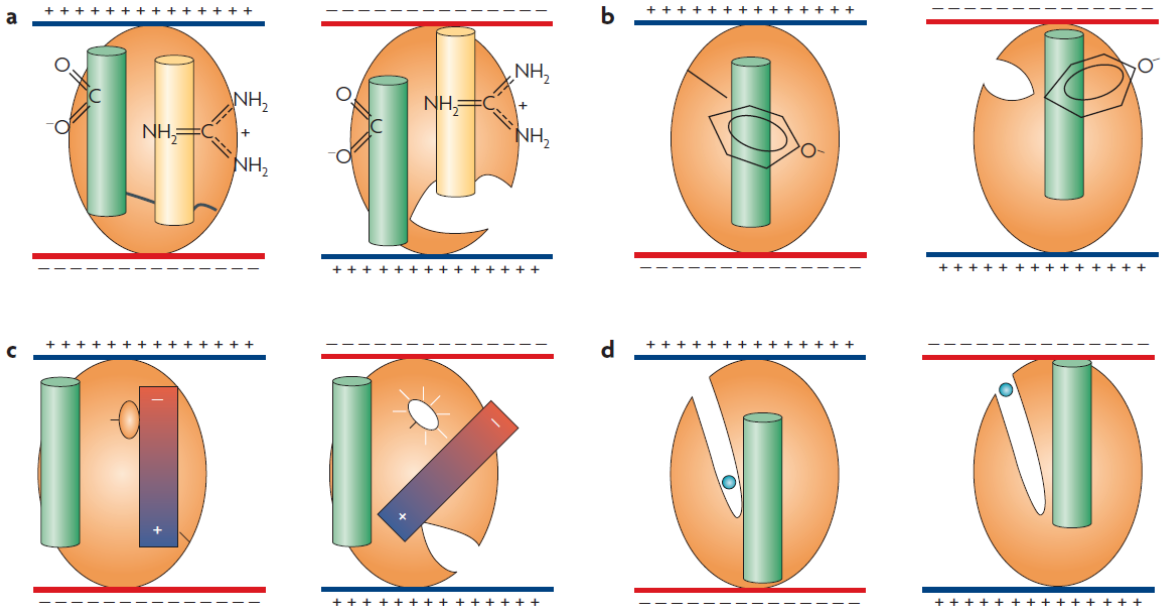

Figure 30. Possible mechanisms of voltage sensing. The schematic drawing of a transmembrane protein (orange oval) and different voltage-sensing active sites are shown. (a) Charged amino acids (Asp and Arg) move within the membrane in response to membrane potential changes. (b) Reorientation of an intrinsic residue dipole, such as Tyr, through changes in the electric field. (c) A membrane-spanning α-helix possesses a dipole moment (red to blue gradient) equivalent to the length of the helix that separates ±0.5 electronic charges (e0); the oval attached to the α-helix represents a fluorophore that changes emission according to the protein conformation. (d) A channel within the protein can redistribute ions (light blue circle) according to the direction of the electric field and initiates a conformational change (Bezanilla, 2008).

A notable example of voltage-sensing domain (VSD) is the S1–S4 transmembrane segments of voltage-activated ion channels. When these channels were first cloned, the fourth putative membrane-spanning segment, S4, stood out because of its several positively charged residues (Arg or Lys) (Noda et al., 1986; Tempel et al., 1987). S1–S3 segments also contain charged

residues, and the four segments collectively form the VSD. Although S1–S4 voltage-sensing domains were originally thought only to exist in voltage-activated ion channels, it has been recently shown that a VSD exists in a phosphatase from the Ciona intestinalis to regulate the hydrolysis of membrane phosphoinositides (Figure 31) (Murata et al., 2005; Kohout et al., 2008). Another S1–S4 domain protein without a separate pore domain was shown to function as a voltage-activated proton channel (Figure 31) (Sasaki et al., 2006; Ramsey et al., 2006).

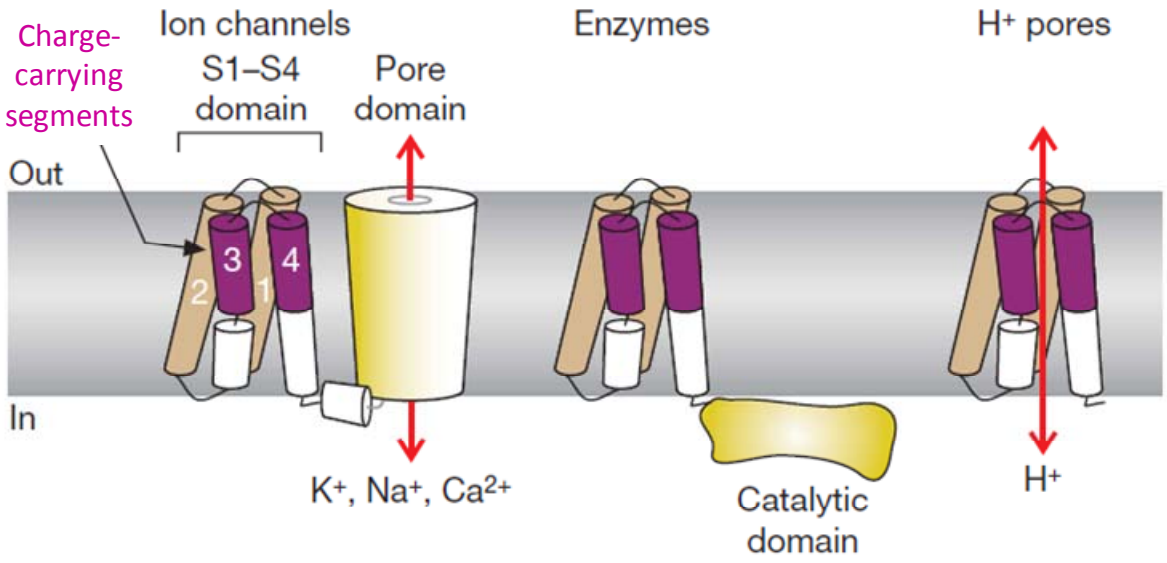

Figure 31. Scheme of S1–S4 VSDs in different types of membrane proteins. In voltage-activated ion channels, the S1–S4 domains (VSD) couple to an ion-selective pore domain (yellow); only one of four VSD is shown for clarity. In enzymes such as the Ci-VSP, VSD couples to a phosphatase domain (yellow), while in voltage-activated proton channels, protons are thought to directly permeate the VSD (Swartz, 2008).

The X-ray structures of the bacterial K_VAP and the eukaryotic Kv1.2 channel provided information about the tridimensional distribution of S1–S4 domains with respect to the pore: the VSD adopts transmembrane orientation and appears loosely attached to the pore domain (Jiang et al., 2003b; Long et al., 2005; Long et al., 2007).

In the BK channel, conserved transmembrane helices S1-S4 constitute the VSD together with the S0 segment. In fact, in addition to the role of S0 in mediating functional assembly of BK channel α and β subunits (Meera et al., 1997; Wallner et al., 1996), S0 can contribute to the VSD function (Koval et al., 2007; Pantazis et al., 2010b). Electrophysiological studies estimate that the four VSD carry overall 2.4 charges per channel (Horrigan and Aldrich, 1999; Horrigan et al., 1999; Diaz et al., 1998), remarkably less than a typical Kv channel (up to ~16 charges per channel (Jensen et al., 2012). In fact, the S4 segment of the BK channel typically contains four positively-charged Arg residues (R0, R2, R3, and R4 equivalent to Kv channels) (Figure 32); however only R4 plays a role in voltage sensing (Ma et al., 2006). A further difference of BK

VSD from a typical Kv channel resides in the fact that charged amino acids in S2 and S3 contribute significantly to voltage sensing (Ma et al., 2006); thus the voltage-sensing charges in the BK channel are fewer and more “decentralized” than in Kv channels (Figure 32). Specifically, S2 harbors two voltage-sensing residues, Asp135 and Arg167, and an additional voltage-sensing charge is located in S3 (Asp186) (Ma et al., 2006). This arrangement may allow BK channel to respond in a finely graded manner under diverse conditions. This charge distribution results in complex relative motions occurring during voltage-dependent activation: fluorometry experiments suggest that, upon depolarization, S4 diverges from S0, S1 and S2, while S2 approaches S1 (Pantazis and Olcese, 2012; Pantazis et al., 2010b).

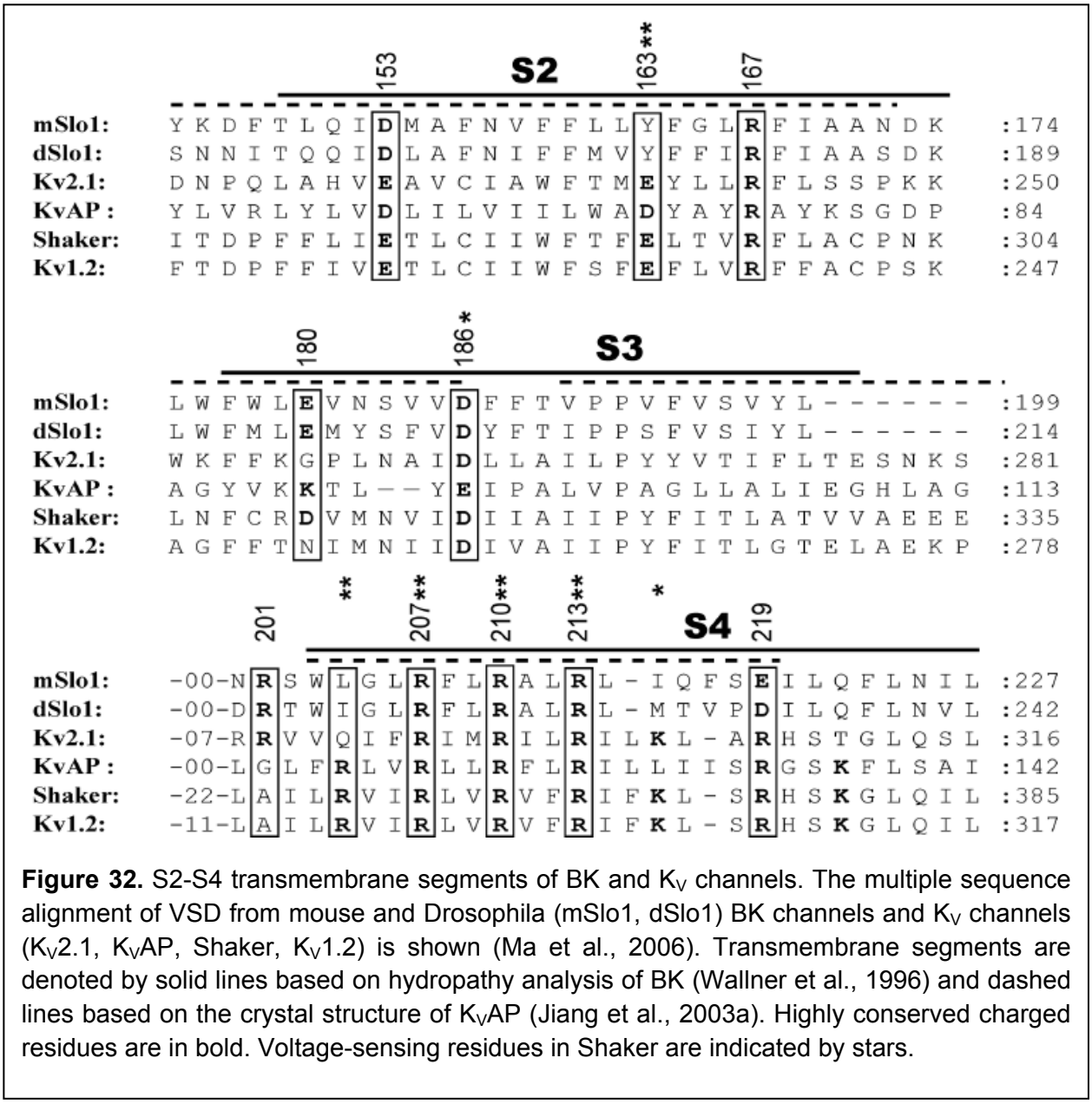

Figure 32. S2-S4 transmembrane segments of BK and K_V channels. The multiple sequence alignment of VSD from mouse and Drosophila (mSlo1, dSlo1) BK channels and K_V channels (K_V2.1, K_VAP, Shaker, K_V1.2) is shown (Ma et al., 2006). Transmembrane segments are denoted by solid lines based on hydropathy analysis of BK (Wallner et al., 1996) and dashed lines based on the crystal structure of K_VAP (Jiang et al., 2003a). Highly conserved charged residues are in bold. Voltage-sensing residues in Shaker are indicated by stars.

Moreover, S2 and S4 segments reciprocally enhance their voltage-sensing properties in a cooperative fashion (Pantazis et al., 2010a). Consistent with the idea that multiple voltage-sensing charges at different loci are involved in the voltage-sensing process, BK gating currents may show multiple kinetic components (Contreras et al., 2012). In Kv channels, the S4-S5 linker appears to work as a linkage mechanism connecting the VSD movement to opening of the ion conduction gate at the cytoplasmic ends of the four S6 segments (Jensen et al., 2012; Long et al., 2007). In the BK channel, the structural correlates of the VSD-gate coupling mechanism have not been clearly revealed yet. The S6-RCK1 linker, connecting the transmembrane region of the protein with the gating ring domain, may contribute to the VSD-gate coupling process. Shortening or lengthening of this linker segment in the absence of Ca^{2+} alter the the Po-V curve position on the voltage axis without a major change in their curve steepness (Niu et al., 2004). Furthermore, a Leu residue and a Phe residue located in the middle of S6 have been suggested to mediate the influences of VSD activation and Ca^{2+} binding on the ion conduction gate equilibrium (Wu et al., 2009).

Ca^{2+} sensors and the gating ring

Under physiological conditions, BK channels are activated by Ca^{2+} binding to the Ca^{2+}-sensing sites in RCK1 and RCK2, the constituents of the gating ring structure. Changes in $[Ca^{2+}]i$, in the range of 100 nM to 300 μM, alter different aspects of BK channel gating. For example, single-channel Po increases; the mean closed duration decreases, while the mean open duration increases (Rothberg and Magleby, 1999). Moreover, the half-activation potential (V_{half}) of macroscopic ionic currents shifts from >150 mV to ~0 mV when the Ca^{2+} sensors are fully activated by 300 μM of Ca^{2+} (Horrigan and Aldrich, 2002; Sweet and Cox, 2008). Greater concentrations of Ca^{2+} as well as of other divalent cations ions such as Mg^{2+} (>1 mM) produce additional activation (Zeng et al., 2005). This “low-affinity” response is often referred to as Mg^{2+}-dependent activation because the underlying mechanism has been studied primarily with Mg^{2+} (Shi and Cui, 2001; Shi et al., 2002). The “low-affinity” (Mg^{2+}-dependent) activation and the “high-affinity” (Ca^{2+}-dependent) activation processes are electrophysiologically different, reflecting their distinct molecular mechanisms (Horrigan and Ma, 2008; Yang et al., 2007). Thus, the BK gating ring operates as a chemomechanical transducer, converting the free energy of divalent cation binding into structural rearrangements. These structural transitions constitute the molecular basis by which this second messengers ultimately favor gate opening and VSD activation.

The RCK2 high-affinity Ca^{2+} sensor was identified soon after the BK channel gene was cloned (Adelman et al., 1992): it comprises five consecutive negatively charged Asp residues and it is named Ca bowl (Schreiber and Salkoff, 1997). The recent crystal structure of BK gating ring shows that the Ca bowl is located in a loop segment (~16-20 residues) of the RCK2 domain (Figure 33) (Yuan et al., 2010; Yuan et al., 2011). The oxygen atoms that coordinate Ca^{2+} are provided by the backbone carbonyl groups of Gln889 and Asp 892, and by the side chains of Asp895 and Asp897. In the absence of bound Ca^{2+}, the Ca^{2+}-coordinating oxygen atoms are more dispersed in space, presumably because their electronegative oxygen atoms repel each

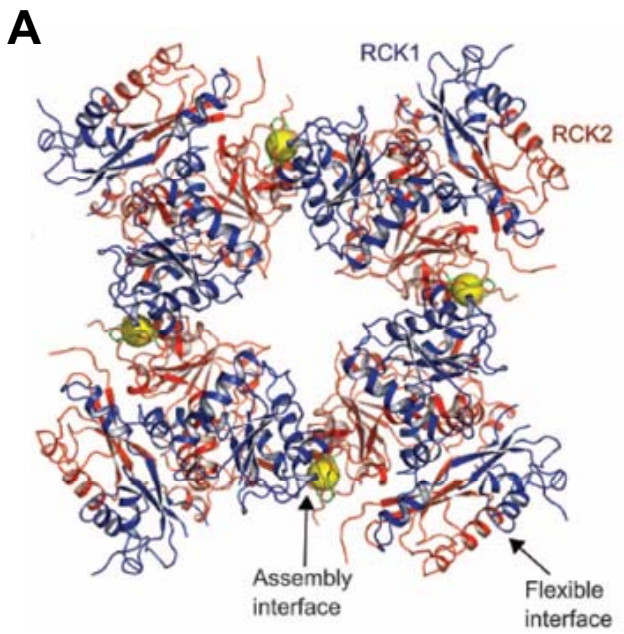

Figure 33. Gating ring structure. (A) Top view of the tetrameric gating ring structure using 6.0 Å diffraction data. RCK1 is shown in blue, RCK2 in red and Ca^{2+} ions as yellow spheres. (B) Structure of the Ca bowl, showing key residues coordinating the Ca^{2+} ion (Yuan et al., 2010).

other (Wu et al., 2010). These structural changes induced by Ca^{2+} coordination in the Ca bowl likely lead to experimentally detectable changes in the whole gating ring assembly, culminating in the stabilization of the open conformation of the ion conduction gate. The apparent Ca^{2+} dissociation constant (Kd) of the RCK2 Ca^{2+} sensor has been electrophysiologically estimated to be ~3 and ~0.9 μM, depending on whether the ion conduction gate is closed or open, respectively (Sweet and Cox, 2008). The neutralization of Ca^{2+}-coordinating residues within the Ca bowl partially impairs the negative shift of the Po(V) curve by Ca^{2+} and binding of Ca^{2+} to C-terminal protein fragments (Bao et al., 2004; Bian et al., 2001; Schreiber and Salkoff, 1997), suggesting that the Ca bowl is indeed a Ca^{2+} sensor. However, the mutations do not fully abolish the BK Ca^{2+} sensitivity in either electrophysiological (Schreiber and Salkoff, 1997) or biochemical assays (Bao et al., 2004; Bian et al., 2001; Javaherian et al., 2011), hinting the existence of a second Ca^{2+} sensor. However, the atomic structures of the isolated gating ring domain (PDB IDs 3MT5 and 3U6N) solved in the presence of mM levels of Ca^{2+} (Yuan et al., 2010; Yuan et al., 2011) do not show any Ca^{2+} bound other than to the Ca bowl. To date, the consensus is that at least three amino-acid residues, non-contiguous in the primary sequence, participate in Ca^{2+} coordination in RCK1: Asp367 side chain (Xia et al., 2002), the Glu535 side chain and Arg514 backbone (Zhang et al., 2010). In addition, Met513 may participate in formation of the RCK1 sensor (Bao et al., 2002). The apparent Ca^{2+} dissociation constants of the RCK1 sensor are electrophysiologically estimated to be ~23 and 4.9 μM when the ion

conduction gate is closed and open, respectively (Sweet and Cox, 2008); thus, greater concentrations of Ca^{2+} are required to activate the RCK1 sensor than the RCK2 sensor.

As already mentioned above, the BK gating ring is a tetramer of RCK1-RCK2 tandems. Its atomic structures obtained with or without Ca^{2+} reveal that the gating ring assumes different conformations (Yuan et al., 2010; Yuan et al., 2011; Wu et al., 2010). In particular, it appears that Ca^{2+} binding to the RCK2 sensors rearranges the gating ring so that the layer of the gating ring domain immediately juxtapositional to the transmembrane segments opens up (Yuan 2011). Presumably, it is the free energy change associated with these conformational changes in the cytoplasmic gating ring domain that ultimately promotes opening of the ion conduction gate. Spectroscopic studies of the isolated tetrameric gating ring domain in solution show that Ca^{2+} binding reversibly causes the gating ring domain to assume a more hydrodynamic shape (Javaherian et al., 2011).

An allosteric model for BK channels

In BK channels, the VSD or the Ca^{2+} sensors ability to influence a concerted conformational change (pore opening) in a nonobligatory fashion is well described as allosteric mechanisms (MONOD et al., 1965). A dual allosteric model (Figure 34) has been implemented to account for the features of BK channel activation and provides a useful framework for analyzing BK channel gating in terms of domain/domain interactions (Horrigan and Aldrich, 1999; Horrigan et al., 1999; Horrigan and Aldrich, 2002; Horrigan, 2012). The HA (Horrigan-Aldrich) model asserts that the pore can undergo a closed to open (C-O) transition, regulated by four independent and identical voltage- and Ca^{2+}-sensors. VSDs can be in a resting (R) or activated (A) conformation, whereas Ca^{2+} sensors can be Ca^{2+} free (X) or Ca^{2+} bound (X-Ca^{2+}) (Figure 34). The function of each domain is defined by equilibrium constants for gate opening (L), voltage-sensor activation (J), and Ca^{2+} binding (K). The degree of cooperativity between domains is represented by allosteric factors (C, D, and E), which define the ability of a transition in one domain to affect the equilibrium constant in another (Horrigan and Aldrich, 2002).

In the absence of Ca^{2+} and when the ion conduction gate is closed, the VSD of the BK channel is more stable in the resting conformation. Large depolarizations are required to fully drive the VSD to the activated conformation. However, binding of Ca^{2+} to the BK channel dramatically biases the VSD equilibrium towards the activated conformation both indirectly through the sequential coupling of the Ca^{2+} sensor to the ion conduction gate (allosteric factor “C” in the HA model) and to the VSD (allosteric factor “D”) and directly through the coupling between the Ca^{2+} sensor and the VSD (allosteric factor “E”) (Horrigan and Aldrich, 2002). Thus, Ca^{2+}-binding promotes BK channel activation at more physiological potentials. Similarly, binding of Ca^{2+} to the Ca^{2+} sensors of the channel increases the probability the ion conduction gate is open, and opening of the gate in turn increases the affinity of the sensors to Ca^{2+}. Finally, VSD activation also increases the Ca^{2+} affinity, and Ca^{2+} binding, in turn, promoting VSD activation.

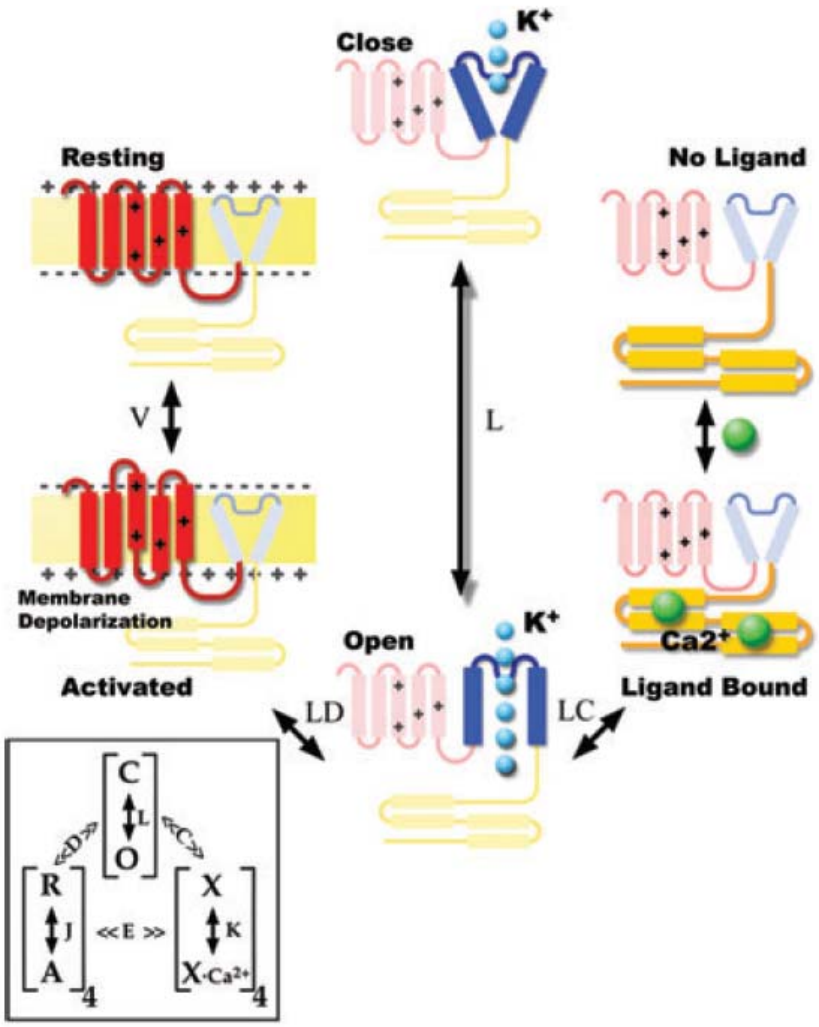

Figure 34. Horrigan and Aldrich (HA) allosteric model for BK activation. The cartoon represents one BK channel subunit whose pore can undergo a transition from the closed to the open configuration, according to the equilibrium constant L. Depolarizations activate VSDs facilitating pore opening by the allosteric factor D. Ca^{2+} binding also facilitates the channel opening (allosteric factor C) (Latorre et al., 2010). In the inset, the HA allosteric model scheme is reported (Horrigan and Aldrich, 2002).

2.B METHODS

Molecular biology

Mutagenesis: Single point mutations were generated with the QuikChange Site-Directed Mutagenesis Kit (Stratagene, CA). In vitro site-directed mutagenesis is a very useful tool to study the relationship between protein structure and function. The QuikChange site-directed mutagenesis method allows site specific mutation in double-stranded plasmids. It is performed using PfuUltra™ high-fidelity DNA polymerase. The PCR product is controlled on a 1% agarose gel and then transformed into competent bacteria, XL1-blue, using the appropriate selective antibiotics. The mutations were then confirmed by sequencing.

A hSlo clone (#U11058) without extracellular Cysteines (C14S-C141S-C277S) was used. Background mutations also included R207Q and W203V to increase P_O (Diaz et al., 1998; Ma et al., 2006) and fluorescence signal (Savalli et al., 2006), respectively. A single Cysteine was substituted in position 202 in the short S3-S4 linker (S202C) for site directed fluorescence labeling (Pantazis et al., 2010a; Savalli et al., 2006; Savalli et al., 2007). Throughout the thesis, this clone is referred-to as pseudo-WT (pWT). The two high-affinity Ca^{2+} sensors were separately neutralized generating the D362A/D367A (in RCK1) and the D894-898N (in RCK2 / Ca bowl) mutants. We also used the non-inactivating Shaker K^+ channel (Sh-IR, #M17211). For site-directed fluorescent labeling, we introduced a unique cysteine in the S3-S4 linker, generating the Sh-IR-M356C channel (Cha and Bezanilla, 1997; Mannuzzu et al., 1996).

In vitro transcription: The plasmids carrying cDNAs of pWT and mutant channels were linearized with a specific single-cutter restriction enzyme (generally Not I, New England Bioloab). The linear cDNA was then used as the template for the in vitro transcription (1-2 μg per reaction) to produce capped cRNAs (mMESSAGE MACHINE; Ambion, Austin, TX). Capped RNA mimics most eukaryotic mRNAs found in vivo, because of a 7-methyl guanosine cap structure at the 5' end. The reaction of the in vitro transcription kit includes the cap analog [m7G(5')ppp(5')G], which is incorporated as the first or 5' terminal G of the transcript because its structure precludes its incorporation at any other position in the RNA molecule. The reaction ran at 37^{o}C for 2h. The cRNA was then precipited with LiCl2 at 20^{o}C and resuspended in water. After assessing RNA concentration with the spectrophotometer (λ= 260 nm) and RNA quality by agarose gel, cRNA was stored at –80^{o}C.

Oocyte preparation and injection

Xenopus laevis (NASCO, Modesto, CA) oocytes are an excellent system where to express ion channels for electrophysiological studies, as their large size (~1 mm diameter) allows the micro-injection of cloned RNA into their cytosol, which they readily translates into functional proteins.

After surgical excision from the frog, the oocytes (stage V-VI) were defolliculated via a mechanical and enzymatic treatment (collagenase type I in a Ca^{2+}-free solution) (Figure 35). The same day of preparation or the day after, oocytes were injected with 50 nl of total cRNA (0.01-0.1 µg/µl) using a Drummond nano-injector. Injected oocytes were maintained at 18°C in an amphibian saline solution supplemented with 50 µg/ml gentamycin (Invitrogen, Carlsbad, CA), 200 µM DTT (to prevent that the external cysteines engage in disulfide bonds) and 10 µM EDTA. Three to six days after injection, oocytes were stained for 30 min with 10 µM membrane-impermeable, thiol-reactive fluorophore, tetra-methyl-rhodamine-5'-maleimide (TMRM) (Molecular Probes, Eugene, OR) in a depolarizing K^+ solution (in mM: 120 K-Methanesulfonate (MES), 2 $Ca(MES)_2$, and 10 HEPES, pH=7). TMRM stock (100 mM) was dissolved in DMSO and stored at ~ -20°C. The oocytes were then thoroughly rinsed in a dye-free solution and loaded with the caged compound DM-Nitrophen (100 nl at 2.5 mM) prior to being mounted in the recording chamber.

Figure 35. Mature *Xenopus* oocytes after defolliculation.

Voltage clamp fluorometry

Voltage clamp fluorometry is a powerful technique to optically track protein conformational rearrangements. It takes advantage of the fact that many fluorophores are sensitive to their local environment (Lakowicz, 2006). It is possible to conjugate such fluorophores to a specific protein site and, if this area undergoes a motion that results in a change of the fluorophore environment, a deflection in the fluorescence emission will be observed. Voltage clamp fluorometry was pioneered in Shaker K^+ channels expressed in oocytes clamped by two-electrode voltage clamp (Mannuzzu et al., 1996), and was shortly after implemented in the Cut-open Oocyte Vaseline Gap (COVG) voltage clamp technique (Cha and Bezanilla, 1997).

The COVG technique (Stefani and Bezanilla, 1998) is a low-noise, fast clamp technique that can allow control of the internal solution. The oocyte is mounted in a triple-compartment Perspex chamber, with a diameter of 600 µm for the top and bottom holes (Figure 36). The voltage clamp circuit is then assembled around the mounted oocyte by the placement of six salt bridges and one intracellular electrode, imposing three simultaneous voltage clamps. The three chambers are electrically-isolated by Vaseline gaps: the upper chamber isolates the oocyte upper domus and maintains it under clamp; the middle chamber provides a guard shield by clamping the middle part of the oocyte to the same potential as the upper chamber; the bottom chamber allows to clamp to ground the intracellular compartment of the oocyte, through the saponin-permeabilized membrane. Changes in fluorescence signal and ionic currents were simultaneously measured from the same area of membrane isolated by the top chamber (Gandhi and Olcese, 2008). The optical setup consists of a Zeiss Axioscope FS microscope

with filters appropriate for TMRM (Omega Optical, Brattleboro, VT). The light source is a 100 W microscope halogen lamp. A TTL-triggered Uniblitz VS 25 shutter (Vincent Associates, Rochester, NY) is mounted on the excitation light path. The Objective (Olympus LUMPlanFI, 40×, water immersion) has a numerical aperture of 0.8 and a working distance of 3.3 mm (Olympus Optical). The emission light is focused on a PIN-08-GL photodiode (UDT Technologies, Torrance, CA). A Dagan Photomax 200 amplifier is used for the amplification of the photocurrent and background fluorescence subtraction. For the UV flash photolysis of caged Ca^{2+}, the Xe flash lamp system JML-C2 was used (Rapp Opto-electronik GmbH, Hamburg, Germany), which delivers high-energy UV flashes of adjustable intensity. An external trigger is used to synchronize flashes with voltage clamp and optical recordings.

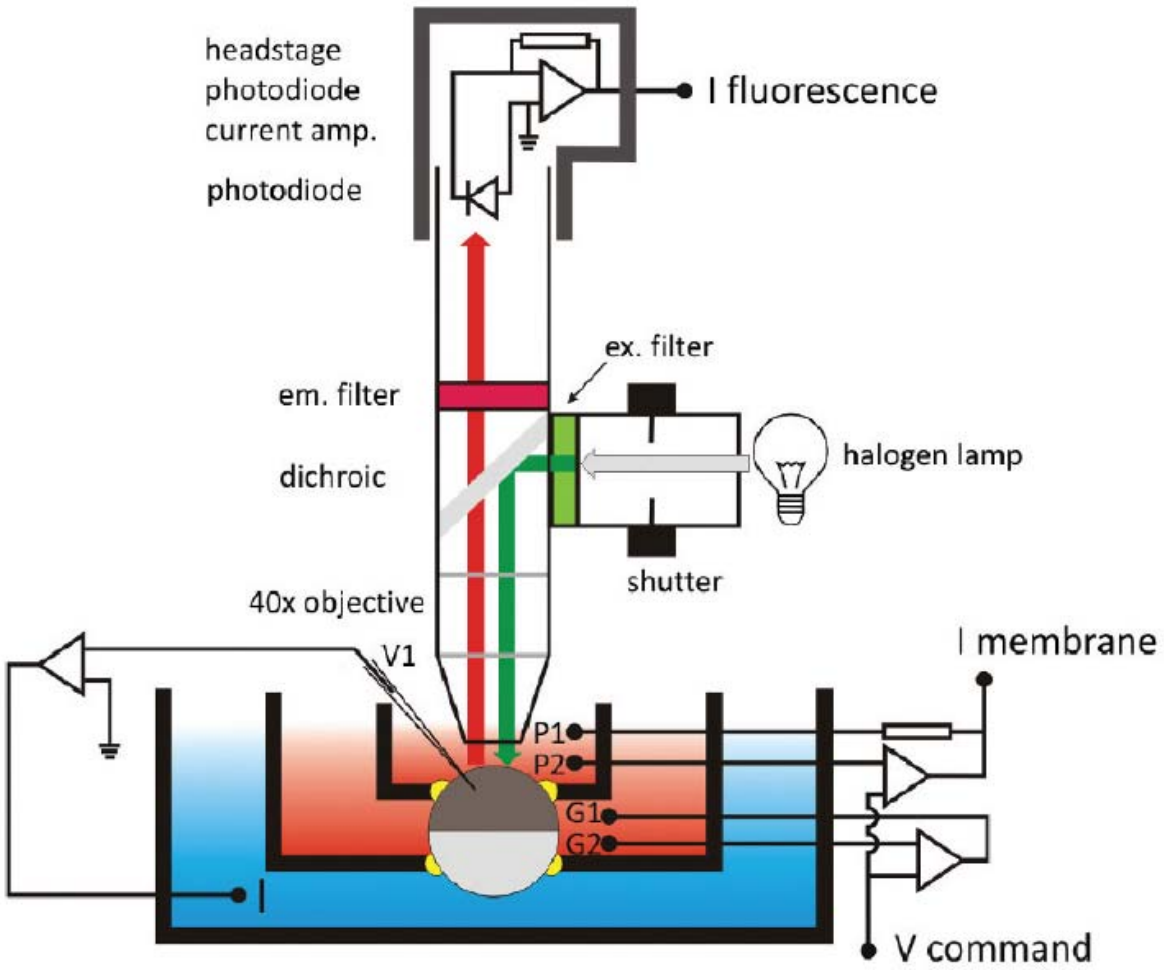

Figure 36. Voltage-clamp fluorometry. It is shown a schematic drawing of the COVG recording chambers, the fluorescence light path, the photodetector circuit, and the COVG circuit. The bottom chamber (filled with internal solution) is held at ground, and the middle chamber and upper chambers (filled with external solution) are clamped to the command membrane potential. Fluorescence emission and ionic current are recorded from the oocyte membrane isolated in the upper chamber. The fluorescence is detected by a photodiode connected to a low noise current amplifier (Gandhi and Olcese, 2008).

A quartz water immersed light guide was positioned ~0.5 mm away from the oocyte. The external solution contained (mM): 60 Na-MES, 50 K-MES, 2 Ca-$(MES)_2$, 10 Na-HEPES (pH=7.0). The internal solution contained (mM): 120 K-Glutamate, 10 HEPES (pH=7.0). Solution for the intracellular micro-pipette was (mM): 2700 Na-MES, 10 NaCl. Low-access resistance to the oocyte interior was obtained by permeabilizing the oocyte with 0.1% saponin dissolved in the internal solution.

Analysis: Experimental data were analyzed with a customized program developed in our Division and using fitting routines running in Microsoft Excel. The G(V) curves were calculated dividing the current-voltage relationships (I-V curves) by the driving force (V_m~E_K), where V_m is the membrane potential and E_K the equilibrium potential for K^+, estimated using the Nernst equation. Data for the membrane conductance (G(V)) and the fluorescence (F(V)) curves were fitted to one Boltzmann distributions of the form:

$$G(V) = \frac{G_{\max}}{1 + e^{\left[z(Vhalf - Vm)\left(\frac{F}{RT}\right)\right]}}$$

$$F(V) = \frac{F_{\max} - F_{\min}}{1 + e^{\left[z(Vhalf - Vm)\left(\frac{F}{RT}\right)\right]}} - F_{\min}$$

where G_{max} and F_{max} are the maximal G and F; F_{min} is the minimal F; z is the effective valence of the distribution; V_{half} is the half-activating potential; V_m is the membrane potential; F, R and T are the usual thermodynamic values. For each experiment, G(V) and F(V) curves were constructed before and after UV flash-induced Ca^{2+} release.

Statistical Analysis: Scatter plots of ΔV_{half} vs. $\Delta kTln[Ca^{2+}]i$ were tested for monotonicity using Spearman's rank order correlation coefficient (ρ) using the statistical software SigmaStat (Aspire Software, Ashburn, VA). ΔV_{half} data were normalized to unitless quantities by multiplying by the fitted values for charge displacement (z_L for ΔGV_{half} and $4z_J$ for ΔFV_{half}) and dividing by the change in chemical potential for calcium $\Delta\mu = \Delta kTln[Ca^{2+}]i$. The collective mean of these normalized quantities, which can be interpreted as a measure of thermodynamic linkage between Ca^{2+}- and voltage–sensing elements of the channel, was assessed for nonzero value using Student's t-test.

Caged Ca^{2+} compounds

The term "caged compounds" was first used in 1978 by physiologists to refer to the functional encapsulation of ATP by use of a photochemical protecting group. Chromophore excitation leads to photolysis of a covalent bond, liberating the caged chemical messenger (Ellis-Davies,

2007). Among other molecules, Ca^{2+} is efficiently released by photochemical lysis of the chelator backbone, converting a high affinity, tetracarboxylic acid chelator into two low affinity dicarboxylic acid molecules.

In this thesis, to induce a fast increase of $[Ca^{2+}]$ in the oocytes, a caged Ca^{2+} compound was used: DM-nitrophen (1-(4,5-dimethoxy-2-nitrophenyl)-1,2-diaminoethane-N,N,N′,N′-tetraacetic acid). DM-nitrophen is an EDTA moiety, which strongly binds Ca^{2+} (Kd ~5 nM), fused with a 2-nitophenyl group that makes the molecule light sensitive (Figure 37). When a UV photon hits DM-nitrophen, it breaks a covalent bond in the EDTA backbone, rapidly producing two products with much lower affinity for Ca^{2+} (~3 mM) and thus releasing Ca^{2+} (Faas and Mody, 2012) .

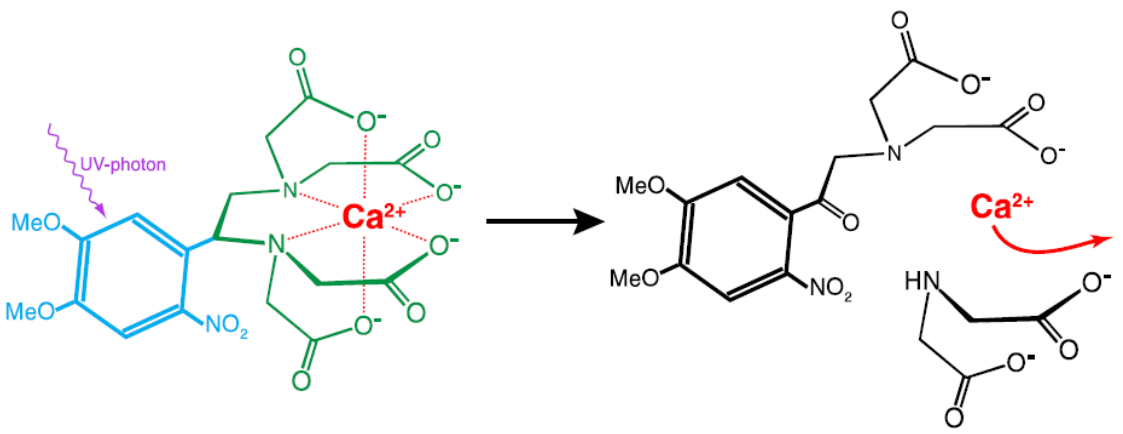

Figure 37. DM-nitrophen is a photo-sensitive Ca^{2+} chelator. DM-nitrophen is an EDTA molecule (green) attached to a 2-nitophenyl group (blue). When the 2-nitophenyl group absorbs a UV photon, the EDTA group breaks into two molecules with lower affinity for Ca^{2+}, effectively releasing Ca^{2+} (Faas and Mody, 2012).

Patch clamp

To construct a calibration curve for BK channel activation at different $[Ca^{2+}]i$, the patch clamp technique was used (see Methods in the first chapter for a brief historical mention on the patch clamp).

BK channels were overexpressed in Xenopus oocytes. 1-2 days after injection, the vitelline layer of the oocytes was removed with two forceps to expose the plasmamembrane. Membrane patches in the inside-out configuration were perfused with bath solutions containing (mM) 115 K-MES, 5 KCl, 5 HEDTA, 10 HEPES (pH 7.0). The $[Ca^{2+}]$ in this solution was varied by adding $CaCl_2$. The free $[Ca^{2+}]$ was first theoretically calculated with WEBMAXC v2.10 (http://www.stanford.edu/~cpatton/maxc.html) and then measured using a Ca^{2+} electrode (WPI, Sarasota, FL). The borosilicate glass pipettes (WPI, Sarasota, FL) were filled with the bath solution at the lowest free $[Ca^{2+}]$. The holding potential was 0 mV. Data were filtered to 1/5 of

the sampling frequency. G(V) curves for different BK clones (pWT, D364/367A, D894-898N) at different free $[Ca^{2+}]i$ were constructed as described above. Plotting V_{half} against $[Ca^{2+}]$ produced calibration curves for the three BK clones used. The free $[Ca^{2+}]i$ in the COVG experiments was then calculated, before and after caged Ca^{2+} release, by interpolating the GV_{half} on the calibration curve of the corresponding clone.

Model

The statistical-mechanical model of BK channels presented in this thesis is based on the allosteric model implemented by Horrigan and Aldrich in 2002 (Horrigan and Aldrich, 2002) and expanded by our collaborator Dr. Daniel Sigg. It comprises a pore domain, four VSDs, four RCK1 Ca^{2+} sensors and four RCK2 Ca^{2+} sensors. The fitting of the model to the experimental data points was performed using the Berkeley Madonna software (www.berkeleymadonna.com/).

The equations of the model are as follow:

Equilibrium properties for the BK model are derived from the partition function *Z*, which can be expressed as a polynomial of equilibrium constants *J*, K_1, K_2, and *L*:

$$Z = \sum_{j,k_1,k_2,l} \Theta_{jk_1k_2l} J^j K_1^{k_1} K_2^{k_2} L^l \ .$$

The activation numbers (*j*, k_1, k_2, and *l*) run from 0 to 4, with the exception of the pore number *l*, which has two values: 0 (closed) and 1 (open).

The equilibrium constants are given by:

$$J = \exp\left(\frac{\Delta q_J (V_m - V_J)}{kT}\right);\ K_1 = \left(\frac{[Ca^{2+}]}{Kd_1}\right);\ K_2 = \left(\frac{[Ca^{2+}]}{Kd_2}\right);\ \text{and}\ L = \exp\left(\frac{\Delta q_L (V_m - V_L)}{kT}\right).$$

The partition factors $\Theta_{jk_1k_2l}$ are a function of both coupling constants (C_1, C_2, *D*, E_1, E_2, and *F*) and combinatorial factors. The value of Θ_{0000} is set to unity (consistent with the usual practice of setting the lowest activated state to zero energy).

It is convenient to write the expression of *Z* in a hierarchical manner, starting with terms for the closed (C) and open (O) states of the channel, followed by distinctions between the voltage sensor J residing in the resting (R) or active (A) state, and finally subdividing between Ca^{2+}-binding of RCK1 and RCK2. Thus,

$$Z = Z_C^4 + LZ_O^4,$$

where,

$$Z_C = Z_{CR} + JZ_{CA}$$

$Z_O = Z_{OR} + JDZ_{OA}$

and,

$Z_{CR} = (1 + K_1) + K_2(1 + K_1F)$,

$Z_{CA} = (1 + K_1E_1) + K_2E_2(1 + K_1E_1F)$,

$Z_{OR} = (1 + K_1C_1) + K_2C_2(1 + K_1C_1)$.

$Z_{OA} = (1 + K_1C_1E_1) + K_2C_2E_2(1 + K_1C_1E_1F)$.

It should be noted that the last group of sub-partitions are voltage independent (functions of $[Ca^{2+}]$ only). We wish to know the mean number of activated domains A_X as a function of V_m and $[Ca^{2+}]$. The corresponding quantity for the J regulatory domain is:

$$A_J = \frac{\sum_{j,k_1,k_2,l} j\Theta_{jk_1k_2l} J^j K_1^{k_1} K_2^{k_2} L^l}{\sum_{j,k_1,k_2,l} \Theta_{jk_1k_2l} J^j K_1^{k_1} K_2^{k_2} L^l} = \frac{J\dfrac{\partial Z}{\partial J}}{Z} = \frac{\partial \ln Z}{\partial \ln J},$$

with similar expressions for A_{K_1}, A_{K_2}, and A_L.

The relevant quantities for this paper are A_J (proportional to the fluorescence changes of the voltage sensor label) and A_L (proportional to channel conductance). These are given by:

$$A_L = LZ_O^4 / Z,$$

$$A_J = \left(\frac{4J}{Z}\right)\left(Z_{CA}Z_C^3 + LDZ_{OA}Z_O^3\right).$$

The normalized G(V) and F(V) are proportional to the activation curves of their respective regulatory domains: G(V) = A_L; and F(V) = A_J/4.

To obtain half-maximal voltage (GV_{half}) of the G(V) curve, we set A_L = 0.5, from which we derive:

$L(Z_{OR} + JDZ_{OA})^4 - (Z_{CR} + JZ_{CA})^4 = 0$. [condition for GV_{half}].

From the voltage dependence of L and J given earlier in this supplement, one can numerically obtain the value GV_{half} satisfying the above equation, which was done using the root finder algorithm in Berkeley Madonna.

2.C RESULTS

The BK channel voltage sensor undergoes voltage-dependent structural changes that precede channel activation

The human BK channel was engineered to allow for specific fluorescent labeling of the extracellular tip of the S4 transmembrane segment (pWT, see Methods), which is an important component of the BK VSD. After labeling the cysteine at position 202 with TMRM fluorophore, the oocytes were voltage-clamped using the Cut-open Oocyte Vaseline Gap (COVG) technique modified for epifluorescence measurement. K^+ currents were recorded at different imposed membrane potentials. Simultaneously, TMRM fluorescence traces were acquired and a voltage dependent change of the fluorescence emission was detected (Figure 38). The voltage dependence of the fluorescence signal (F(V)) preceded the channel activation curve (G(V)) by ~ 80 mV, as expected for protein rearrangement associated to the movement of the VSD. The half activation potentials (V_{half}) were FV_{half} = -81.18 ± 2.80 mV and GV_{half} = -4.07 ± 8.35 mV (n=4).

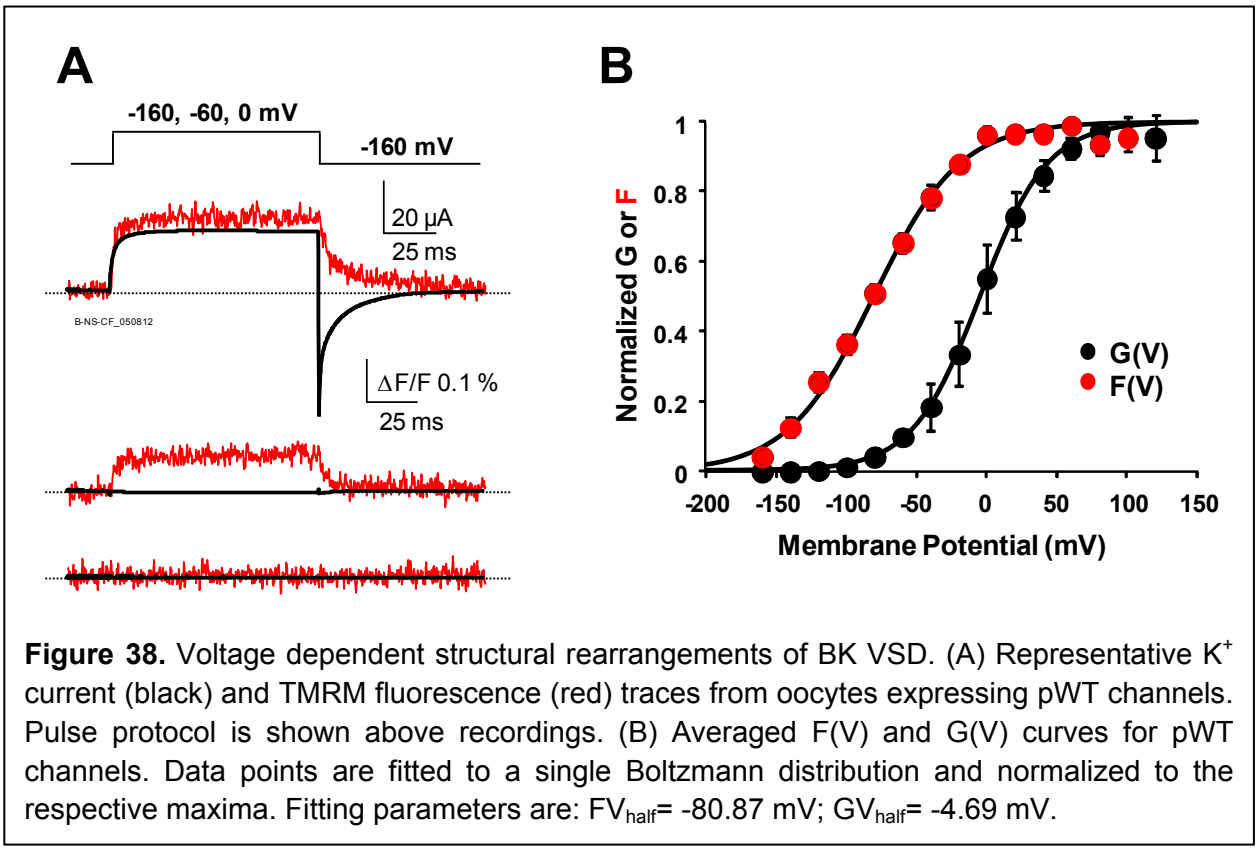

Figure 38. Voltage dependent structural rearrangements of BK VSD. (A) Representative K^+ current (black) and TMRM fluorescence (red) traces from oocytes expressing pWT channels. Pulse protocol is shown above recordings. (B) Averaged F(V) and G(V) curves for pWT channels. Data points are fitted to a single Boltzmann distribution and normalized to the respective maxima. Fitting parameters are: FV_{half}= -80.87 mV; GV_{half}= -4.69 mV.

Ca^{2+} binding to the intracellular BK gating ring produces a structural change that propagates to the transmembrane VSD, as detected by voltage clamp fluorometry

To study the Ca^{2+}-induced conformational changes of BK VSD, Xenopus oocytes expressing pWT BK (prelabeled with TMRM) were injected with DM-Nitrophen, a caged Ca^{2+} compound that undergoes UV photolysis, releasing Ca^{2+}. While under voltage clamp (using the COVG technique modified for epifluorescence measurement), we induced rapid increase of intracellular Ca^{2+} concentration ($[Ca^{2+}]_i$) by delivering UV flashes focused on the upper oocyte membrane.

Simultaneous recordings of K^+ currents and fluorescence emission from oocytes expressing pWT channels are shown in Figure 39A. Once the ionic current reached steady-state, the rapid increase of $[Ca^{2+}]_i$, triggered by the UV flash photolysis of DM-Nitrophen, increased the P_O of BK channels, manifested as a downward or upward deflection in the ionic current traces for potentials above or below the K^+ reversal potential, respectively. Notably, UV-induced Ca^{2+} uncaging also induced an increase of the simultaneously-recorded TMRM fluorescence emission (Figure 39A, red traces), suggesting that Ca^{2+} binding to the intracellular gating ring induces structural rearrangements in the transmembrane VSD.

The voltage dependence of the fluorescence deflections (F(V)) and macroscopic K^+ conductance (G(V)) were calculated from the fluorescence and ionic current recordings, 2 ms before and 10 ms after UV flashes (Figure 39B). The rapid increase in $[Ca^{2+}]$i produced a hyperpolarizing shift of the G(V) curve ($\Delta GV_{half} \approx$ -50 mV) associated with a smaller, but well-resolved, translation of the F(V) curve in the same direction ($\Delta FV_{half} \approx$ -25 mV). Note that the Ca^{2+} release induced a cross-over of G(V) and F(V) curves (Figure 39B), evidence for BK channels undergoing conformational transitions while in the open state. This result is consistent with the established view that BK channels possess multiple open states sequentially populated during activation (Stefani et al., 1997; Horrigan and Aldrich, 2002; Magleby, 2003; Moczydlowski and Latorre, 1983).

Ionic current and fluorescence traces from pWT BK channels expressed in oocytes not loaded with DM-Nitrophen were unaffected by UV flashes (Figure 39C). G(V) and F(V) curves calculated before and after UV-flashes were superimposed, underlining that the UV flash *per se* did not affect the properties of the recordings and the effects observed in oocytes injected with DM-Nitrophen were genuinely produced by Ca^{2+} (Figure 39D).

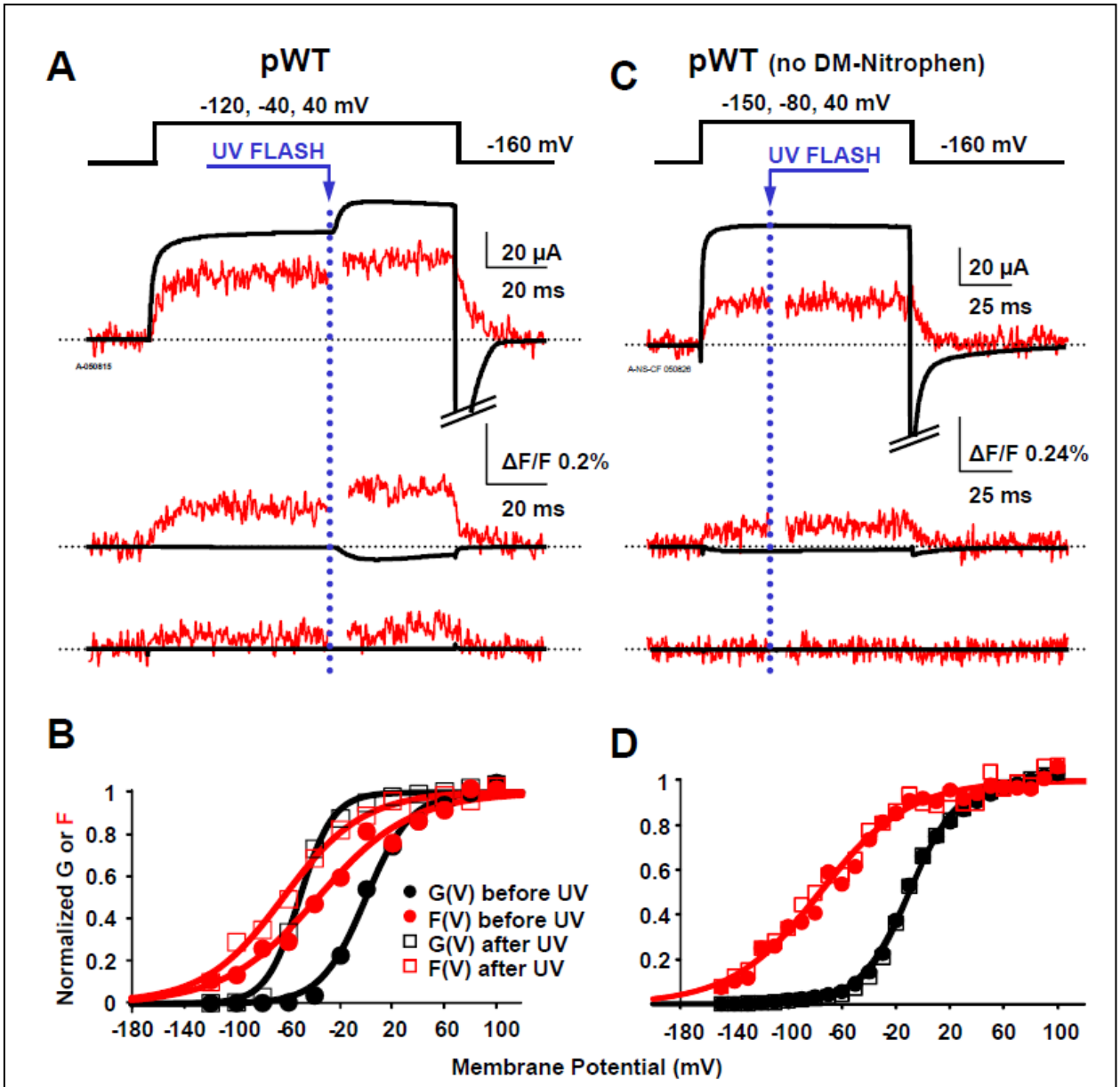

Figure 39. Intracellular Ca^{2+} photo-release induces conformational changes of the BK channel VSD. (A) K^+ current and TMRM fluorescence traces simultaneously recorded during depolarizations to the indicated potentials from an oocyte expressing pWT channels and pre-injected with DM-nitrophen are shown. UV-flashes were delivered onto the oocyte 60 ms after the onset of depolarization. $[Ca^{2+}]i$ increased from 10 µM to 84 µM. The photodiode amplifier was blanked for 3 ms during the UV flash to prevent overload. (B) Normalized fluorescence (F) and K^+ conductance (G) data from the experiment in A, before and after UV flashes, were fit to a single Boltzmann distribution (before UV, GV_{half} = 0 mV and FV_{half} = -37 mV; after UV, GV_{half} = -51 mV and FV_{half} = -63 mV). (C) As in A, but the oocyte was not pre-injected with DM-nitrophen. (D) F(V) and G(V) curves were constructed before ($[Ca^{2+}]i$= 8.2 µM) and after ($[Ca^{2+}]i$= 7.9 µM) UV flashes from the experiment in C and fitted to a single Boltzmann distribution (before UV, GV_{half} = -10 mV and FV_{half} = -75 mV; after UV, GV_{half} = -10 mV and FV_{half} = -76 mV).

The two high-affinity Ca^{2+} sensors of BK channels, in RCK1 and RCK2, are not functionally equivalent

Two high-affinity Ca^{2+} sensors are located within the BK gating ring ligand-binding apparatus: one, in RCK1, includes residue D367, which is critical for Ca^{2+} sensing (Xia et al., 2002; Yusifov et al., 2010); the other, in the RCK2 domain, coordinates Ca^{2+} via the five Asp (D894-D898) comprising the Ca bowl (Yuan et al., 2010; Schreiber and Salkoff, 1997).

To assess their respective contribution to the Ca^{2+}-induced rearrangement of the VSD, the two high-affinity Ca^{2+} sensors were separately neutralized. The D362A/D367A mutations were introduced to impair high-affinity Ca^{2+} sensing in RCK1 (Xia et al., 2002). Following UV flash photolysis, the rapid increase of $[Ca^{2+}]_i$ induced a shift towards more negative potentials in both the G(V) and F(V) curves, as observed in pWT channels although to a smaller extent (Figure 40). This result suggests that an intact RCK1 Ca^{2+} sensor is not necessary to mediate the propagation of Ca^{2+}-induced gating ring rearrangements to the VSD.

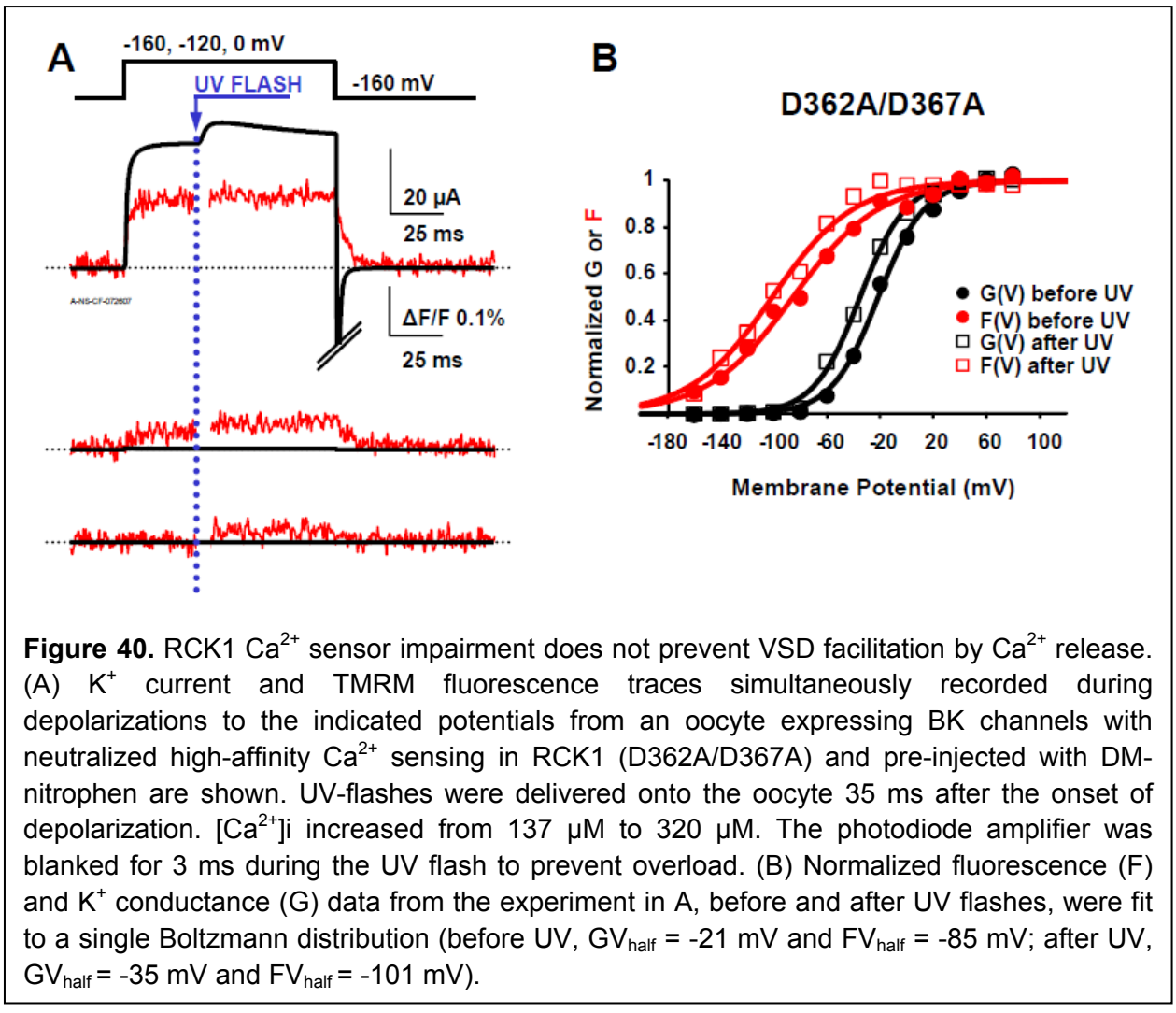

Figure 40. RCK1 Ca^{2+} sensor impairment does not prevent VSD facilitation by Ca^{2+} release. (A) K^+ current and TMRM fluorescence traces simultaneously recorded during depolarizations to the indicated potentials from an oocyte expressing BK channels with neutralized high-affinity Ca^{2+} sensing in RCK1 (D362A/D367A) and pre-injected with DM-nitrophen are shown. UV-flashes were delivered onto the oocyte 35 ms after the onset of depolarization. $[Ca^{2+}]i$ increased from 137 µM to 320 µM. The photodiode amplifier was blanked for 3 ms during the UV flash to prevent overload. (B) Normalized fluorescence (F) and K^+ conductance (G) data from the experiment in A, before and after UV flashes, were fit to a single Boltzmann distribution (before UV, GV_{half} = -21 mV and FV_{half} = -85 mV; after UV, GV_{half} = -35 mV and FV_{half} = -101 mV).

Conversely, when the Asp in the Ca bowl (in RCK2) were mutated into Asn (D894-898N) (Schreiber and Salkoff, 1997), intracellular Ca^{2+} release no longer induced the F(V) curve shift (Figure 41). Still, the P_O of this mutant was increased by the elevation of $[Ca^{2+}]i$, demonstrated by the leftward-shifted G(V) curve following Ca^{2+} release (Figure 41B). Incidentally, the absence of a change in VSD fluorescence excludes the possibility of a direct effect (e.g., charge screening) of Ca^{2+} on the BK VSD. This also shows that TMRM fluorescence was not perturbed by the Ca^{2+}-dependent motions of the pore. These experiments point to the view that there is a functional coupling between RCK2 Ca^{2+} sensor and the VSD, and that no such link exists between RCK1 Ca^{2+} sensor and the VSD.

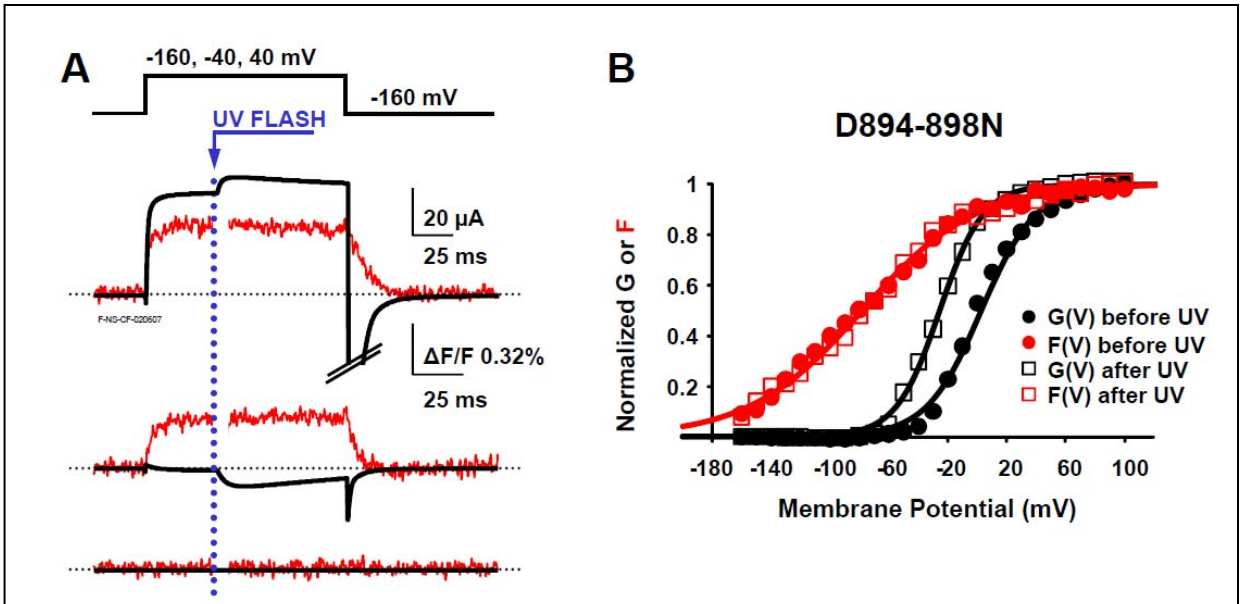

Figure 41. RCK2 Ca^{2+} sensor is necessary for VSD facilitation by Ca^{2+} release. (A) K^+ current and TMRM fluorescence traces simultaneously recorded during depolarizations to the indicated potentials from an oocyte expressing BK channels with neutralized Ca bowl in RCK2 (D894-898N) and pre-injected with DM-nitrophen are shown. UV-flashes were delivered onto the oocyte 35 ms after the onset of depolarization. $[Ca^{2+}]i$ increased from 105 µM to 210 µM. The photodiode amplifier was blanked for 3 ms during the UV flash to prevent overload. (B) Normalized fluorescence (F) and K^+ conductance (G) data from the experiment in A, before and after UV flashes, were fit to a single Boltzmann distribution (before UV, GV_{half} = 3 mV and FV_{half} = -79 mV; after UV, GV_{half} = -26 mV and FV_{half} = -78 mV).

Results from all experiments performed are shown in Figure 42. The Ca^{2+}-induced shift of the half-activation potential of G(V) curves (ΔGV_{half}) was consistently associated with a shift of the F(V) curves (ΔFV_{half}) in the same direction, but only in BK channels with an intact Ca bowl (Figure 42). To quantify the dependence of observed shifts in G(V) and F(V) curves on Ca-release in pWT and mutants channels, we performed a statistical analysis (see Methods). A strong monotonic correlation between Ca^{2+} release ($\Delta kT\ln[Ca^{2+}]$) and G(V) and F(V) voltage shifts was found in pWT and in the D362A/D367A mutant (Figure 43A&B). This was also true for

the D894-898N mutant in the case of z_L*GV_{half} (P<0.001), but not in the case of $4z_J$*ΔF-V_{half} (P=0.705) (Figure 43C). Thus, with the exception of the RCK2 mutant, an increase in intracellular [Ca^{2+}] consistently produced a leftward shift in the activation curves (ΔGV_{half}) associated with a statistically-significant shift of the voltage sensor activation (ΔFV_{half}) in the same direction.

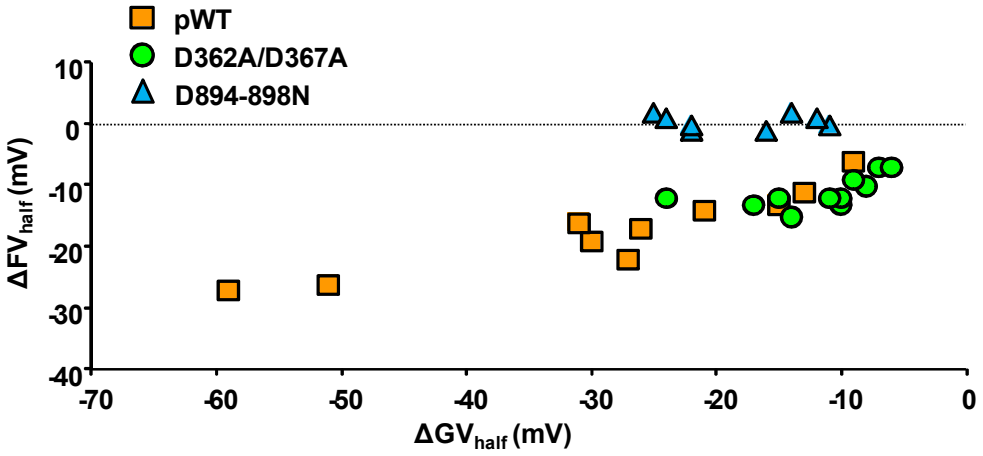

Figure 42. The Ca bowl is required for the Ca^{2+}-mediated effect on VSD movements. The plot shows the shifts in GV_{half} (ΔGV_{half}) and FV_{half} (ΔFV_{half}) measured in response to calcium release for all the experiments performed.

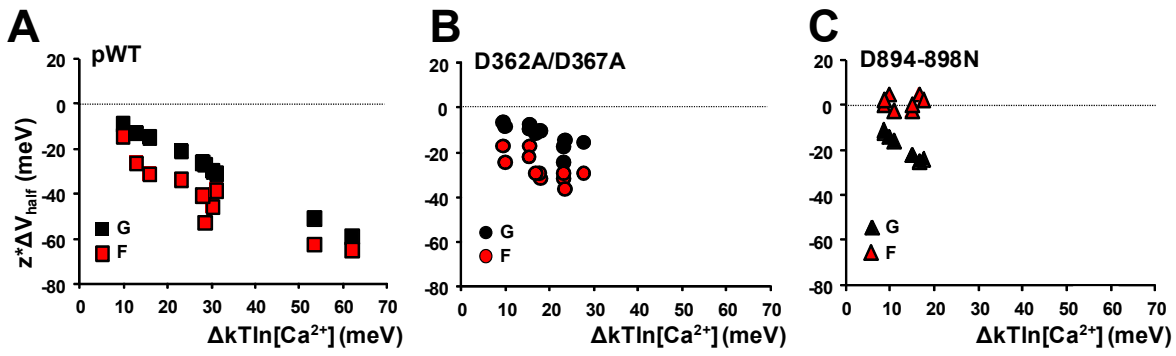

Figure 43. Set of experiments measuring shifts in GV_{half} and FV_{half} in response to calcium release. (A, B, C) These plots show the changes in activation energy produced by Ca^{2+} photo-release ($zL^*\Delta GV_{half}$ and $4zJ^*\Delta FV_{half}$) plotted against the chemical potential $\Delta kTln[Ca^{2+}]$. A strong monotonic correlation exists between Ca-release and G(V) and F(V) voltage shifts in pWT (A) (zL^*GV_{half}: ρ = -1.0, P<0.001; $4zJ^*FV_{half}$: ρ = -0.915, P<0.001) and in the D362A/D367A mutant (B) (zL^*GV_{half}: ρ = -0.868, P < 0.001; $4zJ^*FV_{half}$: ρ = -0.787, P=0.002). This is also true for the D894-898N mutant (C) in the case of $zL^*\Delta GV_{half}$ (ρ = -0.970, P<0.001), but not in the case of $4zJ^*\Delta FV_{half}$ (ρ = 0.146, P=0.705).

BK channels as intrinsic sensor of [Ca^{2+}] at the plamsamembrane level

In order to estimate local intracellular free [Ca^{2+}]i before and after UV photolysis, we took advantage of the BK intrinsic Ca^{2+}-sensing properties, as previously reported in motor neurons and hair cells (Sun et al., 2004; Sy et al., 2010). BK channels were expressed in *Xenopus* oocytes. Patch-clamp experiments were performed in the inside-out configuration. This technique allowed the control and exchange of the solution facing the intracellular portion of the channel where the two Ca^{2+} sensors are located. Solutions at different free [Ca^{2+}]i, ranging between ~1 µM and ~1 mM, were perfused on the excised patch and ionic currents at different potentials were recorded (Figure 44). G(V) curves for different BK clones (pWT, D364/367A, D894-898N) were constructed at each [Ca^{2+}]i (Figure 44B). The midpoints of these curves

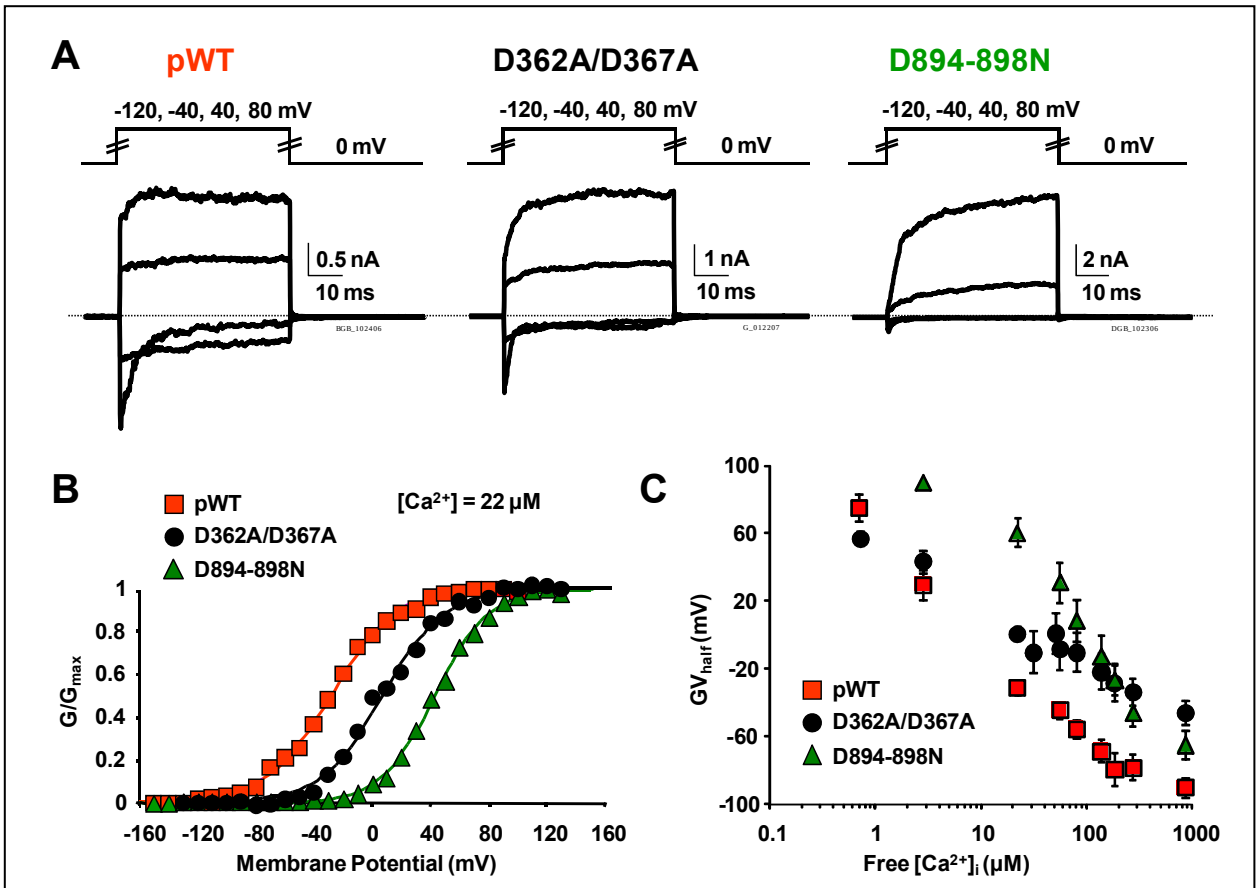

Figure 44. The dependence of GV_{half} *vs.* free [Ca^{2+}]$_i$ when the two BK Ca^{2+} sensors are alternatively neutralized. (A) Representative K^+ current traces were recorded from excised patches of *Xenopus* oocytes in the inside-out configuration expressing pWT, neutralized RCK1 (D362A/D367A) or neutralized RCK2 (D894-898N) channels at free [Ca^{2+}]$_i$ = 22 µM. The voltage protocol is shown above the traces. (B) Normalized G(V) curves from the experiments in A were fit to Boltzmann distributions (lines) to estimate their half activation potential (GV_{half}). (C) Mean GV_{half} *vs.* free [Ca^{2+}]$_i$ plot was constructed from the G(V) curves calculated at different [Ca^{2+}]$_i$ ranging from 0.72 to 830 µM.

(GV_{half}) were plotted versus [Ca^{2+}] to produce calibration curves for the three BK clones used in the Ca-release experiments (Figure 44C). As expected, when one of the two high-affinity Ca^{2+} sensors was impaired, a larger depolarization was necessary to achieve the same degree of channel activation, in agreement with the effects previously observed in WT BK channels (Schreiber and Salkoff, 1997; Xia et al., 2002).The GV_{half} vs [Ca^{2+}] plot was used to estimate [Ca^{2+}]i in the Ca-release experiments by interpolating the GV_{half} before and after UV flashes. These estimated [Ca^{2+}]i were fed into the BK channel model as described in the next section.

A BK channel allosteric model with two high-affinity Ca^{2+} sensors and one voltage sensor per subunit

To quantify the mechanistic interpretation of the experimental results, we fit the data with an allosteric statistical-mechanical model inspired by the seminal Horrigan and Aldrich (HA) model of BK channel activation at steady-state (Horrigan and Aldrich, 2002). The HA model describes the allosteric interactions linking voltage sensing, Ca^{2+} binding and pore opening in BK channels. Since results from the Ca^{2+} photo-release experiments suggest that RCK1 and RCK2 Ca^{2+} sensors employ different allosteric pathways to produce Ca^{2+}-mediated activation, we expanded on the HA model to include two Ca^{2+}-sensing domains (Figure 45). In this model, each Ca^{2+} sensor is capable of interacting with the Pore (allosteric factors C_1 and C_2), with the VSD (allosteric factors E_1 and E_2) and each other (allosteric factor F).

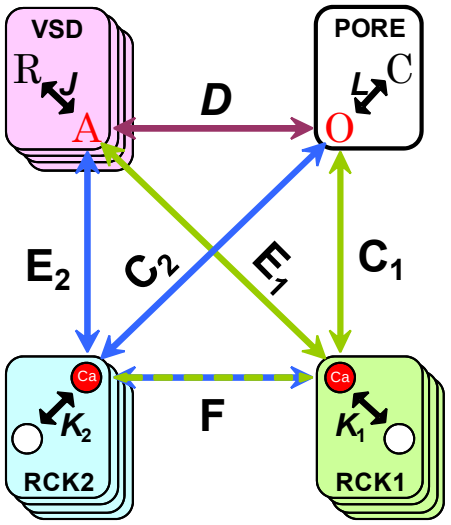

Figure 45. Schematic representation of the allosteric model for BK channel activation. It includes a pore domain and three regulatory domains: the VSD and two Ca^{2+}-sensing domains (RCK1 and RCK2) per subunit. The pore transitions between closed (C) and open (O) states according to the equilibrium constant L; the VSD can be found either in the resting (R) or active (A) state according to equilibrium constant J; Ca^{2+} sensors can exist in unbound or Ca^{2+}-bound states according to equilibrium constants K1 and K2. D, C1, C2, E1, E2 and F are allosteric factors.

Data points (normalized G(V) and F(V) curves) from representative experiments of the three BK channel clones (pWT, RCK1 and RCK2 mutants), each at two Ca^{2+} concentrations (before and after UV photolysis), were simultaneously fit by the model: F(V) data were fit to the model prediction of VSD activation while G(V) data were fit with P_O. As a further constraint, we simultaneously fit averaged values of GV_{half} as a function of [Ca^{2+}] for the three BK channel clones (Figure 45). In fitting the mutant channels, we minimized the number of changing parameters needed to obtain good fits, while constraining the remaining variables to their pWT equivalent. Since it appears that RCK1 retains its

high-affinity Ca^{2+}-binding properties when D362/D367 are neutralized (Yusifov et al., 2010), Kd1 in the RCK1 mutant was constrained to be equal to the corresponding pWT value. Inter-subunit interactions between BK regulatory domains were not included: single-channel studies indicated that such interactions do not play a major role (Niu and Magleby, 2002). $[Ca^{2+}]i$ was estimated by interpolating the GV_{half} value in the plot in Figure 44C, taking advantage of BK intrinsic ability to report $[Ca^{2+}]i$ at the membrane level.

The model parameters that best account for the data are listed in Table 1. The valence of the VSD charge is z_J = 0.6 e^0; the opening of the channel (C-O transition) is also intrinsically voltage-dependent (z_L = 1 e^0), in agreement with previous works (Horrigan and Aldrich, 2002; Ma et al., 2006). During the simultaneous fitting (Figure 46A), the intrinsic Ca^{2+} dissociation constants for RCK1 (Kd_1) and RCK2 (Kd_2) were constrained to the range reported by a recent

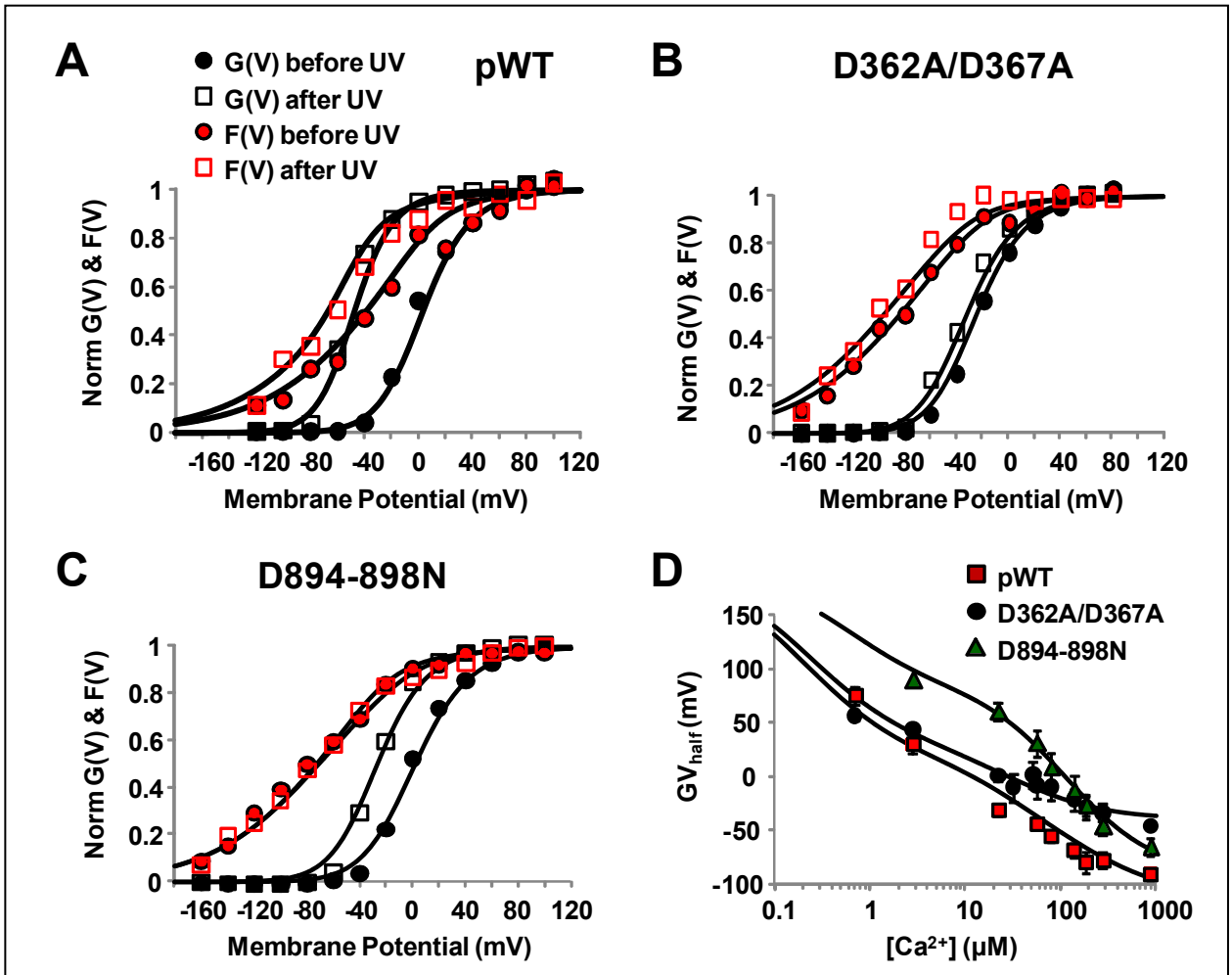

Figure 46. The allosteric model for BK channel activation fits experimental data from three different BK channel mutants. The experimental GV and FV data for pWT (A), RCK1 mutant D362A/D367A (B) and RCK2 mutant D894-898N (C) were fitted simultaneously together with the data points describing the $[Ca^{2+}]$ dependence of the GV_{half} . Continuous lines are the prediction of the BK allosteric model while experimental data points are as in Figures 39B, 40B, 41B, 44C.

study (Sweet and Cox, 2008), resulting in Kd_1 = 10.03 μM and Kd_2 = 2.98 μM for pWT channels. We also found that, in the Ca^{2+}-bound state, RCK1 strongly stabilized VSD activation (E_1 = 10) and, to a lesser extent, the conducting state (C_1 = 2.84). On the other hand, RCK2 efficiently facilitated pore operation (C_2 = 10.41) and exerted a positive cooperativity on VSD activation (E_2 = 2.28). A negative cooperativity was exhibited between the two Ca^{2+}-sensing domains (F = 0.02), as also suggested by a previous investigation (Sweet and Cox, 2008). In the RCK1 mutant channels (Figure 46B), D362/367A mutations abolished the RCK1-Pore cooperativity (C_1 = 1) and slightly affected the allosteric factor F (from 0.02 to 0.06), leaving unaltered the RCK1-VSD interaction. In agreement with the consolidated knowledge that the neutralization of the Ca bowl (D894-898N) impairs high-affinity Ca^{2+}-sensing (Yusifov et al., 2010), the model predicted a marked increase in Kd_2 in the D894-898N mutant (Kd_2 = 4820 μM) (Figure 46C). The allosteric interaction RCK2-Pore (C_2) did not vary compared to the pWT channel. Instead, a negative cooperativity was found between RCK2 and VSD (E_2 = 0.7). In addition, RCK1-RCK2 interaction becomes stronger (F = 11.6).

Table 1. Fitting parameters (for the mutants only parameters different from pWT are reported).

Parameters		**Ca^{2+}-sensing mutations**		
Domain or Interaction		**pWT**	**D362/367A**	**D894-898N**
Pore	z_L (e^0)	1.00		
	V_L (mV)	307		
S4	z_J (e^0)	0.60		
	V_J (mV)	20		
RCK1	Kd_1 (μM)	10.03		
RCK2	Kd_2 (μM)	2.98		4820
S4-Pore	D	3.34		
RCK1-Pore	C_1	2.84	1.00	
RCK1-S4	E_1	10.00		
RCK2-Pore	C_2	10.41		
RCK2-S4	E_2	2.28		0.70
RCK1-RCK2	F	0.02	0.06	11.60

2.D DISCUSSION

BK channels integrate properties of both voltage- and ligand-gated ion channels, a feature that allows them to achieve the fine task of coupling the membrane potential with $[Ca^{2+}]i$ to control key physiological processes such as smooth muscle tone, cochlear hair cell tuning, neuronal excitability, neurotransmitter release, insulin secretion, and oxygen sensing (Fettiplace and Fuchs, 1999; Hu et al., 2001; Salkoff et al., 2006; Braun et al., 2008; Wu and Marx, 2010). The interaction between voltage- and Ca^{2+}-sensing mechanisms was proposed for native BK channels reconstituted in lipid bilayer (Moczydlowski and Latorre, 1983) and further investigated in cloned BK channels, demonstrating the allosteric nature of the dual activation mechanism, synergistically facilitating channel gating (Horrigan and Aldrich, 2002; Horrigan, 2012; Magleby, 2003; Cui et al., 2009; Sweet and Cox, 2008). To investigate how the Ca^{2+}-induced conformational changes of the gating ring at the intracellular portion of the channel can propagate to, and be resolved as, structural rearrangements of the VSD, the voltage-clamp fluorometry technique (Mannuzzu et al., 1996; Cha and Bezanilla, 1997; Gandhi and Olcese, 2008) was combined with the UV-photolysis of a Ca^{2+} cage compound, DM-Nitrophen (Escobar et al., 1997; Ellis-Davies, 2003), to simultaneously trigger the voltage- and Ca^{2+}-dependent activations of BK channels.

The intracellular region of BK channels encompasses two high-affinity Ca^{2+} sensors per subunit (one in RCK1 and one in RCK2 domains). The RCK1 and RCK2 domains are structurally similar (Yusifov et al., 2008; Yusifov et al., 2010; Yuan et al., 2010; Yuan et al., 2011; Wu et al., 2010) and assemble into the ligand-sensitive gating ring complex. However, they share little primary sequence homology (<25%) and are not topologically equivalent within the gating ring super-structure. These underlying differences could account for their apparent functional discrepancy. In fact, their Ca^{2+}-sensing sites differ in several respects, including: structure and relative positions within the gating ring and RCK domains (Figure 29) (Wu et al., 2010; Yuan et al., 2010; Yuan et al., 2011); affinity and selectivity for divalent cations (Zeng et al., 2005); apparent voltage dependence of Ca^{2+}-binding (Sweet and Cox, 2008); and role in epilepsy/dyskinesia-causing BK channel mutants (Yang et al., 2010). Given these established differences, do the two high-affinity Ca^{2+} sensors also exert different contributions to the pore and VSD activations?

In pWT BK channels, the rapid increase of $[Ca^{2+}]i$ by UV-photolysis of DM-Nitrophen induces a conformational change that, originating in the gating ring upon Ca^{2+}-binding, propagates to the VSD, facilitating its activation (Figure 39). Indeed, the purified BK gating ring in solution can undergo Ca^{2+}-driven structural rearrangements resulting in an overall decrease of its hydrodynamic radius (Javaherian et al., 2011). To understand the contribution of each Ca^{2+} sensor, they have been alternatively neutralized such that only one at the time is functional in the BK channel. The impairment of Ca^{2+} sensing in RCK2 (Ca bowl neutralization), but not in RCK1, abolishes the effect of the $[Ca^{2+}]i$ elevation on VSD activation, underlining a functional difference of the two Ca^{2+} sensors.

Using a statistical-mechanical model inspired by the HA model (Horrigan and Aldrich, 2002), but accounting for two distinct Ca^{2+} sensors (Figure 45), we quantified the allosteric interactions between pore, VSD and the two RCK domains. In pWT channels, the model predicts salient

differences in the allosteric coupling between RCK1 and RCK2 with the VSD and the pore (Table 1), suggesting that they are functionally separable, in spite of their structural homology. RCK1 and RCK2 are allosterically coupled by negative cooperativity, such that the activation of one domain disfavors the activation of the other, recapitulating the findings of Sweet & Cox (Sweet and Cox, 2008). The functional impairment of Ca^{2+} sensing either in RCK1 or in RCK2 highlights their functional diversity. In D362A/D367A mutants, a rapid increase in $[Ca^{2+}]i$ significantly facilitates pore and VSD activation (Figure 40), as indicated by the consistent leftward shifts of both G(V) and F(V) curves at the highest $[Ca^{2+}]i$. This effect is likely mediated by intact Ca bowls in RCK2 domains. In the model, the effect of the D362A/D367A mutations is mostly accounted by the loss of cooperativity between RCK1 and the pore (allosteric factor C_1) (Table 1). It is interesting that the model can predict the effects of the D362A/D367A mutations without reducing the intrinsic Ca^{2+} affinity of the RCK1 domain (Kd_1). This prediction would be in agreement with the lack of direct experimental evidence that D362/D367 residues are essential for Ca^{2+} coordination. However, a potential Ca^{2+}-binding site involving D367 and other residues has been proposed based on electrophysiological evidence (Xia et al., 2002) and inference from the gating ring crystal structure (Zhang et al., 2010). Conversely, the neutralization of the Ca bowl abolishes the Ca^{2+}-induced facilitation of the VSD activation: indeed, the F(V) curves were not significantly modified by the Ca^{2+} release (Figure 41B, 42). To account for these experimental data, three model parameters are considerably altered compared to the corresponding pWT values (Table 1), suggesting that the neutralization of the five Asps not only abolishes a high-affinity Ca^{2+}-binding site (Ca bowl) but also alters the energetics of gating ring operation, likely because of a structural perturbation.

Recent work has pointed out an important functional difference between RCK1 and RCK2: Ca^{2+}-binding to the RCK1 domain (but not to RCK2) is voltage-dependent (Sweet and Cox, 2008). To test the validity of our model prediction, we computed the steady-state occupancy of the Ca^{2+}-bound state for RCK1 and RCK2. For a wide range of membrane potentials, the occupancy of RCK1 Ca^{2+}-bound state is voltage-dependent, while RCK2 Ca^{2+}-binding is weakly affected by membrane potential (Figure 47). Thus, in spite of their structural homology, RCK1 and RCK2 domains provide different contribution to the Ca^{2+}-dependent activation of BK channels.

The precise structural basis of the model energetic couplings is as yet unknown. It is possible to speculate that the S6-RCK1 linker, which operates like a spring, connecting the gating ring with the channel pore functionally as well as structurally (Niu et al., 2004), could account for the allosteric factor C_1; Mg^{2+} dynamically coordinated between RCK1 and S4 (Horrigan and Hoshi, 2008; Yang et al., 2008; Chen et al., 2010) could mediate the allosteric factor E_1; in addition, hydrophobic residues between RCK1 and RCK2 (Kim et al., 2006) and properties of the RCK1-RCK2 linker (Lee et al., 2009) could contribute to the allosteric factor F. Mutations in the critical Ca^{2+}-sensing sites of RCK1 and RCK2, in some cases, result in stronger interactions between channel domains (Table 1), even though Ca^{2+} sensitivity and channel activation are impaired. It is possible that these mutations not only impair Ca^{2+} binding, but also could cause subtle structural alterations, which would in turn perturb the free energy transduction to distal regulatory domains.

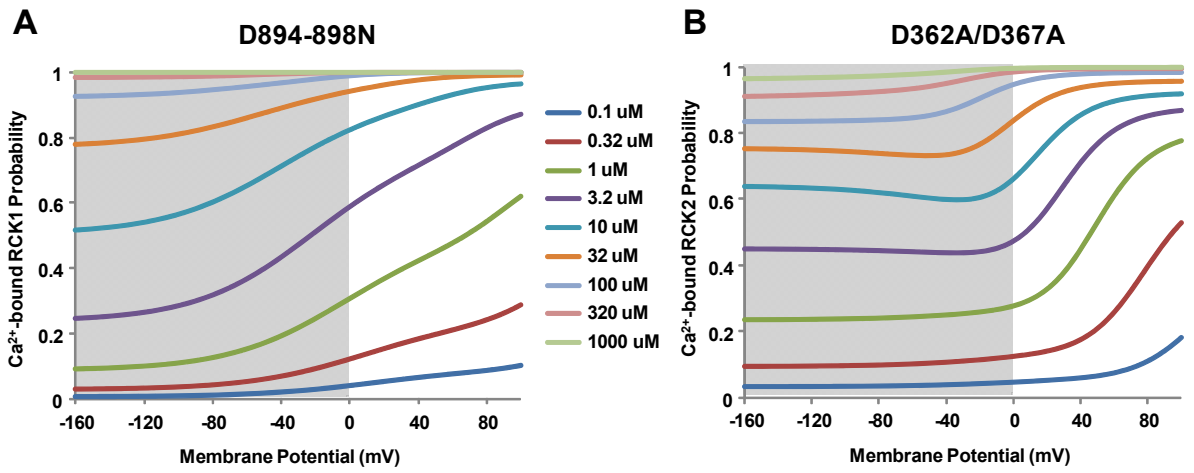

Figure 47. Model predictions of the voltage dependence of the Ca^{2+}-bound state of RCK1 and RCK2. The plots show the steady-state occupancy of the Ca^{2+}-bound state for RCK1 (A) in the D894-898N BK channel and for RCK2 (B) in the D362A/D367A BK channels, as predicted by the model. For a wide range of membrane potentials (grey background), Ca^{2+} binding is strongly voltage-dependent in RCK1 domain (A), but weakly in RCK2 domain (B).

The importance of achieving deeper understanding of BK channel biophysical properties resides in its involvement in several diseases, such as hypertension, epilepsy, schizophrenia and diabetes (Yang et al., 2010; Grimm and Sansom, 2010; Braun et al., 2008). In particular, elucidating the mechanisms underlying the functional coupling between VSD and the two distinct Ca^{2+} sensors is fundamental for the physiology and pathophysiology of excitable cells. For instance, the Slo1 epilepsy/dyskinesia-causing mutation affects Ca^{2+}-dependent activation originating from the Ca^{2+}-binding site in RCK1, but not in RCK2, by altering the coupling mechanism between Ca^{2+} binding and gate opening (Yang et al., 2010).

In summary, the allosteric nature of BK channel Ca^{2+}-dependent activation has been directly probed by optically tracking VSD movements perturbed by Ca^{2+}-binding to the gating ring, under voltage clamp. By investigating channels impaired in high-affinity Ca^{2+}-sensing sites, it is unraveled that the two BK Ca^{2+} sensors are not functionally equivalent: although both contribute to Ca^{2+}-dependent channel activation, the efficiency of the allosteric interactions appears different. A functional Ca Bowl (RCK2) is required to observe the propagation of Ca^{2+}-induced “wave” of rearrangements from the cytoplasmic portion to the transmembrane VSD. The results are fit with a statistical-mechanical allosteric model to quantify the cooperative interactions among the prominent BK regulatory domains.

REFERENCE LIST

1. Adelman,J.P., K.Z.Shen, M.P.Kavanaugh, R.A.Warren, Y.N.Wu, A.Lagrutta, C.T.Bond, and R.A.North. 1992. Calcium-activated potassium channels expressed from cloned complementary DNAs. *Neuron* 9:209-216.

2. Armstrong,C.M. and F.Bezanilla. 1973. Currents related to movement of the gating particles of the sodium channels. *Nature* 242:459-461.

3. Averaimo,S., R.H.Milton, M.R.Duchen, and M.Mazzanti. 2010. Chloride intracellular channel 1 (CLIC1): Sensor and effector during oxidative stress. *FEBS Lett.* 584:2076-2084.

4. Baccelli,I. and A.Trumpp. 2012. The evolving concept of cancer and metastasis stem cells. *J. Cell Biol.* 198:281-293.

5. Bao,L., C.Kaldany, E.C.Holmstrand, and D.H.Cox. 2004. Mapping the BKCa channel's "Ca2+ bowl": side-chains essential for Ca2+ sensing. *J Gen. Physiol* 123:475-489.

6. Bao,L., A.M.Rapin, E.C.Holmstrand, and D.H.Cox. 2002. Elimination of the BK(Ca) channel's high-affinity Ca(2+) sensitivity. *J Gen. Physiol* 120:173-189.

7. Bao,S., Q.Wu, R.E.McLendon, Y.Hao, Q.Shi, A.B.Hjelmeland, M.W.Dewhirst, D.D.Bigner, and J.N.Rich. 2006. Glioma stem cells promote radioresistance by preferential activation of the DNA damage response. *Nature* 444:756-760.

8. Barnett,S.C., L.Robertson, D.Graham, D.Allan, and R.Rampling. 1998. Oligodendrocyte-type-2 astrocyte (O-2A) progenitor cells transformed with c-myc and H-ras form high-grade glioma after stereotactic injection into the rat brain. *Carcinogenesis* 19:1529-1537.

9. Berdiev,B.K., J.Xia, L.A.McLean, J.M.Markert, G.Y.Gillespie, T.B.Mapstone, A.P.Naren, B.Jovov, J.K.Bubien, H.L.Ji, C.M.Fuller, K.L.Kirk, and D.J.Benos. 2003. Acid-sensing ion channels in malignant gliomas. *J. Biol. Chem.* 278:15023-15034.

10. Berkefeld,H., B.Fakler, and U.Schulte. 2010. Ca2+-activated K+ channels: from protein complexes to function. *Physiol Rev.* 90:1437-1459.

11. Bezanilla,F. 2008. How membrane proteins sense voltage. *Nat Rev Mol Cell Biol* 9:323-332.

12. Bian,S., I.Favre, and E.Moczydlowski. 2001. Ca2+-binding activity of a COOH-terminal fragment of the Drosophila BK channel involved in Ca2+-dependent activation. *Proc. Natl. Acad. Sci. U. S A* 98:4776-4781.

13. Bonnet,D. and J.E.Dick. 1997. Human acute myeloid leukemia is organized as a hierarchy that originates from a primitive hematopoietic cell. *Nat. Med.* 3:730-737.

14. BOYDEN,S. 1962. The chemotactic effect of mixtures of antibody and antigen on polymorphonuclear leucocytes. *J. Exp. Med.* 115:453-466.

15. Braun,M., R.Ramracheya, M.Bengtsson, Q.Zhang, J.Karanauskaite, C.Partridge, P.R.Johnson, and P.Rorsman. 2008. Voltage-gated ion channels in human pancreatic beta-cells: electrophysiological characterization and role in insulin secretion. *Diabetes* 57:1618-1628.

16. Calabrese,C., H.Poppleton, M.Kocak, T.L.Hogg, C.Fuller, B.Hamner, E.Y.Oh, M.W.Gaber, D.Finklestein, M.Allen, A.Frank, I.T.Bayazitov, S.S.Zakharenko, A.Gajjar, A.Davidoff, and R.J.Gilbertson. 2007. A perivascular niche for brain tumor stem cells. *Cancer Cell* 11:69-82.

17. Cha,A. and F.Bezanilla. 1997. Characterizing voltage-dependent conformational changes in the Shaker K+ channel with fluorescence. *Neuron* 19:1127-1140.

18. Chamberlain,M.C. 2010. Emerging clinical principles on the use of bevacizumab for the treatment of malignant gliomas. *Cancer* 116:3988-3999.

19. Charles,N. and E.C.Holland. 2010. The perivascular niche microenvironment in brain tumor progression. *Cell Cycle* 9:3012-3021.

20. Chen,C.D., C.S.Wang, Y.H.Huang, K.Y.Chien, Y.Liang, W.J.Chen, and K.H.Lin. 2007. Overexpression of CLIC1 in human gastric carcinoma and its clinicopathological significance. *Proteomics.* 7:155-167.

21. Chen,J., R.M.McKay, and L.F.Parada. 2012. Malignant glioma: lessons from genomics, mouse models, and stem cells. *Cell* 149:36-47.

22. Chen,R.-S., Y.Geng, and K.L.Magleby. 2010. Voltage Sensor Activation Facilitates Magensium-gated Channel Opening in BK Channels. *Biophys. J* 98:916a.

23. Contreras,G.F., A.Neely, O.Alvarez, C.Gonzalez, and R.Latorre. 2012. Modulation of BK channel voltage gating by different auxiliary beta subunits. *Proc. Natl. Acad. Sci. U. S. A* 109:18991-18996.

24. Cowmeadow,R.B., H.R.Krishnan, A.Ghezzi, Y.M.Al'Hasan, Y.Z.Wang, and N.S.Atkinson. 2006. Ethanol tolerance caused by slowpoke induction in Drosophila. *Alcohol Clin. Exp. Res.* 30:745-753.

25. Cuddapah,V.A. and H.Sontheimer. 2011. Ion channels and transporters [corrected] in cancer. 2. Ion channels and the control of cancer cell migration. *Am. J. Physiol Cell Physiol* 301:C541-C549.

26. Cui,J., H.Yang, and U.S.Lee. 2009. Molecular mechanisms of BK channel activation. *Cell Mol Life Sci.* 66:852-875.

27. del,S.A., C.J.Tsai, B.Ma, and R.Nussinov. 2009. The origin of allosteric functional modulation: multiple pre-existing pathways. *Structure.* 17:1042-1050.

28. Denysenko,T., L.Gennero, M.A.Roos, A.Melcarne, C.Juenemann, G.Faccani, I.Morra, G.Cavallo, S.Reguzzi, G.Pescarmona, and A.Ponzetto. 2010. Glioblastoma cancer stem cells: heterogeneity, microenvironment and related therapeutic strategies. *Cell Biochem. Funct.* 28:343-351.

29. Dey,M., I.V.Ulasov, and M.S.Lesniak. 2010. Virotherapy against malignant glioma stem cells. *Cancer Lett.* 289:1-10.

30. Diaz,L., P.Meera, J.Amigo, E.Stefani, O.Alvarez, L.Toro, and R.Latorre. 1998. Role of the S4 segment in a voltage-dependent calcium-sensitive potassium (hSlo) channel. *J Biol Chem.* 273:32430-32436.

31. Du,W., J.F.Bautista, H.Yang, A.ez-Sampedro, S.A.You, L.Wang, P.Kotagal, H.O.Luders, J.Shi, J.Cui, G.B.Richerson, and Q.K.Wang. 2005. Calcium-sensitive potassium channelopathy in human epilepsy and paroxysmal movement disorder. *Nat. Genet.* 37:733-738.

32. Duran,C., C.H.Thompson, Q.Xiao, and H.C.Hartzell. 2010. Chloride channels: often enigmatic, rarely predictable. *Annu. Rev. Physiol* 72:95-121.

33. Edwards,J.C. and C.R.Kahl. 2010. Chloride channels of intracellular membranes. *FEBS Lett.* 584:2102-2111.

34. Ellis-Davies,G.C. 2003. Development and application of caged calcium. *Methods Enzymol.* 360:226-238.

35. Ellis-Davies,G.C. 2007. Caged compounds: photorelease technology for control of cellular chemistry and physiology. *Nat. Methods* 4:619-628.

36. Escobar,A.L., P.Velez, A.M.Kim, F.Cifuentes, M.Fill, and J.L.Vergara. 1997. Kinetic properties of DM-nitrophen and calcium indicators: rapid transient response to flash photolysis. *Pflugers Arch.* 434:615-631.

37. Faas,G.C. and I.Mody. 2012. Measuring the kinetics of calcium binding proteins with flash photolysis. *Biochim. Biophys. Acta* 1820:1195-1204.

38. Fettiplace,R. and P.A.Fuchs. 1999. Mechanisms of hair cell tuning. *Annu Rev Physiol* 61:809-834.

39. Fodor,A.A. and R.W.Aldrich. 2004. On evolutionary conservation of thermodynamic coupling in proteins. *J Biol Chem.* 279:19046-19050.

40. Fraser,S.P. and L.A.Pardo. 2008. Ion channels: functional expression and therapeutic potential in cancer. Colloquium on Ion Channels and Cancer. *EMBO Rep.* 9:512-515.

41. Friedl,P. and D.Gilmour. 2009. Collective cell migration in morphogenesis, regeneration and cancer. *Nat. Rev. Mol. Cell Biol.* 10:445-457.

42. Furnari,F.B., T.Fenton, R.M.Bachoo, A.Mukasa, J.M.Stommel, A.Stegh, W.C.Hahn, K.L.Ligon, D.N.Louis, C.Brennan, L.Chin, R.A.DePinho, and W.K.Cavenee. 2007. Malignant astrocytic glioma: genetics, biology, and paths to treatment. *Genes Dev.* 21:2683-2710.

43. Galli,R., E.Binda, U.Orfanelli, B.Cipelletti, A.Gritti, V.S.De, R.Fiocco, C.Foroni, F.Dimeco, and A.Vescovi. 2004. Isolation and characterization of tumorigenic, stem-like neural precursors from human glioblastoma. *Cancer Res.* 64:7011-7021.

44. Gandhi,C.S. and R.Olcese. 2008. The Voltage-Clamp Fluorometry Technique. *In* Methods in Molecular Biology, Potassium Channels. J.D.Lippiat, editor. Humana Press, Totowa. 213-231.

45. Goodchild,S.C., M.W.Howell, N.M.Cordina, D.R.Littler, S.N.Breit, P.M.Curmi, and L.J.Brown. 2009. Oxidation promotes insertion of the CLIC1 chloride intracellular channel into the membrane. *Eur. Biophys. J.* 39:129-138.

46. Goodey,N.M. and S.J.Benkovic. 2008. Allosteric regulation and catalysis emerge via a common route. *Nat. Chem. Biol.* 4:474-482.

47. Grimm,P.R. and S.C.Sansom. 2010. BK channels and a new form of hypertension. *Kidney Int.* 78:956-962.

48. Gu,N., K.Vervaeke, and J.F.Storm. 2007. BK potassium channels facilitate high-frequency firing and cause early spike frequency adaptation in rat CA1 hippocampal pyramidal cells. *J. Physiol* 580:859-882.

49. Haas,B.R. and H.Sontheimer. 2010. Inhibition of the Sodium-Potassium-Chloride Cotransporter Isoform-1 reduces glioma invasion. *Cancer Res.* 70:5597-5606.

50. Habela,C.W., N.J.Ernest, A.F.Swindall, and H.Sontheimer. 2009. Chloride accumulation drives volume dynamics underlying cell proliferation and migration. *J. Neurophysiol.* 101:750-757.

51. Hamill,O.P., A.Marty, E.Neher, B.Sakmann, and F.J.Sigworth. 1981. Improved patch-clamp techniques for high-resolution current recording from cells and cell-free membrane patches. *Pflugers Arch.* 391:85-100.

52. Hendrich,J., P.Alvarez, X.Chen, and J.D.Levine. 2012. GDNF induces mechanical hyperalgesia in muscle by reducing I(BK) in isolectin B4-positive nociceptors. *Neuroscience* 219:204-213.

53. Horn,R. and J.Patlak. 1980. Single channel currents from excised patches of muscle membrane. *Proc. Natl. Acad. Sci. U. S. A* 77:6930-6934.

54. Horrigan,F.T. 2012. Perspectives on: Conformational coupling in ion channels: Conformational coupling in BK potassium channels. *J. Gen. Physiol* 140:625-634.

55. Horrigan,F.T. and R.W.Aldrich. 2002. Coupling between voltage sensor activation, Ca2+ binding and channel opening in large conductance (BK) potassium channels. *J Gen. Physiol* 120:267-305.

56. Horrigan,F.T. and R.W.Aldrich. 1999. Allosteric voltage gating of potassium channels II. Mslo channel gating charge movement in the absence of Ca(2+). *J Gen. Physiol* 114:305-336.

57. Horrigan,F.T., J.Cui, and R.W.Aldrich. 1999. Allosteric voltage gating of potassium channels I. Mslo ionic currents in the absence of Ca(2+). *J Gen. Physiol* 114:277-304.

58. Horrigan,F.T., S.H.Heinemann, and T.Hoshi. 2005. Heme regulates allosteric activation of the Slo1 BK channel. *J Gen. Physiol* 126:7-21.

59. Horrigan,F.T. and T.Hoshi. 2008. Integration of an electric-metal sensory experience in the Slo1 BK channel. *Nat Struct. Mol Biol* 15:1130-1132.

60. Horrigan,F.T. and Z.Ma. 2008. Mg2+ enhances voltage sensor/gate coupling in BK channels. *J Gen. Physiol* 131:13-32.

61. Hou,S., S.H.Heinemann, and T.Hoshi. 2009. Modulation of BKCa channel gating by endogenous signaling molecules. *Physiology. (Bethesda.)* 24:26-35.

62. Hu,H., L.R.Shao, S.Chavoshy, N.Gu, M.Trieb, R.Behrens, P.Laake, O.Pongs, H.G.Knaus, O.P.Ottersen, and J.F.Storm. 2001. Presynaptic Ca2+-activated K+ channels in glutamatergic hippocampal terminals and their role in spike repolarization and regulation of transmitter release. *J Neurosci.* 21:9585-9597.

63. Huse,J.T. and E.C.Holland. 2010. Targeting brain cancer: advances in the molecular pathology of malignant glioma and medulloblastoma. *Nat. Rev. Cancer* 10:319-331.

64. Javaherian,A.D., T.Yusifov, A.Pantazis, S.Franklin, C.S.Gandhi, and R.Olcese. 2011. Metal-driven operation of the human large-conductance voltage- and Ca2+-dependent potassium channel (BK) gating ring apparatus. *J. Biol. Chem.* 286:20701-20709.

65. Jensen,M.O., V.Jogini, D.W.Borhani, A.E.Leffler, R.O.Dror, and D.E.Shaw. 2012. Mechanism of voltage gating in potassium channels. *Science* 336:229-233.

66. Jentsch,T.J., V.Stein, F.Weinreich, and A.A.Zdebik. 2002. Molecular structure and physiological function of chloride channels. *Physiol Rev.* 82:503-568.

67. Jiang,Y., A.Lee, J.Chen, V.Ruta, M.Cadene, B.T.Chait, and R.MacKinnon. 2003a. X-ray structure of a voltage-dependent K+ channel. *Nature* 423:33-41.

68. Jiang,Y., V.Ruta, J.Chen, A.Lee, and R.MacKinnon. 2003b. The principle of gating charge movement in a voltage-dependent K+ channel. *Nature* 423:42-48.

69. Jiang,Z., M.Wallner, P.Meera, and L.Toro. 1999. Human and rodent MaxiK channel beta-subunit genes: cloning and characterization. *Genomics* 55:57-67.

70. Jones,T.S. and E.C.Holland. 2010. Molecular Pathogenesis of Malignant Glial Tumors. *Toxicol. Pathol.*

71. Kang,M.K. and S.K.Kang. 2008. Pharmacologic blockade of chloride channel synergistically enhances apoptosis of chemotherapeutic drug-resistant cancer stem cells. *Biochem. Biophys. Res. Commun.* 373:539-544.

72. Kim,H.J., H.H.Lim, S.H.Rho, S.H.Eom, and C.S.Park. 2006. Hydrophobic interface between two regulators of K+ conductance domains critical for calcium-dependent activation of large conductance Ca2+-activated K+ channels. *J Biol Chem.* 281:38573-38581.

73. Kohout,S.C., M.H.Ulbrich, S.C.Bell, and E.Y.Isacoff. 2008. Subunit organization and functional transitions in Ci-VSP. *Nat Struct. Mol Biol* 15:106-108.

74. Koval,O.M., Y.Fan, and B.S.Rothberg. 2007. A role for the S0 transmembrane segment in voltage-dependent gating of BK channels. *J. Gen. Physiol* 129:209-220.

75. Kunzelmann,K. 2005. Ion channels and cancer. *J. Membr. Biol.* 205:159-173.

76. Lakowicz,J.R. 2006. Principles of Fluorescence Spectroscopy. 3rd ed. Springer, New York, NY. -954 pp.

77. Lancaster,B., H.Hu, G.M.Ramakers, and J.F.Storm. 2001. Interaction between synaptic excitation and slow afterhyperpolarization current in rat hippocampal pyramidal cells. *J. Physiol* 536:809-823.

78. Landry,D., S.Sullivan, M.Nicolaides, C.Redhead, A.Edelman, M.Field, Q.al-Awqati, and J.Edwards. 1993. Molecular cloning and characterization of p64, a chloride channel protein from kidney microsomes. *J. Biol. Chem.* 268:14948-14955.

79. Latorre,R., F.J.Morera, and C.Zaelzer. 2010. Allosteric Interactions and the Modular Nature of the Voltage- and Ca2+ -activated (BK) Channels. *J. Physiol*.

80. Lee,J.H., H.J.Kim, H.D.Kim, B.C.Lee, J.S.Chun, and C.S.Park. 2009. Modulation of the conductance-voltage relationship of the BK(Ca) channel by shortening the cytosolic loop connecting two RCK domains. *Biophys. J* 97:730-737.

81. Lee,U.S. and J.Cui. 2010. BK channel activation: structural and functional insights. *Trends Neurosci.* 33:415-423.

82. Lefranc,F., J.Brotchi, and R.Kiss. 2005. Possible future issues in the treatment of glioblastomas: special emphasis on cell migration and the resistance of migrating glioblastoma cells to apoptosis. *J. Clin. Oncol.* 23:2411-2422.

83. Li,R.K., J.Zhang, Y.H.Zhang, M.L.Li, M.Wang, and J.W.Tang. 2012. Chloride intracellular channel 1 is an important factor in the lymphatic metastasis of hepatocarcinoma. *Biomed. Pharmacother.* 66:167-172.

84. Littler,D.R., S.J.Harrop, W.D.Fairlie, L.J.Brown, G.J.Pankhurst, S.Pankhurst, M.Z.DeMaere, T.J.Campbell, A.R.Bauskin, R.Tonini, M.Mazzanti, S.N.Breit, and P.M.Curmi. 2004. The intracellular chloride ion channel protein CLIC1 undergoes a redox-controlled structural transition. *J. Biol. Chem.* 279:9298-9305.

85. Littler,D.R., S.J.Harrop, S.C.Goodchild, J.M.Phang, A.V.Mynott, L.Jiang, S.M.Valenzuela, M.Mazzanti, L.J.Brown, S.N.Breit, and P.M.Curmi. 2010. The enigma of the CLIC proteins: Ion channels, redox proteins, enzymes, scaffolding proteins? *FEBS Lett.* 584:2093-2101.

86. Liu,G., X.Niu, R.S.Wu, N.Chudasama, Y.Yao, X.Jin, R.Weinberg, S.I.Zakharov, H.Motoike, S.O.Marx, and A.Karlin. 2010. Location of modulatory {beta} subunits in BK potassium channels. *J. Gen. Physiol*.

87. Liu,X., Y.Chang, P.H.Reinhart, H.Sontheimer, and Y.Chang. 2002. Cloning and characterization of glioma BK, a novel BK channel isoform highly expressed in human glioma cells. *J. Neurosci.* 22:1840-1849.

88. Long,S.B., E.B.Campbell, and R.MacKinnon. 2005. Voltage sensor of Kv1.2: structural basis of electromechanical coupling. *Science* 309:903-908.

89. Long,S.B., X.Tao, E.B.Campbell, and R.MacKinnon. 2007. Atomic structure of a voltage-dependent K+ channel in a lipid membrane-like environment. *Nature* 450:376-382.

90. Lu,R., A.Alioua, Y.Kumar, M.Eghbali, E.Stefani, and L.Toro. 2006. MaxiK channel partners: physiological impact. *J Physiol* 570:65-72.

91. Ma,Z., X.J.Lou, and F.T.Horrigan. 2006. Role of charged residues in the S1-S4 voltage sensor of BK channels. *J Gen. Physiol* 127:309-328.

92. Magleby,K.L. 2003. Gating mechanism of BK (Slo1) channels: so near, yet so far. *J Gen. Physiol* 121:81-96.

93. Maher,E.A., F.B.Furnari, R.M.Bachoo, D.H.Rowitch, D.N.Louis, W.K.Cavenee, and R.A.DePinho. 2001. Malignant glioma: genetics and biology of a grave matter. *Genes Dev.* 15:1311-1333.

94. Manjunath,N., H.Wu, S.Subramanya, and P.Shankar. 2009. Lentiviral delivery of short hairpin RNAs. *Adv. Drug Deliv. Rev.* 61:732-745.

95. Mannuzzu,L.M., M.M.Moronne, and E.Y.Isacoff. 1996. Direct physical measure of conformational rearrangement underlying potassium channel gating. *Science* 271:213-216.

96. Mantovani,A. 2009. Cancer: Inflaming metastasis. *Nature* 457:36-37.

97. McCoy,E. and H.Sontheimer. 2007. Expression and function of water channels (aquaporins) in migrating malignant astrocytes. *Glia* 55:1034-1043.

98. Meera,P., M.Wallner, M.Song, and L.Toro. 1997. Large conductance voltage- and calcium-dependent K+ channel, a distinct member of voltage-dependent ion channels with seven N-terminal transmembrane segments (S0-S6), an extracellular N terminus, and an intracellular (S9-S10) C terminus. *Proc. Natl. Acad. Sci. U. S A* 94:14066-14071.

99. Menon,S.G. and P.C.Goswami. 2007. A redox cycle within the cell cycle: ring in the old with the new. *Oncogene* 26:1101-1109.

100. Meredith,A.L., S.W.Wiler, B.H.Miller, J.S.Takahashi, A.A.Fodor, N.F.Ruby, and R.W.Aldrich. 2006. BK calcium-activated potassium channels regulate circadian behavioral rhythms and pacemaker output. *Nat Neurosci.* 9:1041-1049.

101. Milton,R.H., R.Abeti, S.Averaimo, S.DeBiasi, L.Vitellaro, L.Jiang, P.M.Curmi, S.N.Breit, M.R.Duchen, and M.Mazzanti. 2008. CLIC1 function is required for beta-amyloid-induced generation of reactive oxygen species by microglia. *J. Neurosci.* 28:11488-11499.

102. Moczydlowski,E. and R.Latorre. 1983. Gating kinetics of Ca2+-activated K+ channels from rat muscle incorporated into planar lipid bilayers. Evidence for two voltage-dependent Ca2+ binding reactions. *J Gen. Physiol* 82:511-542.

103. MONOD,J. and F.JACOB. 1961. Teleonomic mechanisms in cellular metabolism, growth, and differentiation. *Cold Spring Harb. Symp. Quant. Biol.* 26:389-401.

104. MONOD,J., J.WYMAN, and J.P.CHANGEUX. 1965. ON THE NATURE OF ALLOSTERIC TRANSITIONS: A PLAUSIBLE MODEL. *J. Mol. Biol.* 12:88-118.

105. Morange,M. 2012. What history tells us. XXVII. A new life for allostery. *J. Biosci.* 37:13-17.

106. Muller,A., M.Kukley, M.Uebachs, H.Beck, and D.Dietrich. 2007. Nanodomains of single Ca2+ channels contribute to action potential repolarization in cortical neurons. *J. Neurosci.* 27:483-495.

107. Murata,Y., H.Iwasaki, M.Sasaki, K.Inaba, and Y.Okamura. 2005. Phosphoinositide phosphatase activity coupled to an intrinsic voltage sensor. *Nature* 435:1239-1243.

108. Murzin,A.G. 2008. Biochemistry. Metamorphic proteins. *Science* 320:1725-1726.

109. Nduom,E.K., C.G.Hadjipanayis, and E.G.Van Meir. 2012. Glioblastoma cancer stem-like cells: implications for pathogenesis and treatment. *Cancer J.* 18:100-106.

110. Neher,E. and B.Sakmann. 1976. Single-channel currents recorded from membrane of denervated frog muscle fibres. *Nature* 260:799-802.

111. Neher,E. and B.Sakmann. 1992. The patch clamp technique. *Sci. Am.* 266:44-51.

112. Nelson,M.T. and J.M.Quayle. 1995. Physiological roles and properties of potassium channels in arterial smooth muscle. *Am. J Physiol* 268:C799-C822.

113. Niu,X. and K.L.Magleby. 2002. Stepwise contribution of each subunit to the cooperative activation of BK channels by Ca2+. *Proc. Natl. Acad. Sci. U. S A* 99:11441-11446.

114. Niu,X., X.Qian, and K.L.Magleby. 2004. Linker-gating ring complex as passive spring and Ca(2+)-dependent machine for a voltage- and Ca(2+)-activated potassium channel. *Neuron* 42:745-756.

115. Noda,M., T.Ikeda, H.Suzuki, H.Takeshima, T.Takahashi, M.Kuno, and S.Numa. 1986. Expression of functional sodium channels from cloned cDNA. *Nature* 322:826-828.

116. Novarino,G., C.Fabrizi, R.Tonini, M.A.Denti, F.Malchiodi-Albedi, G.M.Lauro, B.Sacchetti, S.Paradisi, A.Ferroni, P.M.Curmi, S.N.Breit, and M.Mazzanti. 2004. Involvement of the intracellular ion channel CLIC1 in microglia-mediated beta-amyloid-induced neurotoxicity. *J. Neurosci.* 24:5322-5330.

117. Ortensi,B., D.Osti, S.Pellegatta, F.Pisati, P.Brescia, L.Fornasari, D.Levi, P.Gaetani, P.Colombo, A.Ferri, S.Nicolis, G.Finocchiaro, and G.Pelicci. 2012. Rai is a new regulator of neural progenitor migration and glioblastoma invasion. *Stem Cells* 30:817-832.

118. Pani,G., T.Galeotti, and P.Chiarugi. 2010. Metastasis: cancer cell's escape from oxidative stress. *Cancer Metastasis Rev.* 29:351-378.

119. Pantazis,A., V.Gudzenko, N.Savalli, D.Sigg, and R.Olcese. 2010a. Operation of the voltage sensor of a human voltage- and Ca2+-activated K+ channel. *Proc. Natl. Acad. Sci. U. S A* 107:4459-4464.

120. Pantazis,A., A.P.Kohanteb, and R.Olcese. 2010b. Relative motion of transmembrane segments S0 and S4 during voltage sensor activation in the human BK(Ca) channel. *J. Gen. Physiol* 136:645-657.

121. Pantazis,A. and R.Olcese. 2012. Relative transmembrane segment rearrangements during BK channel activation resolved by structurally assigned fluorophore-quencher pairing. *J. Gen. Physiol* 140:207-218.

122. Parachikova,A., M.G.Agadjanyan, D.H.Cribbs, M.Blurton-Jones, V.Perreau, J.Rogers, T.G.Beach, and C.W.Cotman. 2007. Inflammatory changes parallel the early stages of Alzheimer disease. *Neurobiol. Aging* 28:1821-1833.

123. Paradisi,S., A.Matteucci, C.Fabrizi, M.A.Denti, R.Abeti, S.N.Breit, F.Malchiodi-Albedi, and M.Mazzanti. 2008. Blockade of chloride intracellular ion channel 1 stimulates Abeta phagocytosis. *J. Neurosci. Res.* 86:2488-2498.

124. Petersen,O.H. and Y.Maruyama. 1984. Calcium-activated potassium channels and their role in secretion. *Nature* 307:693-696.

125. Petrova,D.T., A.R.Asif, V.W.Armstrong, I.Dimova, S.Toshev, N.Yaramov, M.Oellerich, and D.Toncheva. 2008. Expression of chloride intracellular channel protein 1 (CLIC1) and tumor protein D52 (TPD52) as potential biomarkers for colorectal cancer. *Clin. Biochem.* 41:1224-1236.

126. Prevarskaya,N., R.Skryma, and Y.Shuba. 2010. Ion channels and the hallmarks of cancer. *Trends Mol. Med.* 16:107-121.

127. Qiu,M.R., L.Jiang, K.I.Matthaei, S.M.Schoenwaelder, T.Kuffner, P.Mangin, J.E.Joseph, J.Low, D.Connor, S.M.Valenzuela, P.M.Curmi, L.J.Brown, M.Mahaut-Smith, S.P.Jackson, and S.N.Breit. 2010. Generation and characterization of mice with null mutation of the chloride intracellular channel 1 gene. *Genesis.* 48:127-136.

128. Ramsey,I.S., M.M.Moran, J.A.Chong, and D.E.Clapham. 2006. A voltage-gated proton-selective channel lacking the pore domain. *Nature* 440:1213-1216.

129. Redhead,C.R., A.E.Edelman, D.Brown, D.W.Landry, and Q.al-Awqati. 1992. A ubiquitous 64-kDa protein is a component of a chloride channel of plasma and intracellular membranes. *Proc. Natl. Acad. Sci. U. S. A* 89:3716-3720.

130. Reya,T., S.J.Morrison, M.F.Clarke, and I.L.Weissman. 2001. Stem cells, cancer, and cancer stem cells. *Nature* 414:105-111.

131. Reynolds,B.A. and S.Weiss. 1992. Generation of neurons and astrocytes from isolated cells of the adult mammalian central nervous system. *Science* 255:1707-1710.

132. Rothberg,B.S. and K.L.Magleby. 1999. Gating kinetics of single large-conductance Ca2+-activated K+ channels in high Ca2+ suggest a two-tiered allosteric gating mechanism. *J Gen. Physiol* 114:93-124.

133. Sakmann,B. and E.Neher. 1984. Patch clamp techniques for studying ionic channels in excitable membranes. *Annu. Rev. Physiol* 46:455-472.

134. Salkoff,L., A.Butler, G.Ferreira, C.Santi, and A.Wei. 2006. High-conductance potassium channels of the SLO family. *Nat Rev Neurosci.* 7:921-931.

135. Sanai,N., A.varez-Buylla, and M.S.Berger. 2005. Neural stem cells and the origin of gliomas. *N. Engl. J. Med.* 353:811-822.

136. Sasaki,M., M.Takagi, and Y.Okamura. 2006. A voltage sensor-domain protein is a voltage-gated proton channel. *Science* 312:589-592.

137. Savalli,N., A.Kondratiev, S.B.de Quintana, L.Toro, and R.Olcese. 2007. Modes of operation of the BKCa channel beta2 subunit. *J Gen. Physiol* 130:117-131.

138. Savalli,N., A.Kondratiev, L.Toro, and R.Olcese. 2006. Voltage-dependent conformational changes in human Ca(2+)- and voltage-activated K(+) channel, revealed by voltage-clamp fluorometry. *Proc. Natl. Acad. Sci. U. S A* 103:12619-12624.

139. Schreiber,M. and L.Salkoff. 1997. A novel calcium-sensing domain in the BK channel. *Biophys. J* 73:1355-1363.

140. Schwab,A. 2001. Function and spatial distribution of ion channels and transporters in cell migration. *Am. J. Physiol Renal Physiol* 280:F739-F747.

141. Schwab,A., A.Fabian, P.J.Hanley, and C.Stock. 2012. Role of ion channels and transporters in cell migration. *Physiol Rev.* 92:1865-1913.

142. Seibold,M.A., B.Wang, C.Eng, G.Kumar, K.B.Beckman, S.Sen, S.Choudhry, K.Meade, M.Lenoir, H.G.Watson, S.Thyne, L.K.Williams, R.Kumar, K.B.Weiss, L.C.Grammer, P.C.Avila, R.P.Schleimer, E.G.Burchard, and R.Brenner. 2008. An african-specific functional polymorphism in KCNMB1 shows sex-specific association with asthma severity. *Hum. Mol. Genet.* 17:2681-2690.

143. Shen,K.Z., A.Lagrutta, N.W.Davies, N.B.Standen, J.P.Adelman, and R.A.North. 1994. Tetraethylammonium block of Slowpoke calcium-activated potassium channels expressed in Xenopus oocytes: evidence for tetrameric channel formation. *Pflugers Arch.* 426:440-445.

144. Shi,J. and J.Cui. 2001. Intracellular Mg(2+) enhances the function of BK-type Ca(2+)-activated K(+) channels. *J Gen. Physiol* 118:589-606.

145. Shi,J., G.Krishnamoorthy, Y.Yang, L.Hu, N.Chaturvedi, D.Harilal, J.Qin, and J.Cui. 2002. Mechanism of magnesium activation of calcium-activated potassium channels. *Nature* 418:876-880.

146. Singh,H. 2010. Two decades with dimorphic Chloride Intracellular Channels (CLICs). *FEBS Lett.* 584:2112-2121.

147. Singh,H. and R.H.Ashley. 2006. Redox regulation of CLIC1 by cysteine residues associated with the putative channel pore. *Biophys. J.* 90:1628-1638.

148. Singh,H., M.A.Cousin, and R.H.Ashley. 2007. Functional reconstitution of mammalian 'chloride intracellular channels' CLIC1, CLIC4 and CLIC5 reveals differential regulation by cytoskeletal actin. *FEBS J.* 274:6306-6316.

149. Singh,S.K., C.Hawkins, I.D.Clarke, J.A.Squire, J.Bayani, T.Hide, R.M.Henkelman, M.D.Cusimano, and P.B.Dirks. 2004. Identification of human brain tumour initiating cells. *Nature* 432:396-401.

150. Sontheimer,H. 2008. An unexpected role for ion channels in brain tumor metastasis. *Exp. Biol. Med. (Maywood.)* 233:779-791.

151. Stefani,E. and F.Bezanilla. 1998. Cut-open oocyte voltage-clamp technique. *Methods Enzymol.* 293:300-318.

152. Stefani,E., M.Ottolia, F.Noceti, R.Olcese, M.Wallner, R.Latorre, and L.Toro. 1997. Voltage-controlled gating in a large conductance Ca2+-sensitive K+channel (hslo). *Proc. Natl. Acad. Sci. U. S A* 94:5427-5431.

153. Stiles,C.D. and D.H.Rowitch. 2008. Glioma stem cells: a midterm exam. *Neuron* 58:832-846.

154. Sun,X.P., B.Yazejian, and A.D.Grinnell. 2004. Electrophysiological properties of BK channels in Xenopus motor nerve terminals. *J Physiol* 557:207-228.

155. Swartz,K.J. 2008. Sensing voltage across lipid membranes. *Nature* 456:891-897.

156. Sweet,T.B. and D.H.Cox. 2008. Measurements of the BKCa channel's high-affinity Ca2+ binding constants: effects of membrane voltage. *J Gen. Physiol* 132:491-505.

157. Sy,T., A.D.Grinnell, A.Peskoff, and B.Yazejian. 2010. Monitoring transient Ca2+ dynamics with large-conductance Ca2+-dependent K+ channels at active zones in frog saccular hair cells. *Neuroscience* 165:715-722.

158. Tang,X.D., R.Xu, M.F.Reynolds, M.L.Garcia, S.H.Heinemann, and T.Hoshi. 2003. Haem can bind to and inhibit mammalian calcium-dependent Slo1 BK channels. *Nature* 425:531-535.

159. Tempel,B.L., D.M.Papazian, T.L.Schwarz, Y.N.Jan, and L.Y.Jan. 1987. Sequence of a probable potassium channel component encoded at Shaker locus of Drosophila. *Science* 237:770-775.

160. Tonini,R., A.Ferroni, S.M.Valenzuela, K.Warton, T.J.Campbell, S.N.Breit, and M.Mazzanti. 2000. Functional characterization of the NCC27 nuclear protein in stable transfected CHO-K1 cells. *FASEB J.* 14:1171-1178.

161. Tricarico,D., A.Mele, and C.D.Conte. 2005. Phenotype-dependent functional and pharmacological properties of BK channels in skeletal muscle: effects of microgravity. *Neurobiol. Dis.* 20:296-302.

162. Tsai,C.J., S.A.del, and R.Nussinov. 2008. Allostery: absence of a change in shape does not imply that allostery is not at play. *J. Mol. Biol.* 378:1-11.

163. Tulk,B.M., S.Kapadia, and J.C.Edwards. 2002. CLIC1 inserts from the aqueous phase into phospholipid membranes, where it functions as an anion channel. *Am. J. Physiol Cell Physiol* 282:C1103-C1112.

164. Tulk,B.M., P.H.Schlesinger, S.A.Kapadia, and J.C.Edwards. 2000. CLIC-1 functions as a chloride channel when expressed and purified from bacteria. *J. Biol. Chem.* 275:26986-26993.

165. Ulmasov,B., J.Bruno, P.G.Woost, and J.C.Edwards. 2007. Tissue and subcellular distribution of CLIC1. *BMC. Cell Biol.* 8:8.

166. Valenzuela,S.M., D.K.Martin, S.B.Por, J.M.Robbins, K.Warton, M.R.Bootcov, P.R.Schofield, T.J.Campbell, and S.N.Breit. 1997. Molecular cloning and expression of a chloride ion channel of cell nuclei. *J. Biol. Chem.* 272:12575-12582.

167. Valenzuela,S.M., M.Mazzanti, R.Tonini, M.R.Qiu, K.Warton, E.A.Musgrove, T.J.Campbell, and S.N.Breit. 2000. The nuclear chloride ion channel NCC27 is involved in regulation of the cell cycle. *J. Physiol* 529 Pt 3:541-552.

168. Vermeulen,L., M.R.Sprick, K.Kemper, G.Stassi, and J.P.Medema. 2008. Cancer stem cells--old concepts, new insights. *Cell Death. Differ.* 15:947-958.

169. Vescovi,A.L., R.Galli, and B.A.Reynolds. 2006. Brain tumour stem cells. *Nat. Rev. Cancer* 6:425-436.

170. Wallner,M., P.Meera, M.Ottolia, G.J.Kaczorowski, R.Latorre, M.L.Garcia, E.Stefani, and L.Toro. 1995. Characterization of and modulation by a beta-subunit of a human maxi KCa channel cloned from myometrium. *Receptors Channels* 3:185-199.

171. Wallner,M., P.Meera, and L.Toro. 1996. Determinant for beta-subunit regulation in high-conductance voltage-activated and Ca(2+)-sensitive K+ channels: an additional transmembrane region at the N terminus. *Proc. Natl. Acad. Sci. U. S A* 93:14922-14927.

172. Wang,J.W., S.Y.Peng, J.T.Li, Y.Wang, Z.P.Zhang, Y.Cheng, D.Q.Cheng, W.H.Weng, X.S.Wu, X.Z.Fei, Z.W.Quan, J.Y.Li, S.G.Li, and Y.B.Liu. 2009. Identification of metastasis-associated proteins involved in gallbladder carcinoma metastasis by proteomic analysis and functional exploration of chloride intracellular channel 1. *Cancer Lett.* 281:71-81.

173. Wang,L., S.He, Y.Tu, P.Ji, J.Zong, J.Zhang, F.Feng, J.Zhao, Y.Zhang, and G.Gao. 2012. Elevated expression of chloride intracellular channel 1 is correlated with poor prognosis in human gliomas. *J. Exp. Clin. Cancer Res.* 31:44.

174. Warton,K., R.Tonini, W.D.Fairlie, J.M.Matthews, S.M.Valenzuela, M.R.Qiu, W.M.Wu, S.Pankhurst, A.R.Bauskin, S.J.Harrop, T.J.Campbell, P.M.Curmi, S.N.Breit, and M.Mazzanti. 2002. Recombinant CLIC1 (NCC27) assembles in lipid bilayers via a pH-dependent two-state process to form chloride ion channels with identical characteristics to those observed in Chinese hamster ovary cells expressing CLIC1. *J. Biol. Chem.* 277:26003-26011.

175. Watkins,S. and H.Sontheimer. 2011. Hydrodynamic cellular volume changes enable glioma cell invasion. *J. Neurosci.* 31:17250-17259.

176. Werner,M.E., P.Zvara, A.L.Meredith, R.W.Aldrich, and M.T.Nelson. 2005. Erectile dysfunction in mice lacking the large-conductance calcium-activated potassium (BK) channel. *J. Physiol* 567:545-556.

177. Wonderlin,W.F. and J.S.Strobl. 1996. Potassium channels, proliferation and G1 progression. *J. Membr. Biol.* 154:91-107.

178. Wu,R.S. and S.O.Marx. 2010. The BK potassium channel in the vascular smooth muscle and kidney: alpha- and beta-subunits. *Kidney Int.* 78:963-974.

179. Wu,Y., Y.Xiong, S.Wang, H.Yi, H.Li, N.Pan, F.T.Horrigan, Y.Wu, and J.Ding. 2009. Intersubunit coupling in the pore of BK channels. *J. Biol. Chem.* 284:23353-23363.

180. Wu,Y., Y.Yang, S.Ye, and Y.Jiang. 2010. Structure of the gating ring from the human large-conductance Ca(2+)-gated K(+) channel. *Nature*.

181. Xia,X.M., X.Zeng, and C.J.Lingle. 2002. Multiple regulatory sites in large-conductance calcium-activated potassium channels. *Nature* 418:880-884.

182. Yan,J. and R.W.Aldrich. 2012. BK potassium channel modulation by leucine-rich repeat-containing proteins. *Proc. Natl. Acad. Sci. U. S. A* 109:7917-7922.

183. Yang,H., L.Hu, J.Shi, K.Delaloye, F.T.Horrigan, and J.Cui. 2007. Mg2+ mediates interaction between the voltage sensor and cytosolic domain to activate BK channels. *Proc. Natl. Acad. Sci. U. S A* 104:18270-18275.

184. Yang,H., J.Shi, G.Zhang, J.Yang, K.Delaloye, and J.Cui. 2008. Activation of Slo1 BK channels by Mg2+ coordinated between the voltage sensor and RCK1 domains. *Nat Struct. Mol Biol* 15:1152-1159.

185. Yang,J., G.Krishnamoorthy, A.Saxena, G.Zhang, J.Shi, H.Yang, K.Delaloye, D.Sept, and J.Cui. 2010. An epilepsy/dyskinesia-associated mutation enhances BK channel activation by potentiating Ca2+ sensing. *Neuron* 66:871-883.

186. Yuan,P., M.D.Leonetti, Y.Hsiung, and R.MacKinnon. 2011. Open structure of the Ca(2+) gating ring in the high-conductance Ca(2+)-activated K(+) channel. *Nature*.

187. Yuan,P., M.D.Leonetti, A.R.Pico, Y.Hsiung, and R.MacKinnon. 2010. Structure of the Human BK Channel Ca2+-Activation Apparatus at 3.0 A Resolution. *Science*.

188. Yusifov,T., A.D.Javaherian, A.Pantazis, C.S.Gandhi, and R.Olcese. 2010. The RCK1 domain of the human BKCa channel transduces Ca2+ binding into structural rearrangements. *J. Gen. Physiol* 136:189-202.

189. Yusifov,T., N.Savalli, C.S.Gandhi, M.Ottolia, and R.Olcese. 2008. The RCK2 domain of the human BKCa channel is a calcium sensor. *Proc. Natl. Acad. Sci. U. S A* 105:376-381.

190. Zeng,X.H., X.M.Xia, and C.J.Lingle. 2005. Divalent cation sensitivity of BK channel activation supports the existence of three distinct binding sites. *J Gen. Physiol* 125:273-286.

191. Zhang,G., S.Y.Huang, J.Yang, J.Shi, X.Yang, A.Moller, X.Zou, and J.Cui. 2010. Ion sensing in the RCK1 domain of BK channels. *Proc. Natl. Acad. Sci. U. S. A* 107:18700-18705.

192. Zhao,C., W.Deng, and F.H.Gage. 2008. Mechanisms and functional implications of adult neurogenesis. *Cell* 132:645-660.